Interface framework and energy management for microgrids

Minh Cong Pham

▶ **To cite this version:**

Minh Cong Pham. Interface framework and energy management for microgrids. Electric power. Université Grenoble Alpes [2020-..], 2021. English. NNT : 2021GRALT090 . tel-03611852

HAL Id: tel-03611852
https://theses.hal.science/tel-03611852

Submitted on 17 Mar 2022

HAL is a multi-disciplinary open access archive for the deposit and dissemination of scientific research documents, whether they are published or not. The documents may come from teaching and research institutions in France or abroad, or from public or private research centers.

L'archive ouverte pluridisciplinaire **HAL**, est destinée au dépôt et à la diffusion de documents scientifiques de niveau recherche, publiés ou non, émanant des établissements d'enseignement et de recherche français ou étrangers, des laboratoires publics ou privés.

Communauté UNIVERSITÉ Grenoble Alpes

THESE

Pour obtenir le grade de

DOCTEUR DE LA COMMUNAUTE UNIVERSITE GRENOBLE ALPES

Spécialité : **Génie Electrique**

Arrêté ministériel : 25 mai 2016

Présentée par

Minh Cong PHAM

Thèse dirigée par **Seddik BACHA** et codirigée par **Quoc Tuan TRAN**

préparée au sein du **du Laboratoire de Génie Electrique de Grenoble** dans **École Doctorale Electronique, Electrotechnique, Automatique & Traitement du Signal**

Interface framework and energy management for microgrids

Thèse soutenue publiquement le **15 décembre 2021**,
devant le jury composé de :

M. Bruno FRANCOIS
Professeur, L2EP – Ecole Centrale de Lille, Président
Mme. Manuela SECHILARIU
Professeur, Sorbonne Universités - Université de Technologie de Compiègne, Rapporteur
M. Yassine AMIRAT
Maître de Conférence, HDR, ISEN Yncréa Ouest, Brest, Rapporteur
M. Raphael CAIRE
Maître de Conférence, HDR, Université Grenoble Alpes, Examinateur
M. Seddik BACHA
Professeur, Université Grenoble Alpes, Directeur de thèse
M. Quoc Tuan TRAN
Professeur, INSTN, CEA-LITEN / INES, Co-Directeur de thèse
M. Ahmad HABLY
Maître de Conférence, HDR, Université Grenoble Alpes, Encadrant de thèse

Contents

List of figures

List of tables

Acronyms

BESS	Battery Energy Storage System
BTB	Back-to-Back
DER	Distributed Energy Resources
DG	Distributed Generation
DP	Dynamic Programming
ER	Energy Router
EI	Energy Internet
EMS	Energy Management System
FC	Fuel Cell
HESS	Hybrid Energy Storage System
MG	Microgrid
MMG	Multi-microgrid
MSML	Multi-sources Multi-loads
MSSL	Multi-sources Single-load
LCOE	Levelized Cost of Electricity
RES	Renewable Energy Resources
ROCOF	Rate of Change of Frequency
ROCOV	Rate of Change of Voltage
SC	Supercapacitor
SOC	State of Charge
SSML	Single-source Multi-loads
PV	Photovoltaic
VSC	Voltage Source Controller
VSG	Virtual Synchronous Generator

Acknowledgment

First and foremost, I would like to offer my sincere gratitude to my supervisors, M. BACHA Seddik, M. TRAN Quoc Tuan and M. HABLY Ahmad for choosing me as the candidate for this thesis, for dedicating me their time and for supporting me throughout my doctoral research. Thank you for all valuable experience, guidance and advice. It is a great honor for me to pursue my work under your supervision. I would like to thank M. TRAN Quoc Tuan for giving me an opportunity to come to France, working as a PhD student and a member of the European project. All of my work in this thesis cannot be accomplished without his broad and deep knowledge. I would like to thank M. BACHA Seddik and M. HABLY Ahmad for the valuable comments and discussion during my three years of intense work.

Many thanks would go to M. Reza Razi who have worked with me in the m2M project. I have learned many things, especially in power electronic domain from you. You have supported me a lot with simulation and writing reports. I also want to say thank to all my friends, my colleagues and the staffs at G2Elab in Grenoble for their friendship, encourage and assistance with the administrative process.

And last but not least, I would like to thank my family, my wife and my daughter for their unconditional love and their constant encouragement.

ABSTRACT

The large-scale integration of renewable energy leads to numerous technical and regulatory challenges. Recently, distributed system such as a microgrid is an emergent solution in this new electricity mix network. Each microgrid can be seen as a coherent entity, which can support network operation and management by using its distributed energy resources. One of the most important and expensive elements in microgrids is the energy storage system, which enhances the flexibility and reliability for the distributed network. However, despite of their advantages, the massive integration of microgrids leads to crucial challenges for the grid operators in term of policy, operation and energy management. Hence, the concept of microgrid need to be extended to a larger scale, in which multiple MGs are interconnected to form multi-microgrid system. In this new community, microgrids can support each other and improve the overall performance of whole system. The main goals of this thesis are the conceptualization, development and implementation of an appropriate interface among microgrids. This interface is based on the concept of energy router and energy internet. With this new system, the energy router classifies microgrids into grid-forming and grid-following unit. Their roles in the cluster of microgrids are depended on the controllable energy units in their system. The most common controllable energy resources in microgrid system is energy storage system. With that, firstly, the battery energy storage system is discussed. The battery sizing issue and its cooperation with other storage systems are investigated in this thesis. The optimal size of battery aims to minimize the operation cost of the remoted microgrid. The core of the sizing program is an energy management system with a dynamic programming approach. An operation strategy for a hybrid energy storage system is also developed with the respect of the optimal state of charge profile form the battery sizing program. After that, an interface for multi-microgrid system with back-to-back converter architecture is utilized. The core of this energy router topology are voltage source controllers. The microgrids with this interface can work in grid-connected mode, islanded mode and parallel mode. With the DC common line, the microgrids can be electrical isolated. The synchronization and power exchange in among microgrids in this scheme are introduced and examined. The thesis also proposes several methods for frequency supporting in microgrids. Finally, a graph-based theory approach for energy management with energy router application is proposed and validated with comparisons.

RÉSUMÉ

L'intégration à grande échelle des énergies renouvelables entraîne de nombreux défis techniques et réglementaires. Récemment, le système distribué tel qu'un micro-réseaux est une solution émergente dans ce nouveau réseau de mix électrique. Chaque micro-réseaux peut être considéré comme une entité cohérente, qui peut prendre en charge l'exploitation et la gestion du réseau en utilisant ses ressources énergétiques distribuées. L'un des éléments les plus importants et les plus coûteux des micro-réseaux est le système de stockage d'énergie, qui améliore la flexibilité et la fiabilité du réseau distribué. Cependant, malgré leurs avantages, l'intégration massive des micro-réseaux entraîne des défis cruciaux pour les gestionnaires de réseaux en termes de politique, d'exploitation et de gestion de l'énergie. Par conséquent, le concept de micro-réseau doit être étendu à une plus grande échelle, dans laquelle plusieurs MG sont interconnectées pour former un système multi-micro-réseau. Dans cette nouvelle communauté, les micro-réseaux peuvent se soutenir mutuellement et améliorer les performances globales de l'ensemble du système. Les principaux objectifs de cette thèse sont la conceptualisation, le développement et la mise en œuvre d'une interface appropriée entre les micro-réseaux. Cette interface est basée sur le concept de routeur énergétique et d'internet énergétique. Avec ce nouveau système, le routeur d'énergie classe les micro-réseaux en unités de formation et de suivi de réseau. Leurs rôles dans le cluster de micro-réseaux dépendent des unités d'énergie contrôlables dans leur système. Les ressources énergétiques contrôlables les plus courantes dans le système de micro-réseau sont le système de stockage d'énergie. Avec cela, tout d'abord, le système de stockage d'énergie de la batterie est discuté. La question du dimensionnement de la batterie et sa coopération avec d'autres systèmes de stockage sont étudiées dans cette thèse. La taille optimale de la batterie vise à minimiser le coût de fonctionnement du micro-réseau déporté. Le cœur du programme de dimensionnement est un système de gestion de l'énergie avec une approche de programmation dynamique. Une stratégie d'exploitation d'un système de stockage d'énergie hybride est également développée dans le respect du profil d'état de charge optimal du programme de dimensionnement de la batterie. Après cela, une interface pour un système multi-micro-réseau avec une architecture de convertisseur dos à dos est utilisée. Les contrôleurs de source de tension sont au cœur de cette topologie de routeur d'énergie. Les micro-réseaux dotés de cette interface peuvent fonctionner en mode connecté au réseau, en

mode îloté et en mode parallèle. Avec la ligne commune DC, les micro-réseaux peuvent être isolés électriquement. La synchronisation et l'échange d'énergie entre les micro-réseaux de ce schéma sont présentés et examinés. La thèse propose également plusieurs méthodes de support de fréquence dans les micro-réseaux. Enfin, une approche théorique basée sur les graphes pour la gestion de l'énergie avec une application de routeur d'énergie est proposée et validée avec des comparaisons.

CHAPTER I : Introduction

Contents

I.1. The context

I.1.1. Distributed energy resources

I.1.1.a. The concepts

In order to tackle environmental concerns, there is a trend of increasing the penetration of renewable energy sources (RESs) in grid system like solar and wind which are located near the consumers. The distributed energy resources (DERs) concept refers not only to those RESs, but also includes others energy sources that install near loads side such as battery energy storage (BESS) system, fuel cells, combined heat and power units or electric vehicles. With that, the conventional power systems are evolving from a large concentrated system to a more meshed system. With intelligent integration and control of DERs, system operators can handle the natural intermittency and the variability of RESs. Moreover, the overall system can benefit from DERs by reducing the transmission losses in power system.

In term of classification, DERs can be classified based on their interfaces with the system [1] :

- Directed – coupled conventional rotating machine (e.g. fixed – speed wind turbine system).
- Grid – coupled with the inverter (e.g. photovoltaic system).

In addition, DERs can also be categorized based on their functions in the system [2]:

- Grid – forming unit: create a reference value for voltage and frequency (e.g. battery storage system).
- Grid – feeding unit: its role is to extract maximum power from its primary energy source (e.g. rooftop photovoltaic system using maximum power point tracking).
- Grid – supporting unit: this unit are able to adjust its output active and reactive power in order to adapt to frequency and voltage variation caused by load profile changes (e.g. supercapacitor unit).

With the development of controlling method and technology, energy storage systems (ESSs) are vital DERs in future grids. The next part of this section represents the overview, functions and application of these units.

I.1.1.b. Energy storage system in modern power systems

One of the most important and expensive DER units in modern grids is an energy storage system (ESS). The main goals of using ESS are [3]:

- Improving the reliability of the RESs;
- Enhancing the resilience of the power system and resolving its problems;
- Releasing the advantages of smart grids and optimization the energy supply to match the demand.

Based on these goals, there are several applications of ESS in modern power system. These applications bring benefits for both grid operators and customers:

1) Application of ESS for grid operators

- Load tracking: most of electrochemical ESSs are suitable for this application because of their fast response characteristic. ESSs can help grid operators balance the gap between generation and consumption rapidly. Furthermore, ESSs have an ability to charge or discharge the energy so that the grid system can cover both side of the loads variation.
- Peak shaving: by using the energy stored in ESS and a normal capacity of grid, the grid system can supply the peak demand of load without the need of increasing the generation. With that, the operators can optimize the system design.
- Frequency supporting: with the integration of RESs, there are many fluctuations of the frequency in the system. The grid operators can utilize the ESS as a frequency regulator by correcting the frequency deviations (± 0.2 Hz in Continental Europe). There are three levels of frequency regulation for this application: primary (seconds), secondary (minutes) and tertiary (hours). The technologies of ESS must be chosen base on the requirement of the response time in each level of regulation.
- Voltage supporting: with the integration of DERs in distributed fashion, there is an issue with voltage in the grid system. Depending on the DERs behavior, ESS can absorb or release reactive power to regulating the local voltage levels in limitation (± 0.1 p.u).
- Black start: after a black out event, grid operators can utilize ESS for a restored process which is called a black start. ESSs have a capability of generating active power for activate power station.

2) Application of ESS for customers

- Energy management optimization: the goal of this application is to economically optimize the use of energy. ESS owners can storage energy from RES when the electricity from the grid is low and sell it when the price is high. Therefore, customers can maximize their benefit from RES.
- Power quality enhancement: customers' loads can suffer negative effect from the intermittence of RES. With the abilities of instantaneous response and quickly absorb or supply energy, BESS can connect directly with RESs and smoothen the output power of RES. Thus, the quality of the delivered power is improved and the loads are protected against short-term variations.
- Power reliability enhancement: ESS could provide energy continuously for customers in case of system failures. With such a large energy capacity as batteries, ESS can be used as primary generation source in the system running in islanded mode.

I.1.2. Microgrids and multi-microgrid system

I.1.2.a. Microgrid

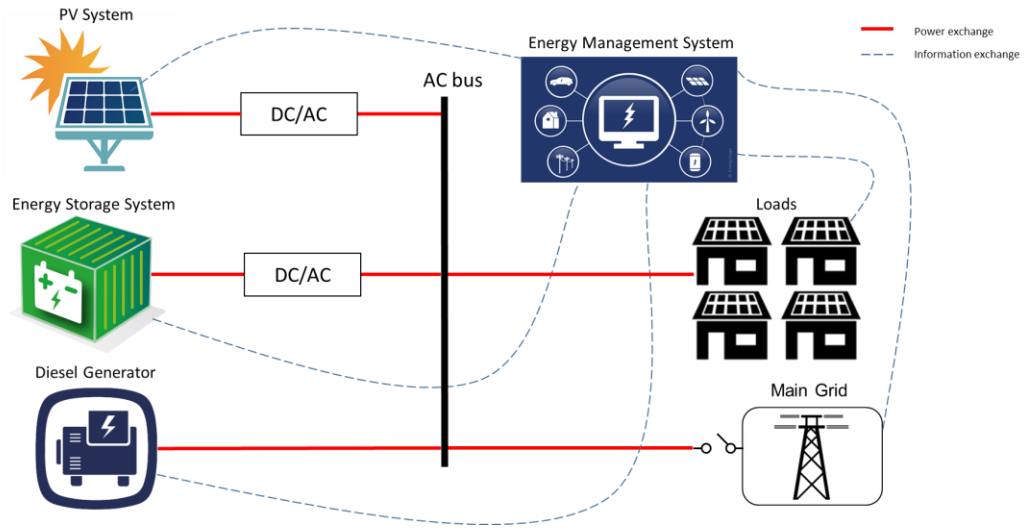

Figure I.1 – An example of a microgrid system with a centralized control system.

The concept of a microgrid is developed through several systematic research and development program, for example: the Consortium for Electric Reliability Technology Solutions (CERTS) effort in the United States [4] and the MICROGRIDS project in Europe [5]. By definition from the U.S. Department of Energy [6]: "a microgrid is a group of

interconnected loads and distributed energy resources (DERs) with clearly defined electrical boundaries that acts as a single controllable entity with respect to the grid and can connect and disconnect from the grid to enable it to operate in both grid-connected or island modes". An example of a microgrid system is shown in Figure I.1. From this definition, there are three main characteristics of the microgrid (MG):

- DERs and loads in a MGs must have electrical boundaries so that a microgrid is distinct from the rest of the system.
- The MG must be controlled as a single entity and the operation and energy management in a MG can be controlled by a single controller (centralized) or several controllers (distributed).
- A MG must be able to cover its own loads so that it can work in isolated mode or grid-connected mode.

In term of motivation, the deployment of MGs can bring benefits to technical, economic and environmental aspects [7]:

1. Technical benefits
    - The development of MGs can improve the reliability and resiliency. In the traditional power system, a blackout happens when a fault in a small part of the system lead to a domino effect that takes down an entire power system. However, thanks to the option of operating in off-grid mode, MGs can be isolated and continue to supply its customers.
    - The local issues of the distribution network can be mitigated with MGs. Unlike conventional system, the local voltage can be regulated by DERs in MGs network. For example, the ESS can adjust the reactive power in case of voltage violation. Moreover, the nature fluctuation of RES inside MGs can be smoothened with proper control method from storage system. Therefore, with the existence of MGs, the power balancing issue can be shared with distributed system operators.
    - With an optimization energy management system and forecasted values, MGs are able to cover their own loads, that can reduce the electricity imported from the main grid and also decrease the losses power in transmission lines.
    - The development of advanced information and communication technologies make the power system become more and more vulnerable with cyberattack.

However, the decentralized MGs remove the single point of failure and become less vulnerable to attacks.

2. Economic benefits
    - The deployment of MGs is located at the distribution network. Therefore, there is no need to develop on a new transmission system or transformers for the large amount of RES integration. MGs solution could avoid investments for replacement and extension of conventional power system. Furthermore, the grid operator can also save the energy losses from that transmission lines, which accounts for around 5 % to 10 % of gross electricity generation [8].
    - The MG can also bring economic benefits for the customers. The electricity tariff of the main grid could be high at the peak hours and by choosing the suitable energy sources with optimization strategy, the customers can buy the lowest cost of electricity from the utility grid or MGs. Moreover, the customers with DERs can sell back the energy to the main grid to make revenue.
3. Environmental benefits
    - The integration of non-controllable RES can bring negative impacts to the conventional system such as voltage rise, power fluctuation and steep ramping. The deployment of MG enhances the penetration of the RES such as solar or wind energy, which leads to the reduction of greenhouse gas emission.
    - In Europe, climate change and the need to integrate large amounts of clean renewable energy generation into the grid are the main driven force of developing MGs [7]. To deal with climate change issue, the main goal of this MG activity is to reduce the use of fossil fuels in generating electricity from 70 % in 2010 to below 20% by 2050 [9].

The installation of microgrid is expected to expanded from 1.1 GW in 2012 to 4.7 GW in 2017 with an forecasted market opportunity of $17.3 billion [10]. MGs are being progressively installed in power networks e.g., the MG capacity exceeded 1.8 GW in 2018 in the U.S [11]. In [12], the total capacity of deployed MGs was roughly 1.4 GW in 2015 and it is estimated to grow to approximately 5.7 GW with a conservative estimation or 8.7 GW with an aggressive scenario by 2024. In the first quarter of 2020, there are approximately 6610 microgrid projects have been proposed, planned and deployed around the world, with the total power capacity of roughly 31.5 GW [13]. In addition, as presented in [7], according

to Navigant Research, in 2018, the Asia Pacific and the North America are sharing the same capacity of microgrid market with 42 % each, following by Europe, Latin America, Middle East and Africa with 11%, 4% and 1% respectively. However, in 2020, the North America has surpassed Asia Pacific to has the highest capacity of microgrid market with 36 % as presented in Figure I.2.

However, despite of this significant development, the expansion of MGs still has to face several policy challenges. The remained issues relate to the legal and regulatory uncertainty, the interconnection policy, utility regulation and opposition, which is deeply discussed in [7]. Moreover, as presented in [14], the integration of MG also brings technical and economic challenges such as voltage collapse, large investment and low-power quality.

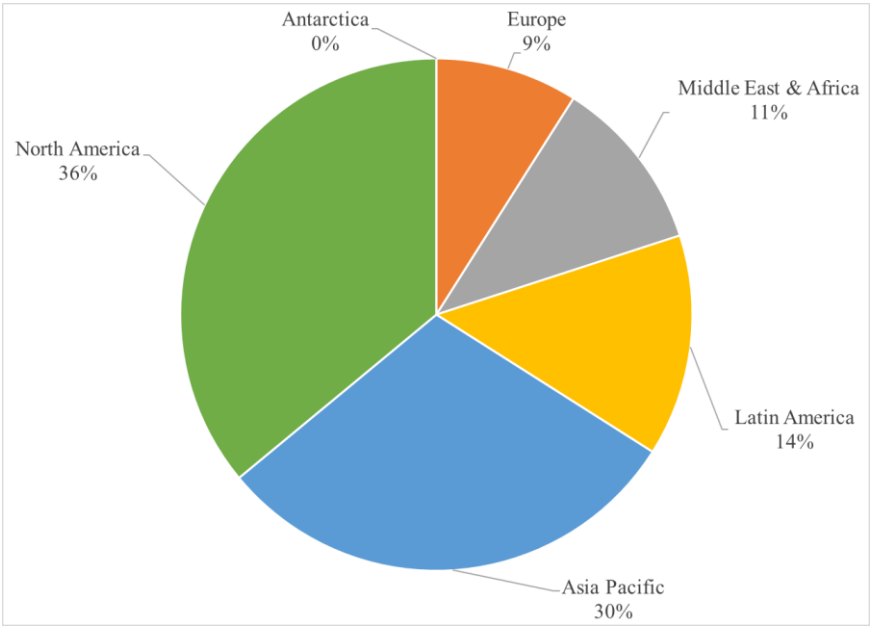

Figure I.2 – Total Microgrid Power Capacity Market Share by Region, World Markets: 1Q 2020. [Source: Guidehouse Insights]

I.1.2.b. Multi-microgrid system

With the massive implementation of microgrids, there could be a crucial challenge for the grid operators in term of operation and energy management. Therefore, the concept of microgrid need to be extended to a larger scale, in which multiple MGs are interconnected to form multi-microgrid system. As defined in [1], a multi-microgrid (MMG) system corresponds to a high-level structure, formed at medium voltage level, which comprises a number of low voltage MGs, DERs and consumers connected to adjacent MV feeders, as

shown in Figure I.3. In MMG system, each MG can act as an active cell to provide flexibilities to the grid operators.

The main driving forces in implementing multi-microgrid system is to alleviate the unstable operation of individual MGs during islanded mode and contribute numerous economic benefits to both main grid and the MG systems participating in the network [13]. The benefits of MMG system for a resilient, sustainable, and cost-effective electricity supply by providing a coordinated operation of individual networks is discussed in [15]. For example, in case of islanded operation, individual MGs could be affected by the fluctuation of RES, which can be overcome by sharing the controllable sources from the other MGs. Moreover, in case of energy shortage, the MGs with surplus energy can transfer their energy to the MGs with insufficiency energy, that reduces the dependency of the MGs on the main grid. In [16], the reliability, the stability and the system security are enhanced by MMG approach. An typical example for MMG project is presented and applied in PARADISE project [17].

Overall, the deployment of multi-microgrid system still need an extensive study to carry out an optimal control method and energy management strategy, which ensures a safe and reliable operation of the entire MG cluster during grid-connected and autonomous mode, as well as guarantees all the potential advantages from the integration of multiple MGs.

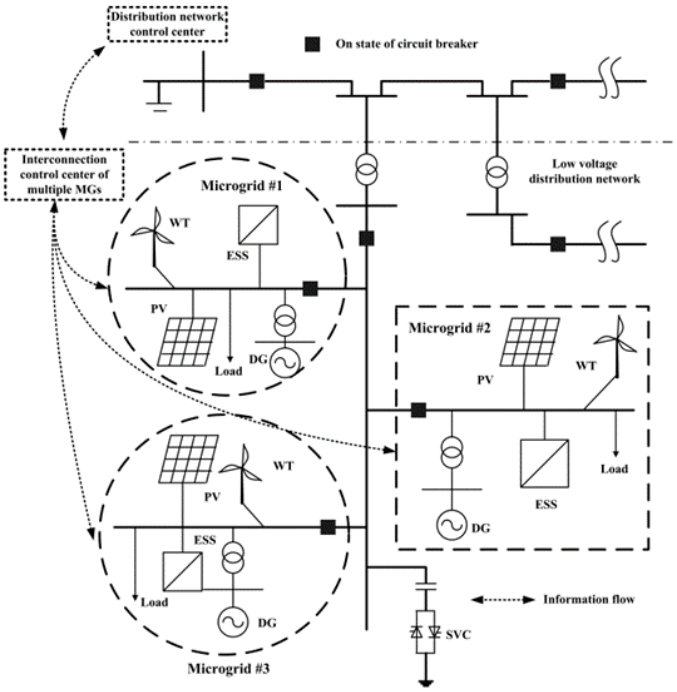

Figure I.3 – A typical structure of a multi-microgrid system [18].

I.2. Research motivation and thesis contribution

This thesis draws its motivation from the grid evolution, one where power system will be soon populated by numerous small and medium sized microgrids. In specific, the work in this thesis is driven by many questions still open to be explored, such as:

- *Can a battery sizing problem be formulated with energy management approaches and how to cooperate multiple energy storages?*
- *Can a cluster of microgrids be interconnected with a DC interface?*
- *What is an Energy Router and what is its roles in the Energy Internet?*
- *How to develop the mathematical models for the energy router and its control system?*
- *How do microgrids interact and exchange power with the energy router interface?*
- *What is the advantage of the DC interface in the multi-microgrid system?*
- *How do microgrids support each other's' stability with the Energy Router interface?*
- *What is the strategy for energy management in the multi-microgrid with the DC transmission lines?*
- *…*

Thus, this thesis, the main objective is to develop an interface among microgrid in the multi-microgrid system. The operation and energy management strategies in the cluster of microgrids are investigated. On the other hand, the sizing and operation issues of energy storage system in an islanded microgrid are also discussed. In term of thesis contribution, first of all, a new BESS sizing method with embedded energy management system is developed for the off-grid system. This method not only estimated an optimal size for the BESS system but also present an optimal power schedule for the MG. The main contribution of the thesis lies on the development of an energy router interface and the operation, energy management strategies for MMG application. Multiple methods for frequency coordination among MGs are proposed. The concept of inertia for frequency supporting in the AC domain is considered in the MMG with the present of DC common line. Finally, a new graph-based routing algorithm application for energy routers in multi-microgrid system is also introduced. Compared to the existing routing solution in the literature, the proposed routing method can deal with the congestion management and load sharing issues more effectively.

I.3. Thesis outline

The contents of this thesis are structured in six chapters. The outline is presented as follow:

- Chapter I: Introduction

  In this chapter, a brief introduction is presented. An emergent element in modern power system – distributed energy resources are introduced and classified. In addition, as one of the most importance DER, an overview and functions of the energy storage system are presented. The concept of microgrid and multi-microgrid system are also introduced in this chapter. These novel grids can work in grid-connected mode or off-grid mode, which enhances the reliability and the flexibility of the system.

- Chapter II: Energy storage system in microgrids

  The chapter focus on energy storage system in microgrids. Energy storage system play a vital role in modern grids. Only with a proper energy storage system, flexible operation and energy management strategies can be applied in microgrids or microgrids community. Therefore, first of all, before developing the interface among microgrids, the battery sizing problem in an isolated microgrid is taken into account. In order to minimize the operation cost of the system, the proposed sizing approach considers energy management system in the sizing process. A dynamic programming method applied for energy management system is developed in MATLAB and the simulation results are compared with the reference for validation. After that, the operation of energy storage system in a single microgrid is also analyzed. An off-grid microgrid with a hybrid energy storage system is studied. The developed operation method aims to follow the signal from the previous energy management system, minimize the fuel consumption and reduce the stress for fuel cell system. The implemented operation approach is tested on MATLAB/Simulink environment and compared with other methods to validate and show the effectiveness of the algorithms proposed.

- Chapter III: Energy Routers: an interface among microgrids

  An interface among microgrids in a multi-microgrid system is developed in this chapter. The chapter introduces the concept of energy internet and energy

router as an interface among MGs, with its characteristics, functionalities and topologies for implementation. The chosen topology for energy router is DC bus-based architecture. This topology has high degree of reuse and integration. In the chapter, a mathematical model of the chosen energy router architecture is developed, with its detail control system structure. In addition, a multi-microgrid system with energy router application is studied. The methodologies for synchronization, stability supporting and load sharing among multi-microgrid members are analyzed with simulation models.

- Chapter IV: Energy Routers: frequency support in a multi-microgrid system

  The application of the DC-link-based energy router for frequency support among microgrids in an islanded multi-microgrid system is proposed in this chapter. Firstly, the energy storage in the DC-link is utilized for enhancing the stability in the system. After that, the chapter proposes the frequency droop method for co-operation between grid-following and grid-forming members in the multi-microgrid system. Moreover, the concept of virtual synchronous generator from the AC domain is also utilized for frequency support in the AC/DC system. All these strategies are implemented and discussed through case studies.

- Chapter V: Graph-based routing algorithm application for energy routers in multi-microgrid system

  In this chapter, with the energy router interface, a novel energy routing algorithm was proposed based on graph theory to achieve peer-to-peer energy trading among microgrids. The main goal of the proposed method is to minimize the power losses of the system while maintaining energy security. Numerous analysis cases are studied to validate the performance and flexibility of the proposed algorithm. A nine – nodes and a thirty – nodes system is investigated in the simulation, which confirmed the superiority of the proposed method over the existing ones.

- Chapter VI: Conclusion and Future works

  This is the conclusive chapter, in which overall comparison among developed methods, results and contribution are discussed. Direction for future work is considered and suggested.

CHAPTER II : Energy storage system in microgrids

Contents

II.1. Introduction

II.1.1. Battery sizing strategies

In term of grid planning and energy management, the main disadvantages of a BESS are a high investment cost and a not very long cycle life. Therefore, in order to maximize the benefits of the microgrids, finding the optimal size of a BESS respecting both economic and technical constrain is essential. Based on the applications and the characteristics of BESS, there are two main approach for the BESS sizing issue: ancillary services approach and economic optimization approach.

The first strategy is applied in [19]–[21]. The authors in [19] propose a sizing method for a BESS with the aim to provide Frequency Containment Reserve (FCR) or Primary Control Reserve (PCR). The proposed sizing method takes into account the functions of BESS as a backup power provision to the system as well as the FCR, along with the investment and operating costs aspect. Similarity, in [20], the optimal size of the BESS for a microgrid is determined with primary frequency control function. The overloading capability of the BESS, state of charge (SOC) of the BESS and the permissible duration for participating in primary frequency control are investigated in the sizing process. The voltage support ability of the BESS is also considered for the BESS sizing process in [21]. The authors determine the optimal size and location of a BESS in distribution network taking into account the lifespan of the battery and its voltage regulation ability, which is formulated as a multi-objective optimization function and solved by genetic algorithm – II (NSGA-II). On the other hand, the BESS sizing issue is also considered with system security concern with bilevel optimization in [22] and in [23] with General Algebraic Modeling System (GAMS) platform.

The second sizing strategy with economic approach is applied widely in the reference [24]–[29]. In [24], with the aim to minimize the total annual operating cost of the grid-connected network with RES system, the authors using Improved Harmony Search Algorithm (IHSA) to solve the objective function. The feed-in-tariff (FIT) and the constrain of SOC of the BESS are considered. In addition, in reference [25], the BESS sizing problem following cost-benefit analysis method in MG is formulated by a two-stage strategy. The first stage is related with sizing model of BESS and the second one is related with MG operating cost model, which are solved by Mesh Adaptive Direct Search (MADS) black box

optimization algorithm and improved Particle Swarm Optimization (IPSO) algorithm respectively. A unit commitment (UC) problem based on the cost-benefit analysis and here-and-now (HN) strategy for BESS sizing problem for both islanded mode and grid-connected mode of MG is developed in [26]. The objective functions are minimizing the size of BESS and maximize the total benefit of the MG. The Particle Swarm Optimization (PSO) tool is utilized in the paper. Another heuristic methods for economic oriented BESS sizing approach are proposed in [27]–[29] A cost-based formulation with the MG operation cost minimization has been formulated to determine the optimal size of BESS and solved by Grey Wolf Optimization (GWO) [27], firefly algorithm (FA) [28] and Genetic Algorithm (GE) [29].

In this chapter, firstly, a new method for sizing BESS in islanded microgrid is presented. The proposed solution follows economic optimization strategy, which not only considers the optimization of operation cost of a MG system but also takes into account the SOC and the aging constrain of the BESS. The optimization problem is developed with the BESS sizing as an outer optimal loop and the economic dispatch of MG based on BESS data from the outer loop is considered as inner loop. An iterative method and a dynamic programming (DP) method are utilized to solve the optimal problems for outer and inner models respectively. A model built in MATLAB environment for an island microgrid is used to evaluate the efficiency of the developed method.

II.1.2. Hybridization of energy storage system

In term of grid operation, a single BESS technology sometime is not able to fulfill the desired operation due to its limited capability and the constrains of lifespan, cost, and power density, and dynamic time responses. Therefore, in the literature, a hybrid energy storage system (HESS), which is a combination of two or more energy storage with appropriate technologies and characteristics, is proposed as an emerged solution for MG application. Normally, a HESS is formed by a high-energy density storage device and a high-power density storage device. A HESS brings benefit to both economic and technical aspects in the grid system. In [30] and [31], by adding a high-power storage system, the size, the deep of discharge and the power losses of the high-energy storage system are significantly reduced.

As can be seen in Figure II.1, the fuel cells (FC) and Li-ion batteries technologies have the highest energy density whereas the ultra-capacitor or supercapacitors (SC) technology have a very fast dynamic response and a very high-power density. Therefore, a combination

of BESS (and/or fuel cell) and SC to form a HESS in the AC (DC) microgrid system have become popular in the recent research [32]–[34]. Moreover, in order to eliminate the use of diesel generator in MG system, Proton Exchange Membrane (PEM) Fuel Cell (FC) system is becoming a promising power source, which has drawn the attention of both academia and industry since the beginning of 21th century [35]. With that, the operation management of a HESS with BESS, FC and SC is investigated for islanded MG application in this chapter.

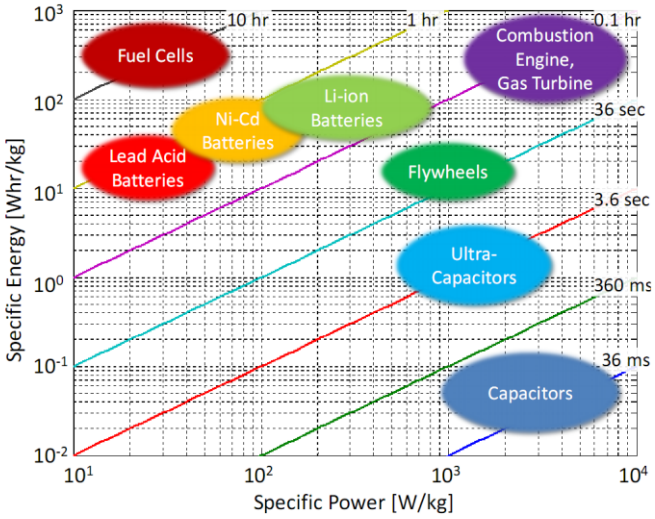

Figure II.1: Ragone plot of various ESS technologies [36]

In term of HESS topology, as shown in Figure II.2, there are two main approaches: series connection and parallel connection [34]. In series connection in Figure II.2 (a), the power distribution cannot be shared properly among ESS because the regenerated power is completely absorbed by the short-term ESS (SC) in this case, so that this topology reduces the flexibility of the HESS. Most of the time, for MG application, ESSs in HESS are connected in parallel topologies because of their flexibility. With a passive configuration in Figure II.2 (b), there is no converter between them so that the current sharing scheme and the common DC voltage between ESSs are completely depended on their internal resistances and the SOC of ESS respectively [37]. This topology has a cheap cost, a simple design and it might be suitable for some rural system with a large long-term storage size. In order to overcome the difficulty of the passive topology, power converters are utilized in the active topologies. With the addition of the power converters, the power flow in HESS can be actively controlled. Figure II.2 (c) and (d) present a semi-active HESS topology in which only the ESS connected with power converter is able to actively control. If the short-term ESS (SC) is connected with DC/DC converter, the SC can be operated with a wider range of voltage and the long-term ESS (BESS) is responsible for regulating the DC bus voltage,

which increases the stress on the BESS because of the high fluctuation and then reduces its life span [38]. On the other hand, if the BESS is connected to the DC/DC converter, the DC bus voltage is depended on the SC. The BESS can operate with a smoother current which reduce its stress. However, this topology requires a large capacity of SC for a stable DC bus. Finally, a full-active HESS topology with the DC/DC converters connected to all the ESS is introduced to improve the flexibility of HESS and enhance the overall system performance. In Figure II.2 (e) a cascaded full-active HESS topology with two bidirectional DC/DC converters allows BESS and SC be isolated from the DC bus. In this connection, the SC is responsible for regulating the DC bus voltage and absorbing the high frequency power variation, which creates a high power losses in the DC/DC converter due to the wide operating voltage of the SC [39]. In Figure II.2 (f), a parallel full-active HESS with a full control of BESS and SC is presented. With an appropriate control strategy, this HESS topology can share the demand power among ESSs effectively and then improve the BESS life span and the stability of the DC bus voltage [40].

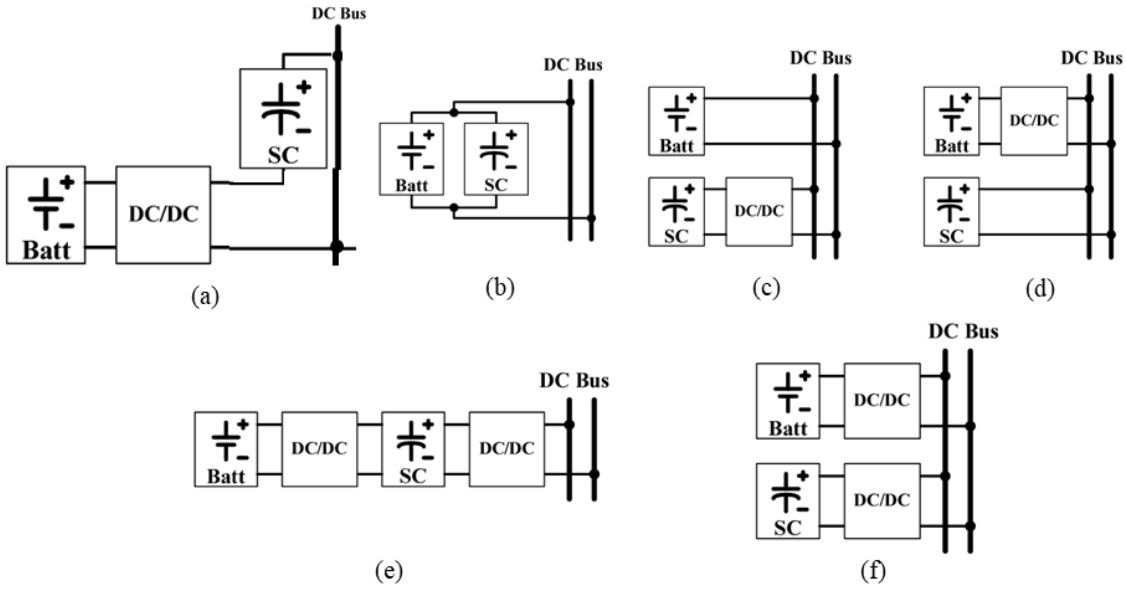

Figure II.2: The available topologies of HESS [33]: (a) Series; (b) Parallel passive; (c) (d) Parallel semi-active; (e) Cascaded full-active; (f) Parallel full-active.

Overall, with the islanded microgrid application, the main objectives of HESS are to enhance the reliability and robustness. Despite of the best controllability, the full-active HESS topologies increase the system complexity and cost. Hence, with a simpler design, reliable and robust operation, the semi-active HESS topologies are the most suitable for remoted application. In this chapter, BESS, SC and FC are formed in semi-active topology is investigated. Furthermore, a strategy for controlling such system is developed with

simulation validation and comparison. The detail of the developed HESS and controlling methodology are presented in section II.3 of this chapter.

II.2. Optimal sizing of battery energy storage system for an islanded microgrid

II.2.1. Configuration of the islanded microgrid system

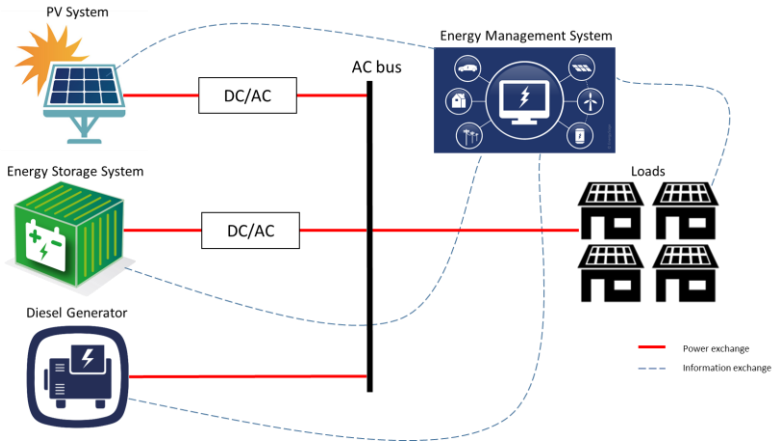

Figure II.3: The PV-diesel-battery islanded microgrid system.

In this section, an islanded microgrid used for BESS sizing process is illustrated in Figure II.3. The studied MG comprises such DERs as PV system, BESS and a backup diesel generator for covering insufficient energy. An energy management system in this off-grid MG is utilized for gathering information and performing operation optimization function. The operation cost of this system depends on the cost model of the ESS, solar and genset. It is essential to find an optimal operation strategy with a given predicted solar radiation curve and load demand curve, which is strongly related to the size of ESS. Furthermore, a proper energy management schedule can reduce the size of ESS and lessen the dependence of diesel generator. On the other hand, the size of ESS must be large enough for charging and discharging to cover the excess and deficit energy from the system. The next part of this section presents the cost-based models of the studied microgrid.

II.2.1.a. Load model

In the studied MG system, only the output power demand of the load is considered. With that, the model for the load in this section is the power demand profile curves. Based on the load demand power, the power supplied from the diesel generator, the sizes of PV

system and BESS are defined, which is related to the investment and operation cost of the whole system. The load power demand ($P_L(t)$ [kW]) is based on hourly data, which is illustrated in Figure II.4.

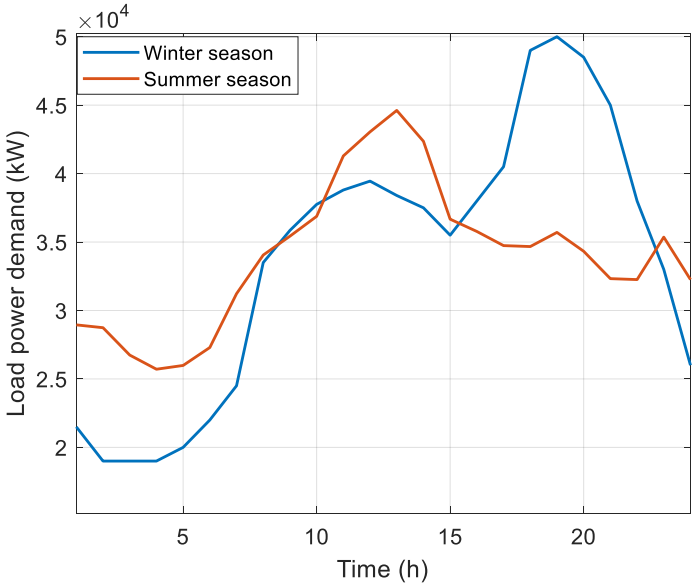

Figure II.4: The predicted daily load demand.

II.2.1.b. Diesel generator model

In islanded MG system, a diesel generator and BESS are the secondary power supply sources for the power system in case of insufficient energy from RES. With a backup of a conventional generator, not only the reliability of the remoted system is improved but also the high investment cost of BESS is lessened. The model for the hourly consumption of diesel generator F(t) [l] is given by [41]:

$$F(t) = 0.246 \, . \, P_{DG}(t) + 0.08415 \, . \, P_R \qquad \text{(II.1)}$$

where $P_{DG}(t)$ [kW] is the output power of diesel generator at time t, P_R [kW] is the rated power of the diesel generator. Therefore, the cost-based function of the diesel generator is calculated:

$$C_{DG}(t) = C_f \, . \, F(t) \qquad \text{(II.2)}$$

where $C_{DG}(t)$ [US$] is operation cost of diesel generator at time t and C_f [US$/l] is the fuel cost of diesel per liter.

II.2.1.c. Solar photovoltaic model

Not only the BESS sizing problem but also the PV sizing is considered in this chapter. However, the main objective of this section is to find an optimal size for BESS. Therefore, the PV sizing problem serves as an input program to provide the PV power data for the BESS sizing model which is presented in II.2.2.a. The PV sizing method is an iterative approach considering the annual cost of the islanded MG system.

Following [42], the total output power of solar photovoltaic system ($P_{PV}(t)$ [kW])is dependent on the solar radiation, the total area of the PV array and the efficiency of the system and given by:

$$P_{PV}(t) = G(t).A_p.N_{PV}.\eta \quad \text{(II.3)}$$

where G(t) [W/m^2] is the solar radiation value, A_p [m^2] is the area of a single PV panel, N_{PV} [unit] is the number of PV panels and η [%] is the overall energy efficiency of the solar PV system. The PV panels technology used in this section is Photowatt PV2300-235 and the detail of this panel can be found in [43]. The predicted data for solar radiation is shown in Figure II.5.

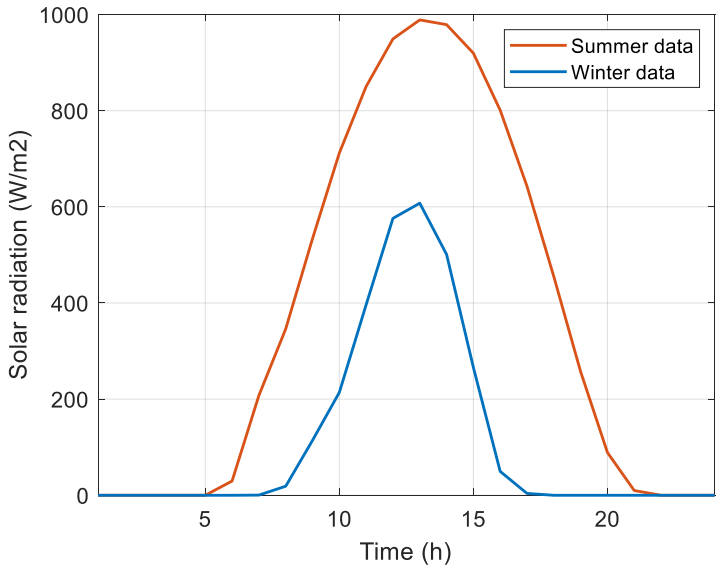

Figure II.5: The predicted daily solar radiation.

Similar with the load model in II.2.1.a, the solar PV model in this chapter only consider the output power of the PV system. However, in this section, only the predicted solar radiation is present. Thus, the model of the PV system, which is an output power curve, must be defined with the number of PV panels in equation (II.3). The method for defining the size of the PV system is presented in II.2.2.

II.2.1.d. Battery energy storage model

The advantages of Lithium-ion batteries are high energy density, high efficiency and long-life cycle. Therefore, in this section, a Lithium-ion battery technology is applied for charging and discharging energy. Following cost-based approach, the model of BESS is presented by its state of charge (SOC) and state of health (SOH), which are related to the (dis)charge power of BESS. The SOC [%] is the ratio of the available BESS capacity C(t) [kWh] at time t and the nominal reference BESS capacity $C_{ref,N}$ [kWh], which is defined by the manufacture data. The SOC of BESS at time t can be given by:

$$SOC(t) = \frac{C(t)}{C_{ref,N}} \tag{II.4}$$

Furthermore, the SOC can also be determined by the previous value of SOC and the charge/discharge power of BESS (P^{ch}_{BESS}/P^{disch}_{BESS} [kW]) between the time step (Δt [h]). Thus, with the time step is taken by 1 hour, the SOC of BESS at time t, from the period (t -1) to t is calculated by:

$$\mathrm{SOC}(t) = \begin{cases} SOC(t-1) + \dfrac{P^{ch}_{BESS}(t-1)}{C_{ref,N}}\Delta t & (1) \\ SOC(t-1) - \dfrac{P^{disch}_{BESS}(t-1)}{C_{ref,N}}\Delta t & (2) \\ SOC(t-1) & (3) \end{cases} \tag{II.5}$$

(1): when the BESS absorbed energy in this period

(2): when the BESS provided energy in this period

(3): when the BESS is idle in this period

On the other hand, to evaluate the battery's ability to charge and discharge energy compared with the new one, it is essential to estimate its state of health (SOH). The SOH [%] is related to the capacity evolution of BESS by the equation [44]:

$$SOH(t) = \frac{C_{ref}(t)}{C_{ref,N}} \tag{II.6}$$

where: $C_{ref}(t)$ [kWh] is the reference capacity defined as the BESS maximum capacity at time t. There are two type of BESS's degradation causing aging effect: cycle aging and calendar aging [45].

With calendar aging mechanism, the most important parameter to estimate this effect is the battery temperature, especially for Lithium-ion battery. In [46], with an experiment, a model for the degradation of SOH after period Δt [h] can be formulated by:

$$\frac{SOH(t+\Delta t)}{SOH(t)} = 1 + c_a . c_V^{\frac{V-V_0}{\Delta V}} . c_T^{\frac{T-T_0}{\Delta T}} . \sqrt{\Delta t} \quad \text{(II.7)}$$

where T_0 [°C] and V_0 [V] are the reference temperature and voltage, T [°C] and V [V] are the temperature and voltage of the battery, ΔT [°C] and ΔV [V] are the reference temperature and voltage variation. c_a, c_T and c_V are the fitting parameters based on accelerated calendar aging test data. From the equation (II.7) above, it is clear that, high temperature and high voltage contribute to the degradation process of BESS. However, the calendar aging mechanism of BESS is not considered the developed sizing process due to the complication of temperature measurement.

In term of cycle aging, which is utilized to for BESS sizing methodology in this chapter, the model for BESS degradation can be formulated by [47]:

$$SOH(t) = SOH(t-\Delta t) - Z.[SOC(t-\Delta t) - SOC(t)] \quad \text{(II.8)}$$

where Z is a linear aging coefficient. Experiment results in [48] defines different Z for different BESS technologies. The coefficient Z of BESS can be estimated as [49]:

$$Z = \begin{cases} 85 . 10^{-6} & (1) \\ \chi . 85 . 10^{-6} & (2) \end{cases} \quad \text{(II.9)}$$

(1): when 20% < SOC (t) < 90%

(2): otherwise

where χ is a scalar strictly greater than one. Moreover, with the equation (II.6), the equation (II.8) can be transformed into:

$$SOH(t) = \frac{C_{ref}(t-\Delta t)}{C_{ref,N}} - Z.[SOC(t-\Delta t) - SOC(t)] \quad \text{(II.10)}$$

In addition, the capacity losses of BESS at time t ($\Delta C_{ref}(t)$ [kWh]) and the new capacity reference of BESS at time t ($C_{ref}(t)$ [kWh]) are given by:

$$\Delta C_{ref}(t) = C_{ref,N} . Z.[SOC(t-\Delta t) - SOC(t)] \quad \text{(II.11)}$$

$$C_{ref}(t) = C_{ref}(t-\Delta t) - \Delta C_{ref}(t) \quad \text{(II.12)}$$

From equations (II.8), (II.11) and (II.12), the variation of SOH is estimated by:

$$\Delta SOH(t) = Z.[SOC(t-\Delta t) - SOC(t)] \quad \text{(II.13)}$$

Overall, by considering the degradation effect of BESS system, the economic model of BESS is described by the investment cost and the aging cost of BESS. The BESS investment cost (BiC [US$]) is calculated:

$$BiC = C_{BESS,cap}.C_{ref,N} \quad \text{(II.14)}$$

where $C_{BESS,cap}$ [US$/kWh] is the capital cost per kWh of the BESS and $C_{ref,N}$ [kWh] is the reference nominal capacity of the BESS. Finally, the cost function of BESS in MG operation is modelled as:

$$C_{BESS}(t) = BiC\frac{\Delta SOH(t)}{1 - SOH_{min}} \quad \text{(II.15)}$$

where $C_{BESS}(t)$ [US$] is the cost of BESS operation at time t SOH_{min} [%] is the minimum state of health value.

II.2.2. The proposed BESS sizing strategy

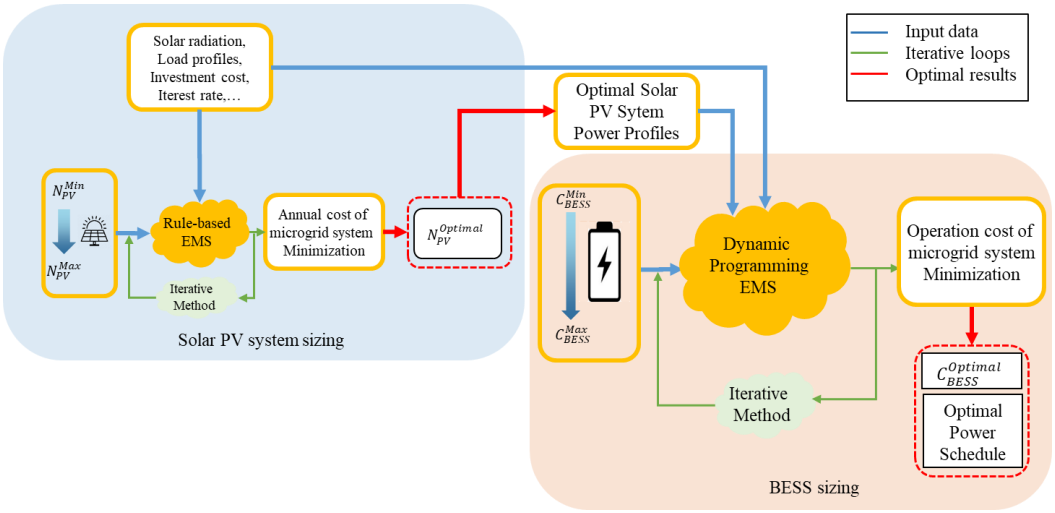

Figure II.6: Scheme of the proposed strategy for BESS sizing problem.

The proposed strategy for finding the optimal size of BESS is presented in Figure II.6. In order to have the optimal solar PV system power curve which serves as an input data for the BESS sizing problem, a sub-problem for finding the optimal size of PV system panel is determined. Overall, with the MG information such as load profiles, solar radiation, investment cost and the like, the proposed strategy not only able to find the optimal size of BESS but also can determine the optimal size of PV system and the optimal power schedule for the islanded MG.

II.2.2.a. Solar PV system sizing

II.2.2.a.i. Problem formulation

Firstly, the sub-problem of sizing solar PV system is illustrated in this part of the section. With the given input data of solar radiation and load profiles, the objective function

for this sub-problem is to find the optimal size of solar PV system in order to minimize the annual cost of the islanded MG system (ACS [US$]). The ACS of the studied MG system consist of the investment cost, maintenance cost and the carbon dioxide (CO_2) emission cost. Therefore, the ACS is given by:

$$ACS = ACC + AOMC + ARC + AFC + AEC \quad \text{(II.16)}$$

where ACC [US$] is the annual capital cost, AOMC [US$] is the annual operation maintenance cost, ARC [US$] is the annual replacement cost, AFC [US$] is the annual fuel cost and AEC [US$] is the annual emission cost. The detail of the ACS function is illustrated in equations from (II.17) - (II.23) [50], [51].

$$ACC = C_{cap} \frac{i.(1+i)^y}{(1+i)^y - 1} \quad \text{(II.17)}$$

$$\text{With} \quad i = \frac{i' - f}{1+f} \quad \text{(II.18)}$$

$$AOMC = C_{cap} \frac{1-\lambda}{\lambda} \quad \text{(II.19)}$$

$$ARC = C_{rep,c} \,.SFF \quad \text{(II.20)}$$

$$\text{With} \quad SFF = \frac{i}{(1+i)^y - 1} \quad \text{(II.21)}$$

$$AFC = C_f \,. \sum_{1}^{8760} F(t) \quad \text{(II.22)}$$

$$AEC = \sum_{1}^{8760} \frac{E_f . E_{cf} . P_{DG}(t)}{1000} \quad \text{(II.23)}$$

where:

C_{cap}	The capital cost	[US$]
y	Project lifetime	[year]
i	Annual real interest rate	[%]
i’	loan interest (%)	[%]
f	annual inflation rate (%)	[%]
λ	reliability of components	[%]
$C_{rep,c}$	Replacement cost of BESS	[US$]
SFF	Sinking fund factor	[unit]
C_f	Fuel cost of diesel per liter	[US$]

F(t)	Hourly consumption of diesel generator	[liter]
E_f	Emission cost function	[kg/kWh]
E_{cf}	Emission cost factor	[unit]
$P_{DG}(t)$	Diesel generator output power at time t	[kW]

II.2.2.a.ii. Methodology

As can be seem in Figure II.6, in order to solve the solar PV sizing problem formulated in equation (II.16), the rule-based methodology for energy management and iterative solution are utilized. The flow chart of the proposed methodology is presented in Figure II.7.

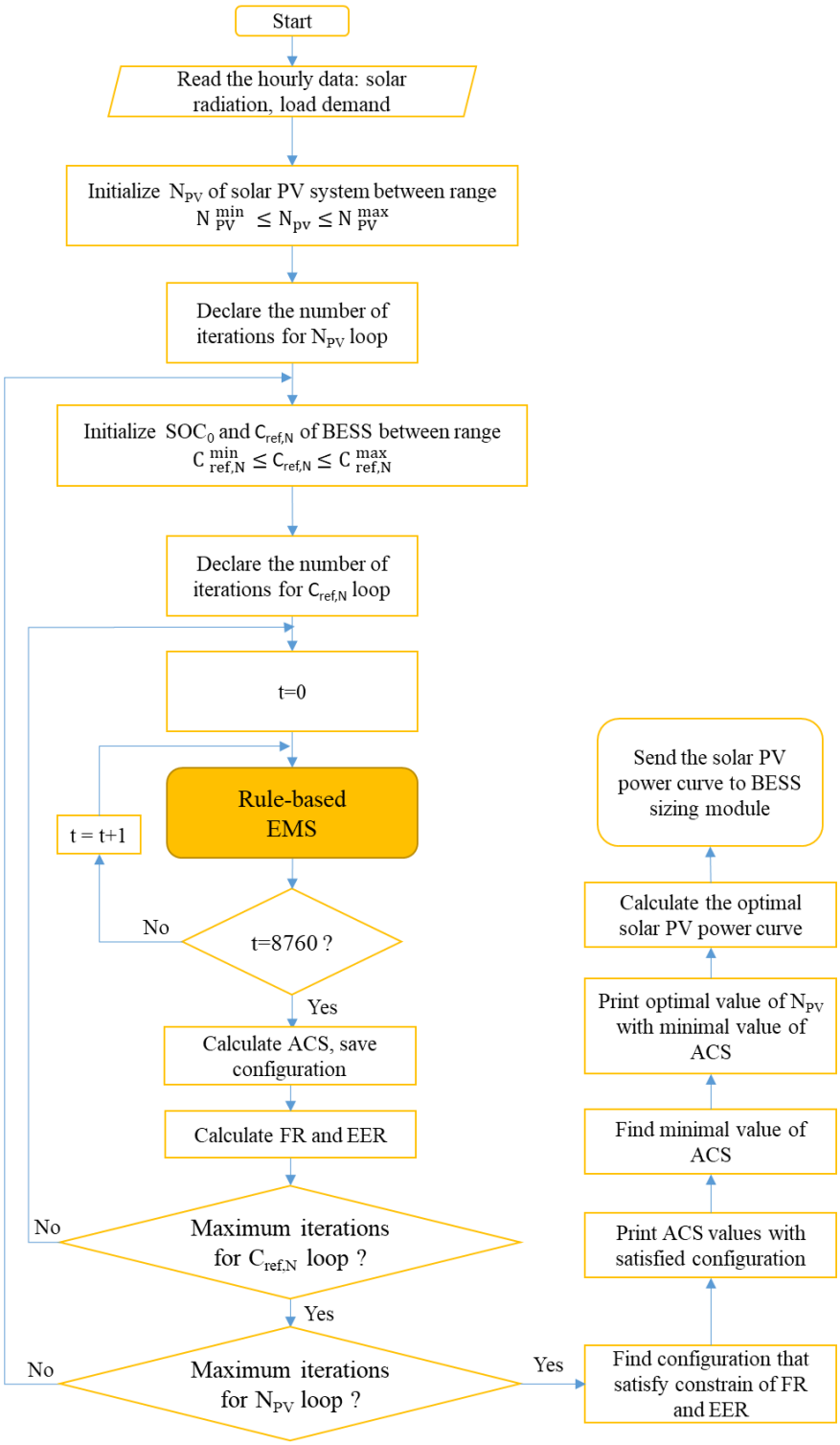

Figure II.7: Flow chart of the Solar PV sizing module.

The proposed strategy including two main parts: the iterative loops of solar PV size, BESS size and the rule-based energy management system (EMS). With iterative loops, the size of BESS and solar PV system are increased until they reach the maximum values. Moreover, in each iteration, with each configuration of solar PV system and BESS, the EMS

in MG is performed to calculate the values of ACS for one year following equation (II.16). When the program reaches the maximum value of all the iteration, all the ACS values are checked with constrains of excess energy ratio (EER) and fraction renewable energy (FR). The detail of the system constrains is presented in II.2.2.a.iii. It is noteworthy that the size of BESS in this solar PV sizing process is just a temporary size, which is used to size the PV panels. The optimal size of BESS will be defined in the next part of the proposed method.

On the other hand, the rule-based EMS strategy illustrated in this section is a method that derives execution instructions from a starting set of data and rules. Following this, based on the specific situation of power of load demand, solar PV power, diesel power and BESS condition, the output power of diesel generator and BESS are defined. With the rule-based EMS, there are several scenarios in islanded MG operation:

- Solar PV system is able to supply sufficient energy to meet the load demand and the BESS is charged by the excess energy.

$$\Delta P_{BESS}^{ch}(t) = (SOC_{max} - SOC(t)).\ C_{ref,N} \quad \text{(II.24)}$$

$$P_{BESS}(t) = P_{BESS}^{ch}(t) = min\ \{P_{PV}(t) - P_L(t),\ \Delta P_{BESS}^{ch}(t)\} \quad \text{(II.25)}$$

- Solar PV system is not enough to supply the load demand. If the deficit power is smaller than the minimum value of diesel power P_{DG}^{min} [kW] and the remaining power of BESS is enough for covering the deficit power demand, the BESS will be discharged to supply the load, the DG is turn off.

$$P_{BESS}(t) = P_{BESS}^{disch}(t) = P_L(t) - P_{PV}(t) \quad \text{(II.26)}$$

- Solar PV system is not enough to supply the load demand. If the deficit power is smaller than the minimum value of P_{DG}^{min} and the remaining power of BESS is not enough for covering the deficit power demand, the DG is will operate at P_{DG}^{min} and the BESS will be charged with the surplus power from the DG.

$$P_{DG}(t) = P_{DG}^{min} \quad \text{(II.27)}$$

$$P_{BESS}(t) = P_{BESS}^{ch}(t) = P_{DG}^{min} - (P_L(t) - P_{PV}(t)) \quad \text{(II.28)}$$

- Solar PV system is not enough to supply the load demand. If the deficit power is higher than the minimum value of P_{DG}^{min} and the deficit power is smaller than the $\Delta P_{BESS}^{disch}(t)$ [kW], the BESS will supply the deficit power and the DG is turn off.

$$\Delta P_{BESS}^{disch}(t) = (SOC(t) - SOC_{min}).\ C_{ref,N} \quad \text{(II.29)}$$

$$P_{BESS}(t) = P_{BESS}^{disch}(t) = P_L(t) - P_{PV}(t) \quad \text{(II.30)}$$

- Solar PV system is not enough to supply the load demand. If the deficit power is higher than the minimum value of P_{DG}^{min} and the deficit power is higher than the sum of $\Delta P_{BESS}^{disch}(t)$ and P_{DG}^{min}, the BESS will discharge at $\Delta P_{BESS}^{disch}(t)$ and the DG will cover the remain deficit power.

$$P_{BESS}(t) = \Delta P_{BESS}^{disch}(t) = (SOC(t) - SOC_{min}).\ C_{ref,N} \quad \text{(II.31)}$$

$$P_{DG}(t) = (P_L(t) - P_{PV}(t)) - \Delta P_{BESS}^{disch}(t) \quad \text{(II.32)}$$

- Solar PV system is not enough to supply the load demand. If the deficit power is higher than the minimum value of P_{DG}^{min} and the deficit power is higher than $\Delta P_{BESS}^{disch}(t)$ but smaller than the sum of $\Delta P_{BESS}^{disch}(t)$ and P_{DG}^{min}, the DG is operate at P_{DG}^{min} and the BESS will be charged.

$$P_{DG}(t) = P_{DG}^{min} \quad \text{(II.33)}$$

$$P_{BESS}(t) = P_{BESS}^{ch}(t) = P_{DG}^{min} - (P_L(t) - P_{PV}(t)) \quad \text{(II.34)}$$

II.2.2.a.iii. The constrains

To apply the flow chart in Figure II.7, there are constrains for the variables of DERs system and grid operation.

a) Constrains of the DERs system

- Diesel generator:

$$P_{DG}^{min} \leq P_{DG}(t) \leq P_{DG}^{max} \quad \text{(II.35)}$$

where P_{DG}^{min} [kW] and P_{DG}^{max} [kW] are the minimum and maximum output power of the DG system respectively.

- BESS:

$$C_{ref,N}^{min} \leq C_{ref,N} \leq C_{ref,N}^{max} \quad \text{(II.36)}$$

$$SOC_{min} \leq SOC(t) \leq SOC_{max} \quad \text{(II.37)}$$

where SOC_{min} and SOC_{max} are the minimum and maximum state of charge of BESS system respectively. $C_{ref,N}^{min}$ [kWh] and $C_{ref,N}^{max}$ [kWh] are the minimum

and maximum reference nominal capacity of the BESS respectively. These limitation values can be estimated as [52]:

$$\begin{cases} C_{ref,N}^{min} = 0 \\ C_{ref,N}^{max} = \dfrac{E_{L\_day}.D}{DOD.\eta_b} \end{cases} \quad \text{(II.38)}$$

where E_{L_day} [kWh] is the total energy from the load demand for one day, D is the number of days, DOD [%] is the depth of discharge of the BESS and η_b is the efficiency of BESS.

- Solar PV system:

$$0 \leq N_{pv} \leq \frac{E_{L\_day}}{W.Hours_{sunshine/day}.\eta_b} \quad \text{(II.39)}$$

where η_b [%] is the efficiency of the BESS, $Hours_{sunshine/day}$ [h] is the number of sunshine hours per day.

b) Constrains of the MG operation

- Fraction renewable energy (FR) [53]:

$$FR = \frac{E_{solar}}{E_{TT}} \quad \text{(II.40)}$$

$$FR_{design} \leq FR \leq 1 \quad \text{(II.41)}$$

where E_{solar} [kWh] is the total energy produced from solar PV system, E_{TT} [kWh] is the total energy received from DERs in the MG. FR_{design} [unit] is the designed value for FR in the studied MG.

- Excess energy ratio (EER):

$$EER = \frac{E_{excess}}{E_{TT}} \quad \text{(II.42)}$$

$$0 \leq EER \leq EER_{design} \quad \text{(II.43)}$$

where E_{excess} [unit] is the excess energy from solar PV system and EER_{design} is the designed value for EER in the studied MG.

II.2.2.b. BESS sizing

II.2.2.b.i. Problem formulation

Next, after the size of solar PV system is defined, the main module of sizing BESS program is introduced in this part of the section. The objective of the proposed BESS sizing

strategy is to find the optimal value size of BESS which minimizes the operation cost (CO) of the islanded MG system with the period of 24 hours. The objective function of the minimization cost operation (CO [US$]) of the studied MG system is given by [54]:

$$CO(t)=C_{DG}(t) + C_{DG}^{Em}(t) + C_{BESS}(t) \quad \text{(II.44)}$$

where $C_{DG}(t)$ and $C_{BESS}(t)$ are the operation cost of DG and BESS at time t and they are calculated in equation (II.2) and equation (II.15) respectively. $C_{DG}^{Em}(t)$ [US$] is the emission cost of DG operation at time t and it is calculated similar with AEC in equation (II.23) but with the period of 24 hours.

II.2.2.b.ii. Methodology

Similar with the previous solar PV sizing approach, an iterative method and an EMS of MG are utilized to deal with the BESS sizing problem. A dynamic programming (DP) with Bellman algorithm is applied to solve the EMS optimization problem of islanded MG in equation (II.44). After reaching the maximum iteration, the developed program can determine the optimal size of BESS and the optimal schedule for MG operation. The flowchart of the proposed method is shown in Figure II.8. The detail of the DP is presented in the next parts.

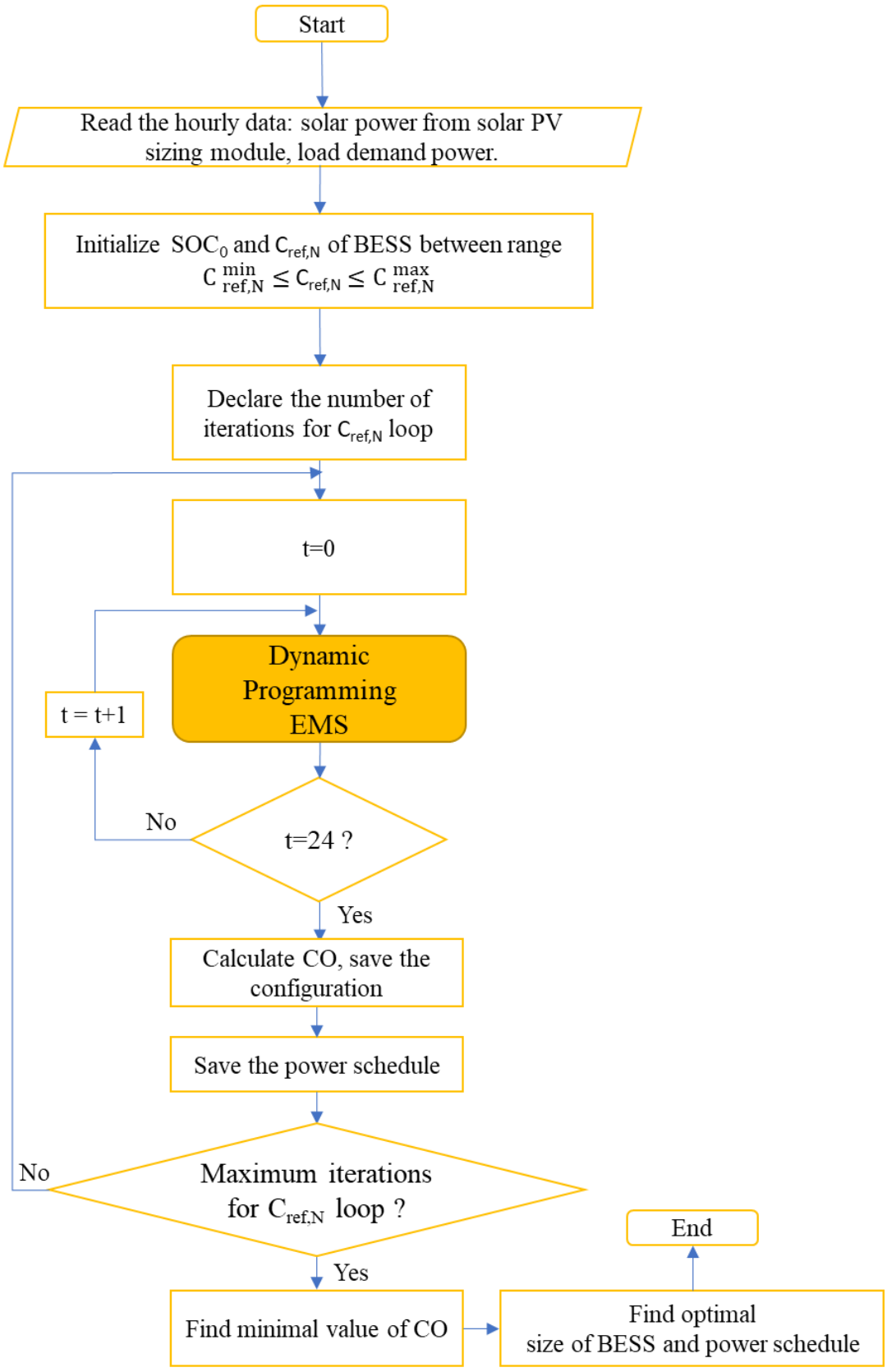

Figure II.8: Flow chart of the BESS sizing module.

a) Introduction of dynamic programming

Dynamic programming is an optimization technique that breaks complex problem into series of sub-problem, which is suitable to deal with discrete time optimization process. DP with Bellman algorithm is an optimization method utilized to find the shortest path from all node of the graph. A graph has a set of elements called nodes or vertices, with edges between some of the nodes. V is used to denote the set of vertices and E to denote the set of edges. A directed graph G = (V, E) is a graph where the edge has a direction. Moreover, a weighted graph is given as a graph where its edges have weight such as cost. Therefore, in order to apply this optimization approach, the optimization problem must be modelled in form of "graph" with "nodes", "edges" and must has a direction. The pseudocode of Bellman algorithm is shown as follow:

Algorithm 1: Bellman Algorithm

Data: Given a directed graph G (V, E), a start node S and the weight W of each edge.
Result: Shortest path from S to all other vertices in G.

```
D[S] = 0;
R =V – S;
C=cardinality(V);
for each vertex k ∈ R do
    D[k] = ∞;
end
for each vertex i = 1 to (C – 1) do
    for each edge (e1, e2) ∈ E do
        Relax(e1, e2);
    end
end
for each edge (e1, e2) ∈ E do
    if D[e2] > D[e1] + W[e1, e2] then
        Print("Graph contains negative weight cycle")
    end
end
Procedure Relax (e1, e2)
for each edge (e1, e2) in E do
```

```
    if D[e2] > D[e1] + W[e1,e2] then
        D[e2]=D[e1]+W[e1,e2];
    end
end
```

b) Application of DP for the EMS problem

The idea is to use SOC of BESS to formulate EMS as a DP problem. Thus, the EMS of the islanded MG must be modelled in form of multi-stage, with SOC as a "node". Thanks to the power balance condition in the MG, one has:

$$P_{BESS}(t)=P_L(t)-(P_{DG}(t)+P_{PV}(t)) \quad \text{(II.45)}$$

From equations (II.5) and (II.45), the power balance equation in MG can be described in form of SOC of BESS as:

$$\frac{SOC(t)-SOC(t-1)}{\Delta t}C_{ref,N}=P_L(t)-(P_{PV}(t)+P_{DG}(t)) \quad \text{(II.46)}$$

Thus, the final equation of power balance in grid system is given as:

$$SOC(t)=SOC(t-1)+\frac{P_{PV}(t)+P_{DG}(t)-P_L(t)}{C_{ref,N}}\Delta t \quad \text{(II.47)}$$

From equation (II.47), it is obvious that by controlling SOC of BESS at each time step, the output power of DG can be controlled. Furthermore, the operation cost of the system at each time step will be regulated via SOC of BESS. With that, the optimization of EMS for 24 hours problem can be divided into 24 sub-problems of optimization.

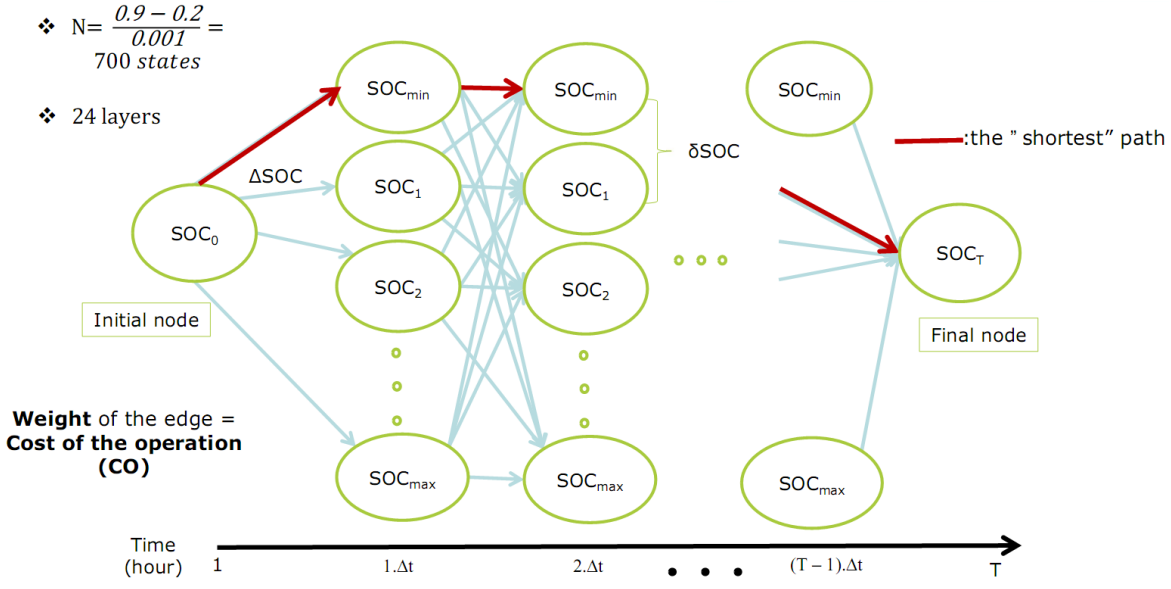

Figure II.9: Dynamic programming for energy management system based on SOC of BESS.

The process of DP application for finding optimal SOC of BESS is described in Figure II.9. In here, the "edge" of the graph are the CO(t) values and the "node" are the SOC(t) of BESS. SOC_0 [%] and SOC_T [%] are the initial and the final SOC respectively. These initial node and final node of SOC are given. There are 24 layers corresponding to 24 hours of a daily MG operation. At each layer, the state of SOC is discretized with a step size which is δSOC [%]. In addition, the transition between two layers of SOC is described by ΔSOC [%] which is the variation of SOC between two step time. The objective of the optimization is to find the optimal flow of SOC from the initial node to the end node. As can be seen clearly that the structure of energy management process can be modeled by a graph. It is obvious that the flow of SOC in this process is a directed graph and all the edges are oriented in one direction from t=0 [h] to t=T [h]. With that, the Bellman algorithm can be applied for searching optimal SOC flow in this problem. The number of state (N) at each layer is estimated by:

$$N = \frac{SOC_{max} - SOC_{min}}{\delta \mathrm{SOC}} \tag{II.48}$$

Now, the weight of each node in the first layer is calculated, which receives the information (SOC_0) from the beginning node. The weight in this DP model represents for the cost of operation (CO) which is calculated in equation (II.44). In addition, the weight of each node in the second layer, which receives the information ($SOC_{0+\Delta t}$) from all nodes in the first layer. Repeat this process until the weights of the final nodes in the last layer are obtained. After that, the weight of the end node, which receives the information from all nodes at the last layer, are obtained by defining the all the CO values from the beginning node. Finally, by minimization of the CO values from the beginning node to the final node, the optimal SOC strategy with the corresponding power schedule are defined.

II.2.2.b.iii. The constrains

There are constrains for system operation. Firstly, the power balance constrain at any instant is described in equation (II.45). Secondly, the constrain of DG is similar with the one presented in equation (II.35).

Secondly, there are addition constrains of SOC for the BESS:

$$\Delta SOC_{\ min} \leq \Delta SOC \leq \Delta SOC_{\ max} \tag{II.49}$$

$$SOH_{min} \leq SOH(t) \quad \text{(II.50)}$$

II.2.3. Simulation results and discussion

II.2.3.a. Input data

In this section, the islanded microgrid system in

Figure II.3 is used for the sizing simulation. The model of the studied microgrid and the sizing program are developed in the MATLAB 2019b environment. The detail of the economic and technical input data is illustrated in Table II-1and Table II-2 [55]. Moreover, the predicted load demand and solar radiation profiles shown in Figure II.4 and Figure II.5 respectively are also utilized.

Table II-1: The economic input data of the MG system for the sizing program

Parameter	Value	Unit
y of PV	20	year
y of BESS	10	year
y of DG	20	year
i’	3	%
f	2	%
λ	98	%
η	98	%
C_{cap} of DG	500	US$/kW
C_{cap} of PV	0.92	US$/W
C_{cap} of BESS	137	US$/kWh
C_f	0.8	US$/l
E_f	0.34	kg/kWh
E_{cf}	55	US$/ton

Table II-2: The technical input data of the MG system for the sizing program

Parameter	Value	Unit
FR_{design} for summer	50	%
FR_{design} for winter	25	%

EER_{design}	1	%
P_{DG}^{min}	15	kW
P_{DG}^{max}	50	kW
DOD	80	%
δSOC	0.0001	unit
SOC_0 for rule-based EMS	60	%
SOC_0 for DP EMS	50	%
SOC_T	50	%
SOC_{min}	20	%
SOC_{max}	90	%
ΔSOC_{max}	70	%
ΔSOC_{min}	0	%
SOH_{min}	70	%

II.2.3.b. Simulation results

In this part of the section, following the simulation results, the optimal size of the BESS and PV solar panel of the islanded microgrid system are presented in Table II-3. From the simulation results, the optimal size of solar PV system is estimated with 410 PV panels. Following this, the optimal capacity of BESS system for the studied MG is approximately 450 kWh. Moreover, with the optimal configuration, the contribution of solar PV system to overall electricity production can reach approximately 59%, which is very good ratio for RES penetration. The contribution of BESS and diesel generator for electricity production record at 18% and 23% respectively. The levelized cost of energy (LCOE) is around 0.1786 US$/kWh, which is reasonable for an isolated system.

Table II-3: The optimal results of the proposed sizing strategy

Name	Value	Unit
$N_{PV}^{Optimal}$	410	panel
$C_{ref,N}^{Optimal}$	450	kWh
ACS	49537	US$

LCOE	0.1786	US$/kWh
CO	135.7	US$/day
Annual load energy	286853.3	kWh
Annual PV system energy	166044.3	kWh
Annual BESS energy	50776.46	kWh
Annual diesel generator energy	70033.27	kWh

With the selected size of solar PV and BESS, Figure II.10 and Figure II.11 describe a typical day of the rule-based operation for MG in summer and winter season. From the figures, it can be seen that the load demands in both seasons are satisfied. Furthermore, with a high solar radiation profile in summer, the island MG system doesn't require any energy from the diesel generator as shown in Figure II.10 (a). However, with high peak power from solar PV system in summer, the size of BESS system is increased. With winter day, with a lower solar radiation and a higher load at the afternoon (from 2 p.m to 12 p.m), the RES energy is not enough so that the remained load is covered successfully from the BESS and diesel generator. In addition, as can be seen in Figure II.10 (b) and Figure II.11 (b), with the start at 60% at the beginning of the operation period, the SOC curves of BESS in both seasons are always in the predefined limits. Therefore, with the given data and simulation results, it can be concluded that the proposed sizing method is able to provide an optimal solar and BESS size for a remoted system while respecting the system and economical constrains.

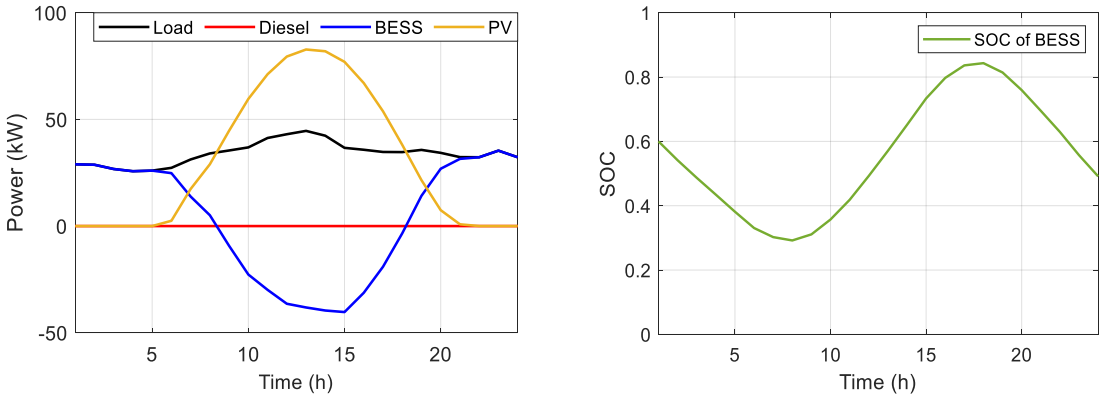

(a) (b)

Figure II.10: (a) The power schedule proposed by rule-based EMS for a typical summer day of the island microgrid; (b) The corresponding SOC of BESS.

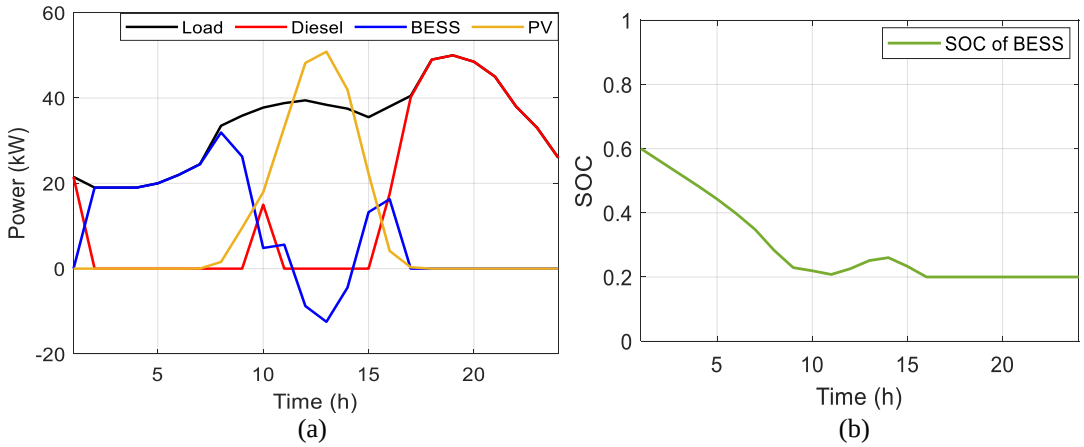

Figure II.11: (a) The power schedule proposed by rule-based EMS for a typical winter day of the island microgrid; (b) The corresponding SOC of BESS.

On the other hand, in order to confirm the performance of the developed method, the proposed BESS sizing method is compared with a reference method which is a simple iterative algorithm proposed in [56]. The input data such as the load power demand profile, solar radiation profiles, the economic parameters and the constrains are inherited from the reference paper. A detail of the comparison is illustrated in Table II-4.

Table II-4: The comparison of the sizing results between the proposed method and the reference method

Parameter	Value		Unit
	Proposed method	Reference method	
$N_{PV}^{Optimal}$	410	410	panel
$C_{ref,N}^{Optimal}$	215	250	kWh
LCOE	0.1786	0.185	US$/kWh
CO	117	139	US$/day

The compared results are shown in Table II-4, it is obvious that, with the same load demand and solar radiation profiles, the two methods estimate the same value of solar PV panels (410 panels). As can be seen in the comparison table, the proposed method not only reduce 14% capacity of the BESS system but also provide a lower cost of electricity (LCOE) and cost of operation (CO). The main contribution to the different in the simulation results between the two methods is the different in the DP EMS in the developed sizing strategy and the iterative with rule-based EMS in the reference sizing strategy.

With the advantage of DP EMS in the sizing process, the SOC of BESS system can be controlled in order to minimize the global cost of the MG operation whereas with the iterative method, there is no operation cost optimization in the process. The different between the two method is indicated in term of optimal power schedules shown in Figure II.12 and Figure II.13. As in Figure II.12, despite of using more energy from diesel generator from 4 p.m to 11 p.m, the operation cost of the system with the proposed method is still lower because of avoiding using BESS with low SOC condition which is clearly presented in Figure II.13. By taking into account the degradation (SOH) of the BESS system in the optimization cost, the diesel generator in the developed method can support BESS system when the SOC level is low. Moreover, the SOC of BESS with DP EMS (Figure II.13(a)) is regulated to return to 50% at the end of day, which is good for BESS condition and provision for the next day of operation. With non-optimization approach, only the constrain of SOC of BESS is satisfied, the degradation of the BESS is not taking into account, which lead to a higher operation cost despite of using less energy from diesel system. As can be seen in Figure II.13(b), the SOC of BESS is depended on the grid situation and stays below 50% most of the time.

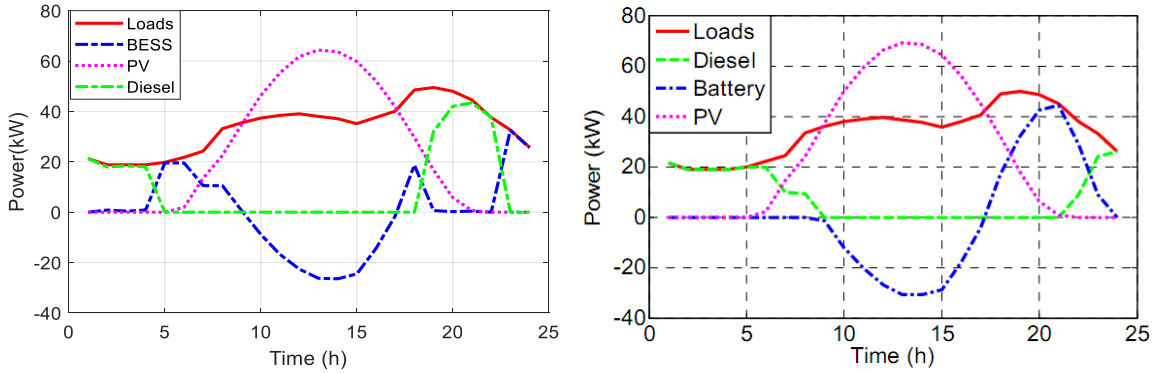

(a) (b)

Figure II.12: The optimal power schedule for a daily MG operation by: (a) The proposed method; (b)The reference method in [56].

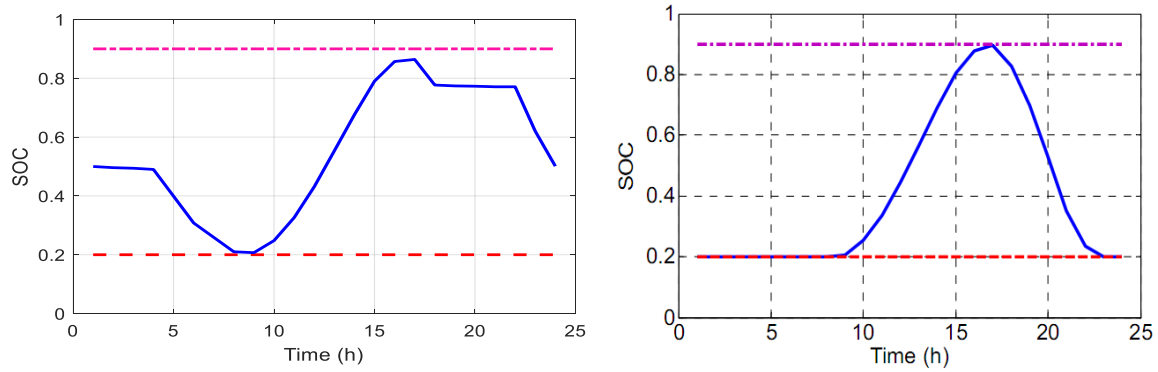

Figure II.13: The optimal SOC profiles of BESS schedule for a daily MG operation by: (a) The proposed method; (b) The reference method in [56].

II.3. Operation strategy of a hbrid energy storage system in a standalone microgrid

II.3.1. Hybrid energy storage system configuration

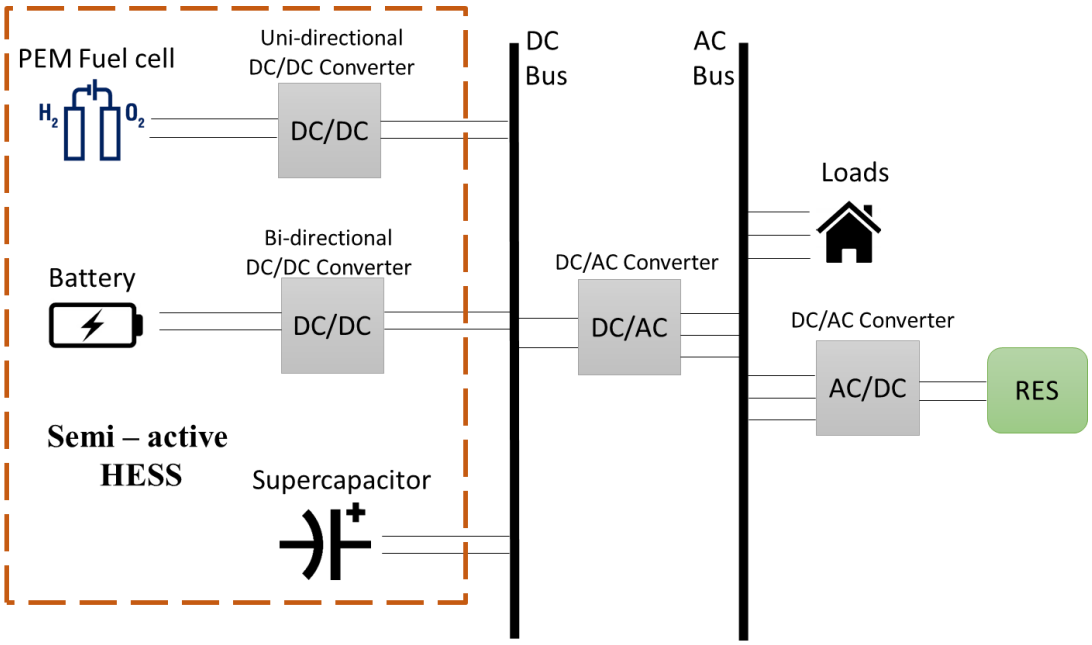

Figure II.14: The case study with an off-grid microgrid system with HESS

In this part of the chapter, an islanded microgrid with battery-supercapacitor-fuel cell is investigated as shown in Figure II.14. All the ESSs are connected to a common DC bus. A semi-active HESS topology with the SC connected directly with the DC bus is chosen. In this way, the BESS and FC can avoid the high fluctuation of the power demand. Furthermore, with the converters, a methodology for optimizing operation can be applied for BESS and

FC system. A PEM fuel-cell system is connected with a unidirectional DC/DC converter, which allows the FC system only produce the energy. With BESS, a bi-directional DC/DC converter is utilized, which allows BESS absorb and release energy following the energy balance condition of the system. With the direct connection, a high-power density and a fast response, the SC is expected to absorb the high frequency and peak load demand so that it can reduce the stress on the FC and BESS. The BESS and FC are controlled via their DC/DC converters with the support from the power management system. The DC bus is converted to AC bus via a DC/AC converter. On the AC side, the load and the RES system are connected to the three phase AC bus. In the next part of the chapter, the models for the MG's elements in the MATLAB/Simulink environment are described.

II.3.2. HESS simulation modelling

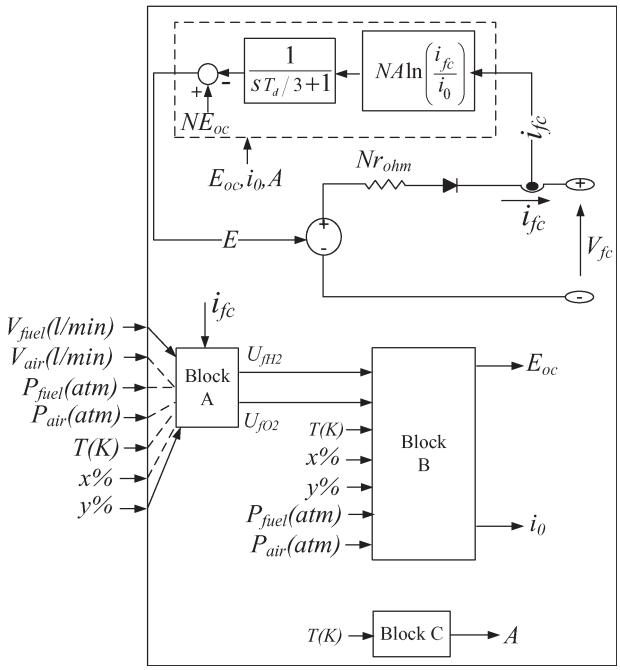

(a)

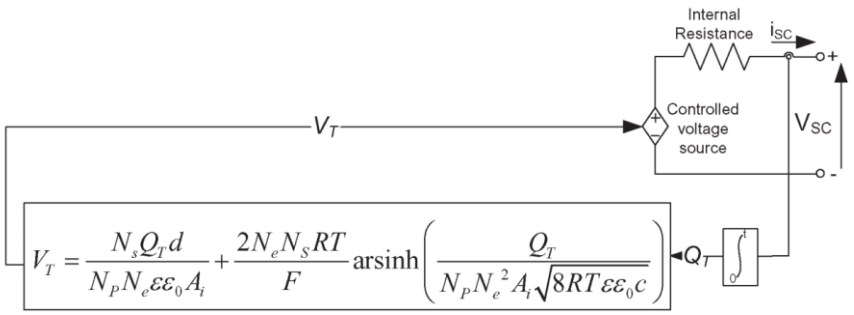

(b)

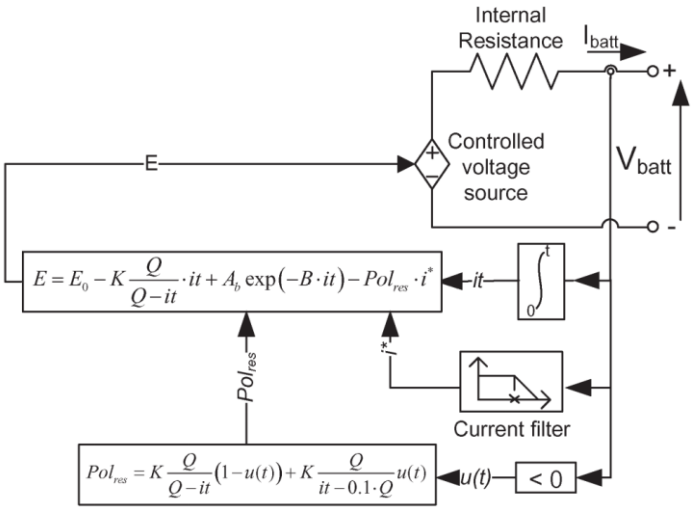

(c)

Figure II.15: HESS models; (a) PEM Fuel-cell; (b) Supercapacitor; (c) Li-ion battery [57].

The models of the HESS are built in MATLAB/Simulink environment using the SimPowerSystems (SPS) toolbox. The mathematical model of the PEM FC system shown in Figure II.15 (a) is described in [58] with the following equation (II.51)-(II.54):

$$V = E_{OC} - V_{act} - V_r \tag{II.51}$$

$$V_{act} = A.ln\left(\frac{i_{fc}}{i_0}\right).\frac{1}{\frac{sT_d}{3}+1} \tag{II.52}$$

$$V_r = r_{ohm}.i_{fc} \tag{II.53}$$

$$V_{fc} = N.V \tag{II.54}$$

$$H\_con = \frac{N}{F}\int i_{fc} \tag{II.55}$$

where V [V] is the cell output voltage, E_{OC} [V] is the open circuit voltage, V_{act} [V] is the activation voltage losses, V_r [V] is the resistive and diffusion losses voltage, A [V] is the Tafel slope, i_{fc} [A] is the output FC current, i_0 [A] is the exchange current, T_d is the cell settling time, r_{ohm} [ohm] is the combined cell and diffusion resistance. With the FC stack, V_{fc} [V] is the total output voltage with N is the number of cells. The hydrogen consumption of the FC system is presented as H_con [g] in equation (II.55), with F [A.s/mol] is the Faraday constant.

In addition, the mathematical model for SC system shown in Figure II.15 (b) is presented with the combination of the Helmholtz and Gouy-Chapman models as described in [59]. This model is illustrated by the equation (II.56)-(II.61).

$$C = \left[\frac{1}{C_H} + \frac{1}{C_{GC}}\right]^{-1} \tag{II.56}$$

$$C_H = \frac{N_e \varepsilon \varepsilon_0 A_i}{d} \tag{II.57}$$

$$C_{GC} = \frac{F Q_c}{2 N_e R T} \sinh\left(\frac{Q_c}{N_e^2 A_i \sqrt{8 R T \varepsilon \varepsilon_0 c}}\right) \tag{II.58}$$

$$C_T = \frac{N_p}{N_s} C \tag{II.59}$$

$$V_{SC} = \frac{Q_T}{C_T} - R_{SC}.i_{SC} \tag{II.60}$$

$$Q_T = N_P Q_c = \int i_{SC} dt \tag{II.61}$$

where C [F], C_H [F], C_{GC} [F] are the SC, Helmholtz and Gouy-Chapman capacitances respectively, N_e [unit] is the number of electrode layers, ε [F/m] and ε_0 [F/m] are the permittivity values of the electrolyte material and free space respectively, A_i [m^2] is the interfacial area between electrodes and electrolyte, d [m] is the Helmholtz layer length, Q_c [C] is the cell electric charge and c [$mol.m^{-3}$] is the molar concentration. With the SC interconnected system, C_T [F] is the total capacitance, Q_T [C] is the total electrical charge, N_p and N_s are the number of cells connected in parallel and series respectively. V_{SC} [V] is the total output voltage, R_{SC} [ohm] and i_{SC} [A] are the SC module resistance and the module current respectively.

Finally, the model of the Li-ion battery system shown in Figure II.15 (c) is developed in [60] with the following mathematical equation (II.62)-(II.63).

$$V_{batt} = E_O - K\frac{Q}{Q - it}.it - R_b.I + A_b \exp(-B.it) - K\frac{Q}{Q - it}.i^* \tag{II.62}$$

$$Pol_{res} = K.\frac{Q}{it - 0.1Q} \tag{II.63}$$

where V_{batt} [V] and E_O [V] are the output voltage and the constant voltage of the battery, K [V/Ah] is the polarization constant. Q [Ah] is the BESS capacity, it [Ah] and i^* [A] are the actual BESS charge and the filtered BESS current respectively, R_b [ohm] is the BESS internal resistance. A_b [V] is the exponential zone amplitude, B [Ah^{-1}] is the exponential

zone time constant inverse. During charging process, the voltage of the BESS increase and Pol_{res} [ohm] is the polarization resistance in this period.

II.3.3. HESS operation strategy

The proposed operation method for the HESS is presented in this section. In order to examine the performance of the method, the state machine and PI approaches in the literatures are also discussed and compared. In the three approaches, the DC-bus voltage in the HESS is presented by the SOC of the SC and is controlled by the BESS. The difference between the operation methods relies on the approach to obtain the FC system reference power, as shown in Figure II.16.

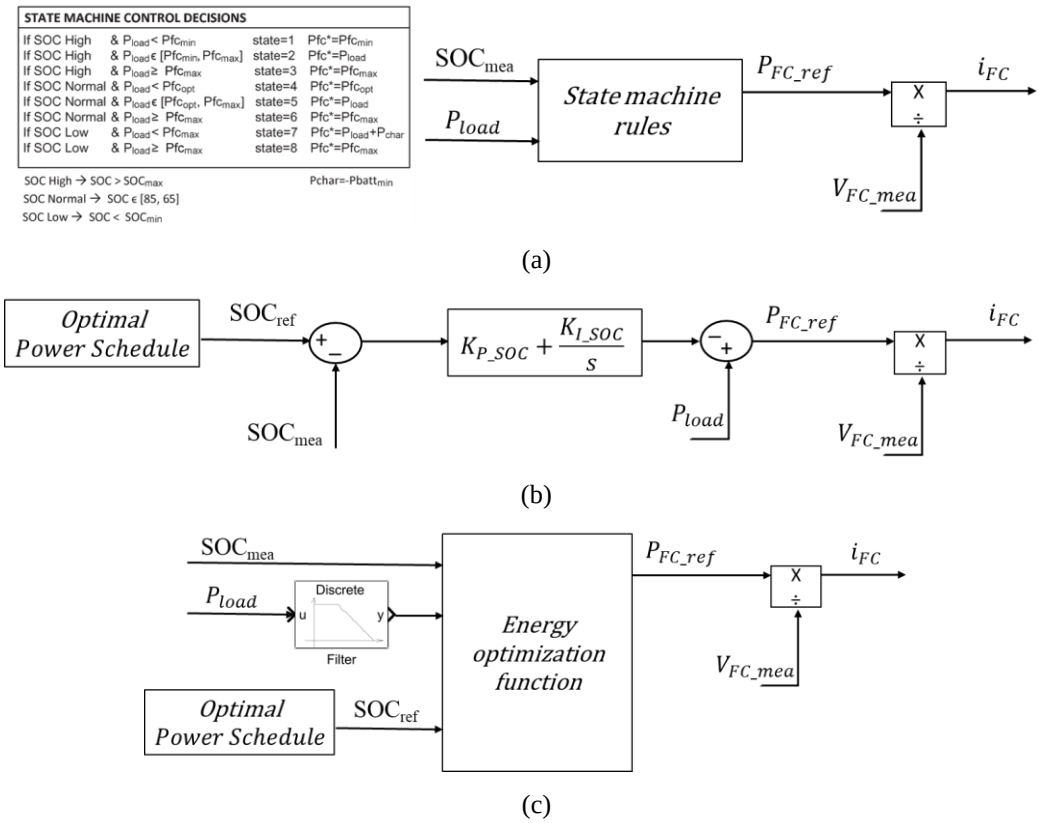

Figure II.16: HESS operation strategies: (a) State machine approach with a control decision rules [57]; (b) PI approach; (c) Proposed approach.

The state machine control method in this part is developed in [61] and presented Figure II.16 (a). With the predefined rule, the power reference of the FC system is calculated based on the measured value of BESS SOC and the load demand. With this control method, a PI controller is used to regulate the SOC of the BESS. Figure II.16 (b) presents a classical PI control method for the HESS [62]. With this approach, BESS power reference is calculated

by the PI controller. Next, the output power of the FC system is obtained by removed the BESS power from the power demand.

Figure II.16 (c) introduces the developed method for the HESS system. The objectives of the proposed method:

- Improve the life expectancy of the fuel-cell.
- Controlling the SOC of BESS in the pre-defined range
- Minimize the fuel consumption of the fuel-cell system and the equivalent fuel consumption of the other energy sources.

Hence, first of all, a filter is utilized to allow the FC system provide energy with a low frequency of load demand. This frequency decoupling approach has been proposed in [63]–[65]. The cut-off frequency of this filter is choose to 8 [mHz], which enables the FC system to provide a nearly constant power as in [57]. After that, an energy management function is applied to minimize the BESS SOC variation and H_2 consumption of the FC system. This function can be described as [66]:

$$\text{Minimize } F = (P_{FC} + \alpha P_{BESS})\Delta T \tag{II.64}$$

where ΔT [s] is the simulation time step, α is a "cost" factor for violation the SOC_{ref} and can be estimated as:

$$\alpha = 1 - 2\mu \frac{(SOC_{mea} - 0.5(SOC_{max} + SOC_{min}))}{SOC_{max} + SOC_{min}} \tag{II.65}$$

where μ is a constant and can be chosen based on the desired of following the SOC, in this part, it is chosen as 0.6, SOC_{max} [%] and SOC_{min} [%] are the maximum and minimum values of the BESS SOC in the simulation period and can be chosen by:

$$[SOC_{max}\ SOC_{min}] = [(SOC_{ref} + 0.5)\ (SOC_{ref} - 0.5)] \tag{II.66}$$

II.3.4. Stress analysis methodology

The stress on the HESS components can be analyzed with the wavelet-transform as in [57] and [67]. The output power profiles of the HESS are decomposed in low and high-frequency components using the three-level Haar wavelet decomposition, which is available in the MATLAB wavelet toolbox. The histogram or standard deviation of the high-frequency component in the output power profiles can provide a good indication of how often each energy source is solicited. An example of the Haar wavelet-transform is presented in Figure

II.17, with *x(n)* is the input signal, $H_i(z)$ with i = 1, 2, … N – 1 and $H_0(z)$ are high-pass filter and low-pass filter respectively. $G_i(z)$ is the reconstruction filters.

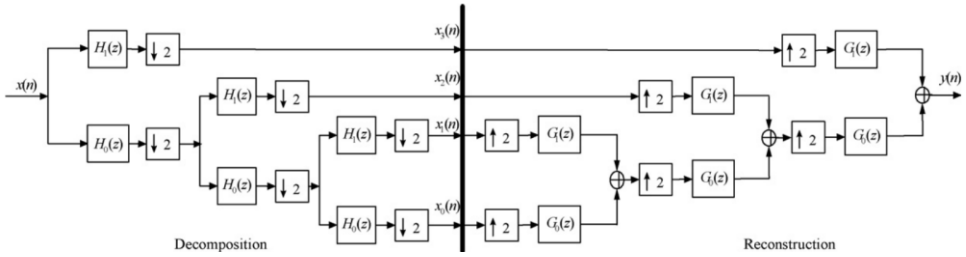

Figure II.17: Three-level Haar decomposition and reconstruction diagram [65].

II.3.5. Simulation and discussion

In this section, the performances of the developed operation strategy are compared with simulations results. An islanded system with HESS shown in Figure II.14 is studied. The simulation parameters are taken as in [57] and presented in Table II-5.

Table II-5: The simulation parameters of the remoted system

PEM Fuel Cell system

Name	Value	Unit
Number of cells	65	cell
Operating temperature	45	Celsius
Nominal air flow rate	732	liter/minute
Nominal supply pressure [Fuel Air]	[1.16 1]	[bar bar]
Nominal operating point [Inom Vnom]	[250 41.15]	[A V]
Maximum operating point [Iend, Vend]	[320 39.2]	[A V]
Nominal composition [H_2 O_2 H_2O]	[99.95 21 1]	[% % %]
PEM Fuel Cell response time	1	s
Fuel Cell current maximum slope	40	A/s

Supercapacitor system

Name	Value	Unit
Rated capacitance	15.6	F
Equivalent DC series resistance	150e-3	ohm
Rated voltage	291.6	V
Number of series capacitors	108	unit
Number of parallel capacitors	1	unit
Initial voltage	270	V
Operating temperature	25	Celsius

Li-ion battery system		
Name	**Value**	**Unit**
Nominal voltage	48	V
Battery response time	20	s
Initial SOC	65	%
Rated capacity	$E_{optimal}$	kWh
SOC_{min}	20	%
SOC_{max}	80	%
SOC_initial	65	%
AC grid system		
Nominal phase-to-phase voltage (Vrms)	0.4	kV
Nominal frequency (fn)	50	Hz

The simulation results of the MG's power profiles and HESS's features with 3 different operation strategies are shown in Figure II.18 and Figure II.19. With the state machine approach, as can be seen in Figure II.18 (a), the FC system is able to follow the load demand and its output power is quite smooth. For the main working operation period, the fluctuation of the load demand is absorbed by the SC and the BESS system. From t = 460 s, when the SOC of the BESS reaches its low level as in Figure II.19 (a), the FC system has to recharge the BESS, which increases the fluctuation in the output power profile of FC system. The performance of this method is mainly depended on the operator's experience hence there is a need for modification in the state machine control decisions when applying for different networks and control's objectives.

With the PI control approach (Figure II.18 (b) and Figure II.19 (b)), during the first 260 s of operation, the BESS tries to get to the SOC_{ref} in the PI controller. Thus, the BESS discharges until the SOC reaches the SOC_{ref} and the output power of the FC system is highly fluctuating because of load demand in this period. After reaching the desired SOC value, the BESS follows the load demand better and the FC system can work with a smoother power profile. However, at the end of the simulation period (t = 450 s), the BESS tries to come back the SOC_{ref} again so it only charges in this period, which is similar case to the first operation period.

The simulation results for the proposed strategy are presented in Figure II.18 (c) and Figure II.19 (c). One of the main objectives of this approach is avoid the high frequency of load demand to the FC system. Therefore, the output power of the FC system is nearly

constant during the operation. However, another important goal of this method is to follow the optimal SOC. From t = 460 s, when the “cost” of the SOC is higher than the cost of FC consumption, the BESS only work in charge mode with the energy from the FC system. The FC and the SC system are responsible for the load demand in this period.

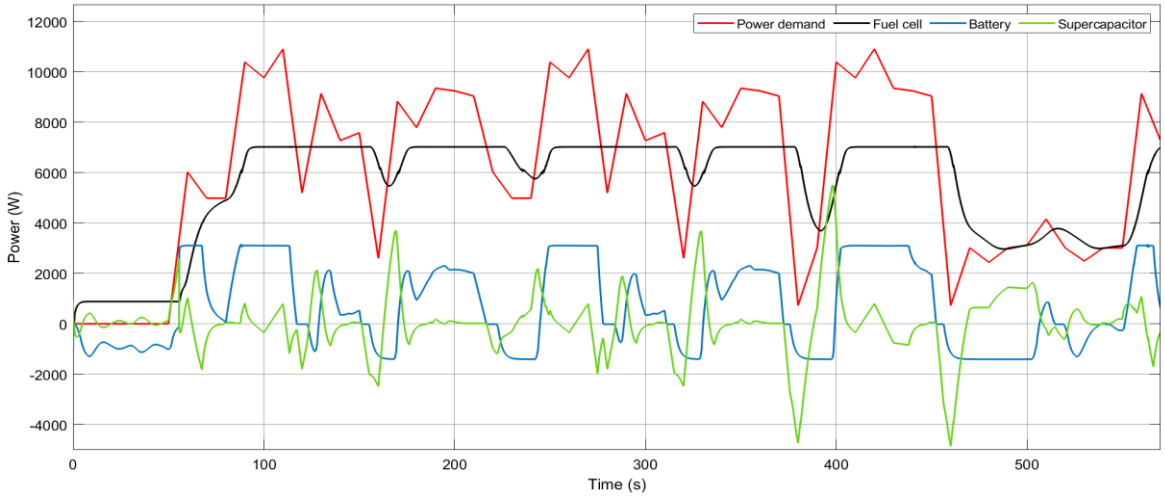

(a)

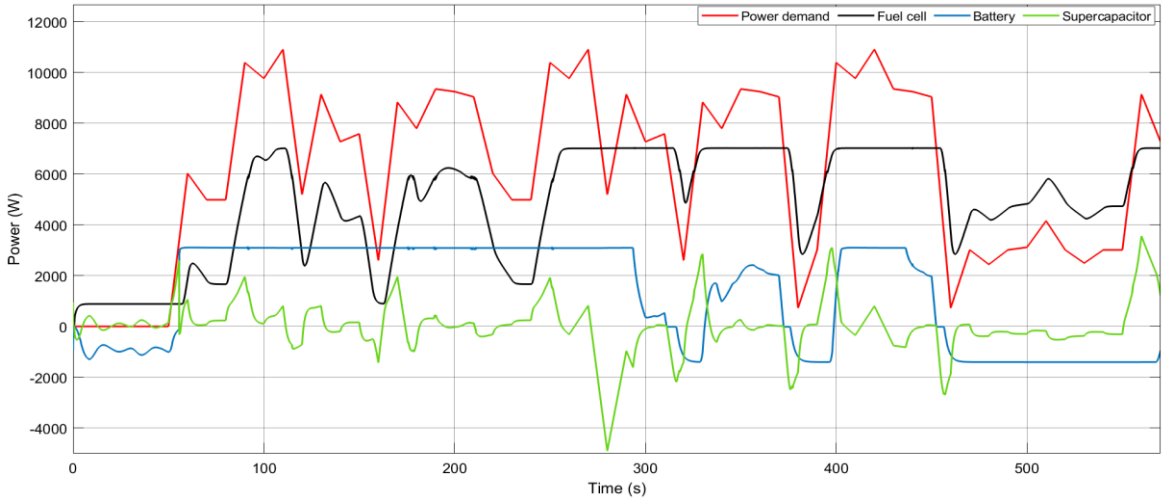

(b)

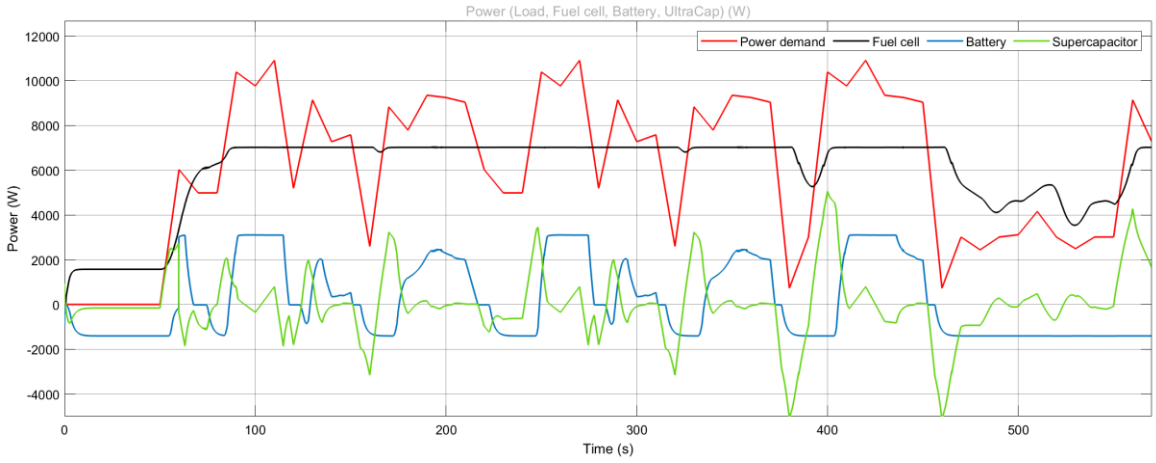

(c)

Figure II.18: MG's power profiles of all the operation strategies:
(a) State machine approach; (b) PI approach; (c) Proposed approach.

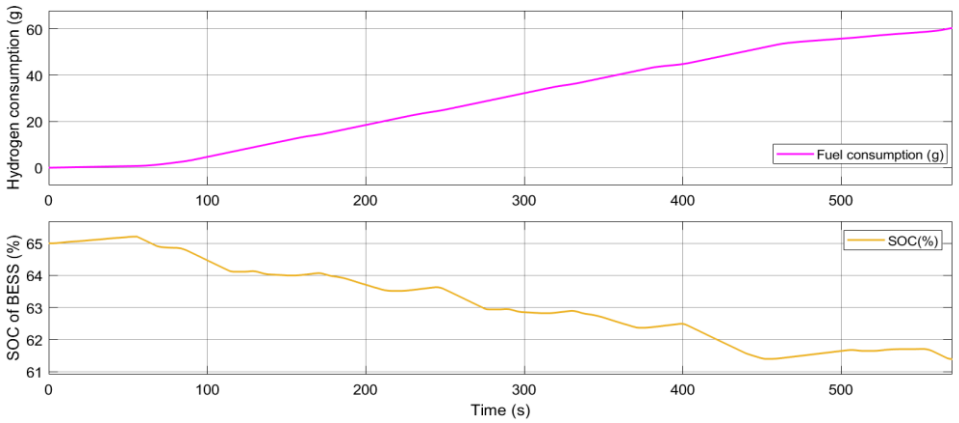

(a)

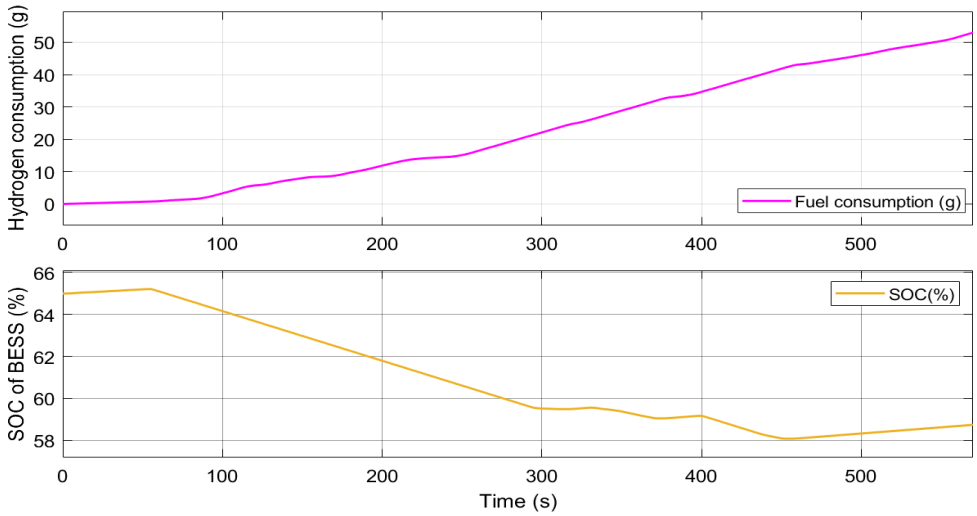

(b)

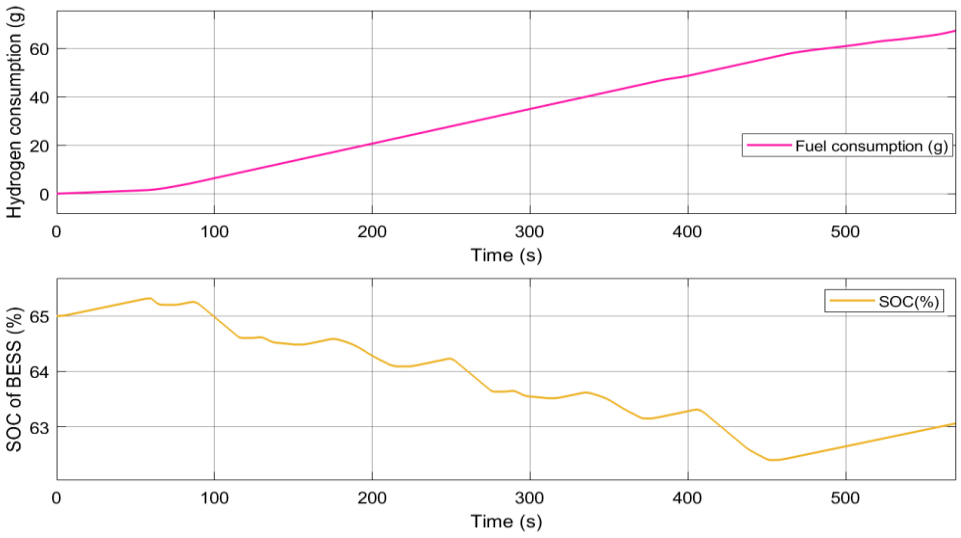

(c)

Figure II.19: SOC of BESS and Hydrogen consumption of FC:
(a) State machine approach; (b) PI approach; (c) Proposed approach.

Another crucial factor considered in these simulations is the stress on the HESS components. As can be seen in Figure II.20, the proposed method presents the smoothest output power profile, which enhance the life cycle of the FC system. With that, the goal of the method is achieved. The Table II-6 summarizes overall performance of the HESS system with different approaches. Due to the direct connection with the DC bus in the investigated HESS topology, the SC system has recorded the highest value of stress in all case study.

As expected, the proposed method records the lowest stress on the FC system and the highest final value of SOC in the BESS system thanks to the frequency filter and the optimization function, which confirms the performance of the method. However, there is a trade off with the proposed method. In order to reduce the fluctuation in the FC's power profile, the stress in the BESS and SC system is increased. The hydrogen consumption if the proposed method also records the highest value because of this reason. The PI strategy introduce the lowest value of hydrogen consumption because of the discharge process of the BESS system.

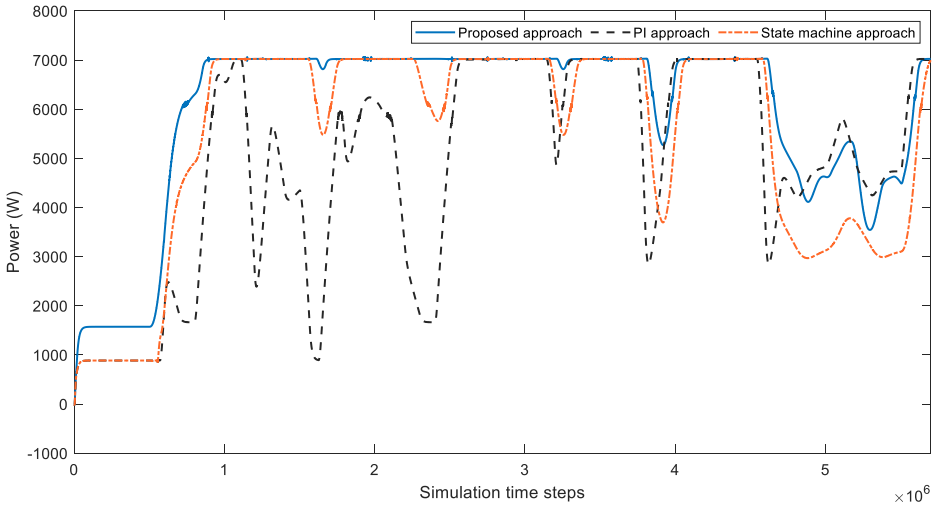

Figure II.20: Fuel cell's power profiles comparison.

Table II-6: The comparison of the HESS's performance

	State machine approach	PI approach	Proposed approach
SOC of BESS range (%)	65-61.4	65-58.7	65-63.6
FC hydrogen consumption (g)	60.4	52.9	67.2
Stress on FC system	4.764	5.372	4.016
Stress on BESS	4.1	4.705	3.879
Stress on SC system	6.905	6.619	7.212

II.4. Conclusion

First of all, this chapter presents the method for battery sizing in an islanded microgrid system. The sizing method is a MATLAB-based program with two parts. In the first part, based on the economic and technical inputs of the system, the optimal size of the solar PV system is defined. The first sizing module includes two loops. The inner loop is a rule-based method with the objective of minimizing the annual cost of the MG system. The outer loop is an iterative loop to vary the number of the PV panel. In addition, the second part of the introduced program is BESS sizing. The inputs for the second part are the economic,

technical parameters and optimal PV size from the first part. The second module of the sizing program also includes two loops. The inner loop is an energy management system with a dynamic programming approach. The objective of the EMS is to minimize the operation cost of the MG system. The SOC of the BESS works as a “node” in the dynamic programming strategy. the Bellman algorithm is utilized for searching optimal SOC flow in this problem. By minimization of the operation cost values from the beginning node to the final node, the optimal SOC strategy with the corresponding power schedule are defined. The outer loop of this module varies the BESS capacity with an iterative method. Following the simulation results, the developed sizing program is able to define the optimal sizes of PV and BESS in the remoted network, which are compared with the optimal results in the literature. It is noteworthy that with the application dynamic programming for the SOC, BESS is allowed to choose the SOC state at the beginning and at the end of the optimal operation day.

The operation of the BESS system with other storage technologies is also investigated in this chapter. A hybrid energy storage system (HESS), which is a combination of two or more energy storage with proper technologies and characteristics, is proposed as an emerged solution for the islanded MG application. This chapter presents an operation strategy with two main objectives: reducing the load fluctuation in FC power profile and following the SOC signal of BESS from the optimal power schedule. Hence, firstly, a low-pass filter is utilized for FC system to remove the high frequency component in the load demand. After that, an energy management system with an optimization function is used to follow the SOC reference. In this function, the cost of hydrogen consumption and the SOC variation are taken into account. The wavelet toolbox in MATLAB is utilized to estimate the stress factor in the HESS. The proposed operation method can reduce the stress on the FC better and has a lower SOC variation compared to other classical methods in the literatures.

CHAPTER III : Energy Routers: an interface among microgrids

Contents

III.1. Introduction

The content of this chapter contributes to work package 4, task 4.2: Interaction between physical micro-grid. A more detail about this contribution can be found in: https://m2m-grid.eu/wp-content/uploads/2020/03/Deliverable-4.2-Interaction-between-physical-micro-grids.pdf

III.1.1. Management approaches in multi-microgrid system

There are several approaches for controlling in MMG system, from fully centralized to fully decentralized strategies. This section introduces these approaches with their advantages and disadvantages.

III.1.1.a. Centralized

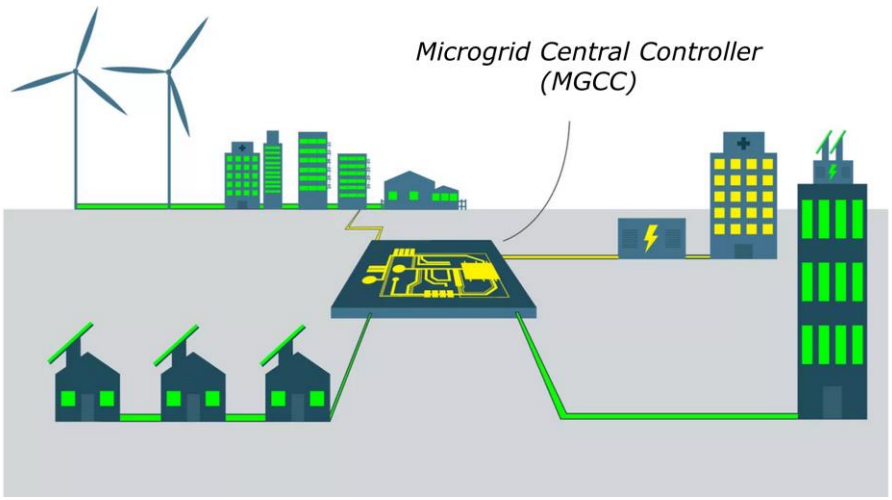

Figure III.1 – Centralized control architecture [68].

In fully centralized control scheme as shown in Figure III.1 , all available measurements and information of the integrated MGs are gathered in a microgrid central controller (MGCC) that imposes the control set points for all units. In [69], the authors introduce an implementation of a centralized controller based on wide area monitoring and control system (WAMC), which can be used to carry out a centralized secondary and tertiary control. In [70], by using WAMC, a centralized secondary voltage controller has been proposed. There are several advantages and disadvantages of this approach.

One of the advantages of centralized control system is that the central controller receives all necessary data from the MGs, which allows the multi-objective controller to

achieve globally optimum performance. Furthermore, because there is only one controller here, the system has a high controllability.

On the other hand, the computational burden in a single controller can be particularly heavy. This approach requires very high quality of communication from all DERs to the central point of control. Moreover, a centralized controller creates a single point of failure and redundancy of the central controller is costly. Thus, a collapse of the overall system can happen if there is a loss of connection with the central controller. Another drawback of the centralized approach is the privacy as this strategy requires all the information from DERs owners, which must also agree to hand over control of their resources to a third party. MGs might be operated by different utilities and the information on production costs cannot be disclosed. Subsequently, central systems are usually considered less scalable and system maintenance demands complete shutdown.

To tackle the above issues, distributed control architectures are developed, as described in the next sections.

III.1.1.b. Hierarchical

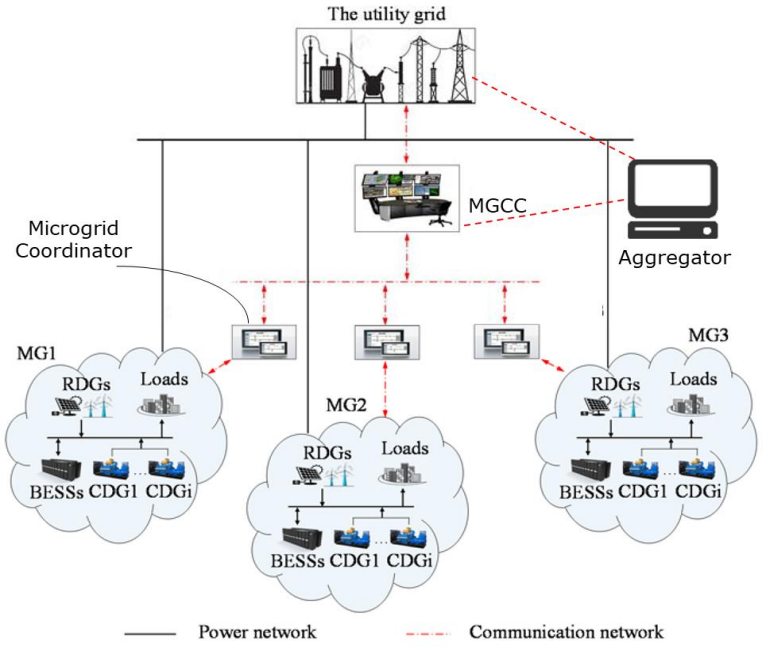

Figure III.2 – Hierarchical control architecture [71].

To overcome the problems of the centralized controller, the hierarchical control strategy is introduced in Figure III.2. In this strategy, there exists some form of aggregation of the central controller then is allowed to transmit the needed source, through a hierarchical

system of aggregators, that determines which DERs should be used at which moment. Thus, this strategy is also mentioned as the *"Aggregate and Dispatch"* solution. Since the sources are represented to the central optimizer in an aggregated way, there is significantly less information required at the central controller and the system is more scalable. This approach is suitable for utilizing demand response resources. For instance, in [72], the demand response reserves are offered by aggregators to a transmission system operator (TSO) e.g., for automatic or manual frequency restoration reserves.

The coordination of multiple, centrally controlled MGs can also be established in a hierarchical way. In that case, a MG central coordinator (MGCC) organize multiple MGs, each controlled by a local MGCC. The MGCC of a single microgrid attempts to obtain an optimal operation point using only its local resources. If the internal resources are not satisfactory, the MGCC shall request the MG central coordinator for external resources from other microgrids [73]. Nevertheless, the single point of failure still exists, and the points of aggregation may even turn into new points of failure.

III.1.1.c. Distributed

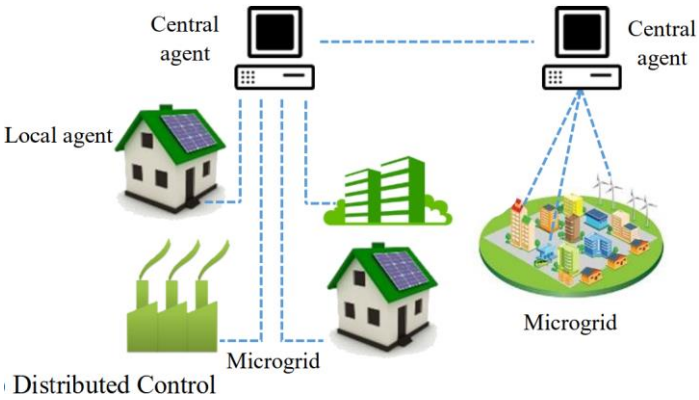

Figure III.3 – Distributed control architecture [74].

The distributed control method for MMG (shown in the Figure III.3) consists of local DERs and central agents that control the global constraints. In both architectures described before, the DERs are regulated by a third party. Nonetheless, as the owners of the DERs appoint the barrier conditions, it is argued that it might be better to maintain a local control of the DER. In addition, not all DERs owners want to exchange all their data with a third party for privacy reasons. However, to achieve a (near) optimal operation of the system, these DERs should still be coordinated. This is the reason why the concept of distributed control is necessary.

The purpose of distributed control is to break down the centralized problem into a definite number of local controllers or agents. Thus, each agent does not have a global perspective of the problem [75], but they can still work at a globally (near) optimal state with the help of coordination. Coordination is arranged by a central agent which is capable of communicating global constraints, such as the maximum power of a transformer, maximum voltage, and frequency limitations. This task can be achieved by the communication of Lagrange multipliers.

In [76], dual decomposition method or alternating direction method of multipliers (ADMM) are applied successfully for distributed approach. Both of them are based on the dual ascent method, where price vectors are transmitted iteratively from the central controller to the DERs. The DERs optimize their consumption in proportion to these vectors and send back demand vectors to the central agents. Then, the central agents analyze the demand vectors and renew the prices, when operational grid constraints are being violated. This process continues until a steady state solution is achieved.

Distributed approaches have several important advantages. First, the computational requirements are reduced due to the change of global optimization problem into several sub-problems. Secondly, the data exchanged between local and central agents is limited, which reduces the requirements of a complex communication system. Finally, the local DERs optimize individually and do not need to send private data to a third party. However, there are still central agents, which potentially form single points of failure.

III.1.1.d. Fully decentralized

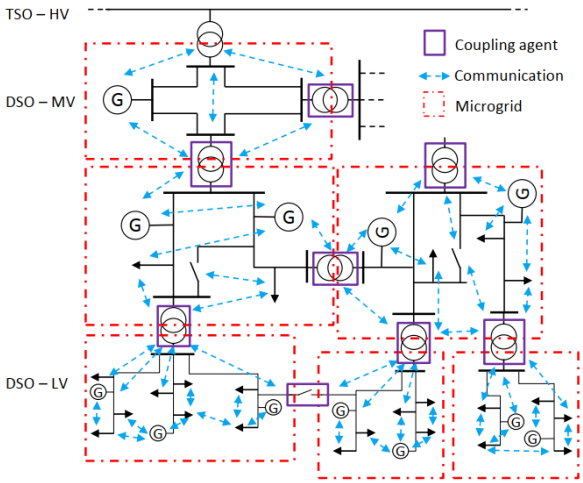

Figure III.4 – Peer-to-peer control architecture [74].

This methodology is characterized by the complete absence of a central controller, which is inspired by P2P computer networking [77]. In this architecture, a single point of failure is completely eliminated and the importance of all agents is equal. Each agent is able to exchange data directly with other agents without the need for a central device [78].

Nowadays, it is preferable to use the control system of a MMG system in a highly decentralized way, because the new DERs are typically distributed in the distribution system, operated by different owners and managed with different goals. Moreover, plug and play property of new resources is crucial to allow for seamless integration over time. In this perspective, P2P control architecture seems to be a good candidate for control of the distribution network.

Still, this architecture may not be applicable to the whole distribution grid, which contains thousands of DERs that are geographically dispersed. To tackle this issue, the grid is usually divided into smaller MGs, containing only a limited amount of DERs. These MGs operate according to the presented P2P control architecture. Points of common coupling are used to connect the different MGs as shown in Figure III.4.

The elimination of central controller leads to the concept of autonomous MGs. The P2P communication is utilized to send the required information in the MGs. The grid–supporting agents are able to determine the set-points with the help of received data from neighbor agents. In this communication scheme, the agents should be able to reach a (near) optimal operation of the considered MGs. When a single agent fails, the other agents can still manage the system. When a single communication channel fails, the required information can still be transmitted to all necessary participants via other agents. In addition, all data is protected, which eliminates any privacy-related concerns. However, in this control architecture, all agents require significant amount of local intelligence to accomplish the fundamental optimizations. There are two popular algorithms for P2P method in the literature: gossiping algorithm [79] and consensus algorithm [80].

An example of the P2P approach in multi-microgrid system application is illustrated in [81]. The authors present a multi-layer and multi-agent architecture to achieve P2P control in an AC islanded MMG system. The control framework is fully distributed with three control layers operated in the agent of each MG. A droop control is adopted for primary control by each MG-agent for localized power sharing. In the secondary control level, a distributed consensus algorithm is utilized for frequency/voltage restoration and arbitrary

power sharing among MGs and with the tertiary level, the power loss in the MMG system is minimized by using alternating direction method of multipliers (ADMM).

III.1.2. Interconnection among microgrids

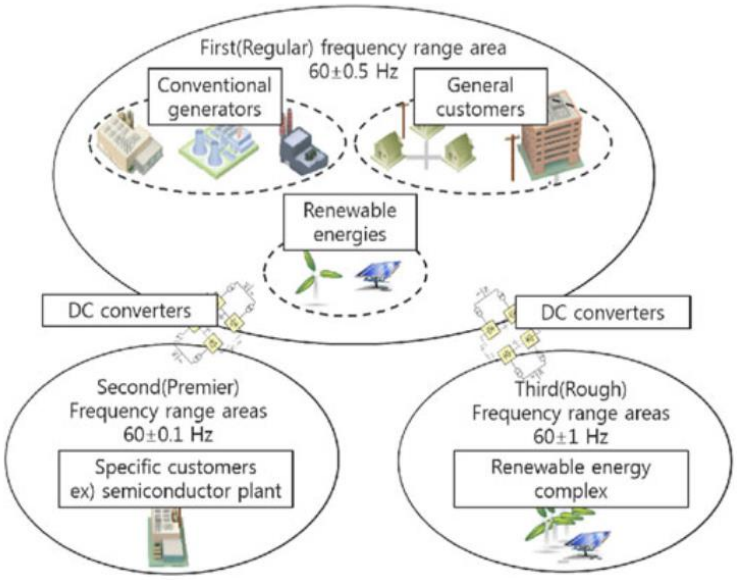

Figure III.5 – MMG system with the use of BTB converters [82].

In most cases, there are two types of interconnection among physical microgrids. In the first type, the MGs can be connected via the AC line with the use of a breaker [83], [84]. With an appropriate synchronization algorithm, this type of connection has a low investment cost. However, the main drawback of this method is the difficulty of power management between MGs. Also, this method is only suitable for the MMG system that has the same frequency and voltage values in all MGs.

In the second type, as shown in Figure III.5, DC connections with back-to-back (BTB) converters can be used as the interface between physical MGs [85]. The topology of the hybrid MG with DC connection at the BTB converter presented in [86] could bring the benefit of multiple AC and DC MGs integration at a common point. In addition, by using BTB converters, each MG can be controlled independently, which leads to flexible voltages and frequencies in MMG system.

In [82], the flexible MMG system can provide some advantages, such as:

- Reduction of the ancillary service cost.
- Improvement of operating efficiency of coal power plants.
- Reasonable pricing system for different customers' needs.

The Ross Island project in Antarctica [87] introduced a physical dual frequency interlinked system (50 Hz and 60 Hz) by using a MG control distributed system. In this chapter, an islanded MMG system with the use of BTB converters for interlinking the adjacent MGs is investigated.

III.2. Energy routers: an emerging agent in the multi-microgrid system

III.2.1. Energy internet – Towards Smart Grid 2.0

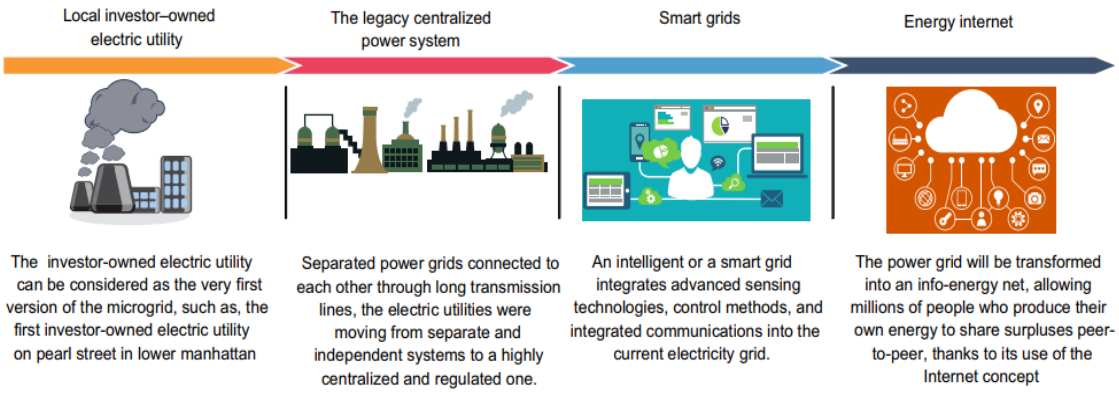

Figure III.6 – The evolution of grids [88].

Energy Internet (EI) or Internet of Energy is a concept that has been regarded as a new evolution stage of the smart grid. EI aims to increase the energy transmission efficiency and optimize the energy dispatching in time and space. In [88], the EI is defined as an Internet-type network of all the elements of a grid system, which closely cooperate with others by sharing both energy and information. Agents or components of this network comprise different prosumers and consumers that have the capability to take and execute decisions individually. MGs, DERs, smart grids, private or governmental energy networks, and any community of prosumers and consumers can be a part of this massive network as agents. The EI is also known as the second generation of the power system because it is provided with advanced sensing and measurement technology, as well as latest control and monitoring technology [89]. The EI also takes advantage of a modern communication network to achieve a higher stage of safety and reliability and enhance the economic and efficient operation of the power system. Moreover, integrating advanced communication network and

smart devices into the power system enables system operators to embed plug-and-play feature and intelligent energy management.

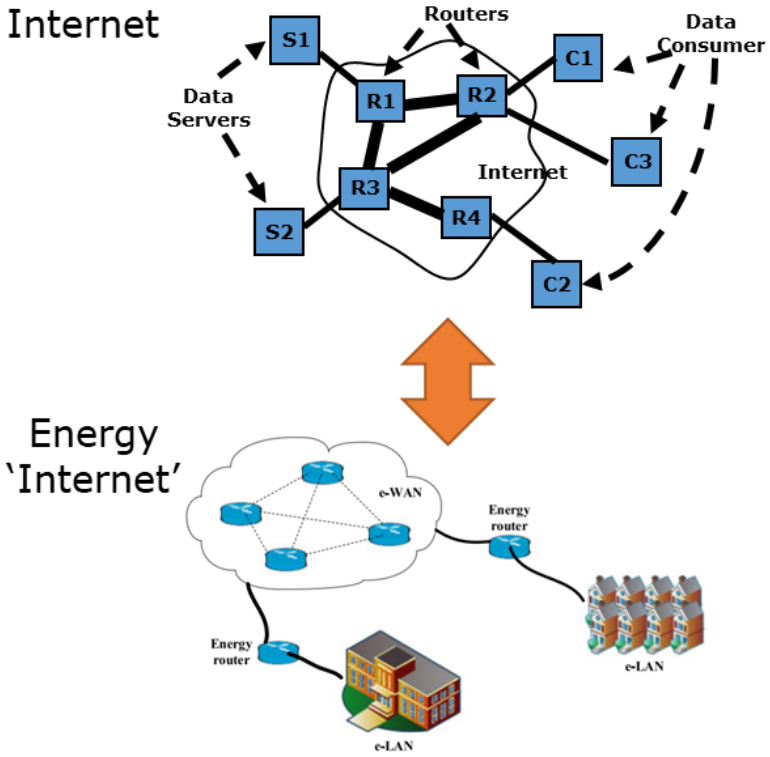

Figure III.7 – Power system in the vision of Energy Internet [90].

As demonstrated in Figure III.7, MGs as agents are main components of the EI network, where they are represented by energy local area networks (e-LANs). MGs have the potential to be the fundamental element of the EI structure, as they are a promising technology that can reinforce the reliability and profitability of energy supply to end consumers [91].

The main characteristics of EI as in [92] are smart plug-and-play characteristics, intelligent energy management, and distributed grid intelligence. On the other hand, the main advantages of MGs are the flexibility in controlling power supplies and loads, flexible operation modes and smart energy management. In addition, with the advanced communication system provided by the future EI, all the information in all MGs can be collected from smart monitor devices to optimize energy management among MGs. Therefore, the present of MGs is an essential step in developing the EI of the future system.

III.2.2. Energy routers concept

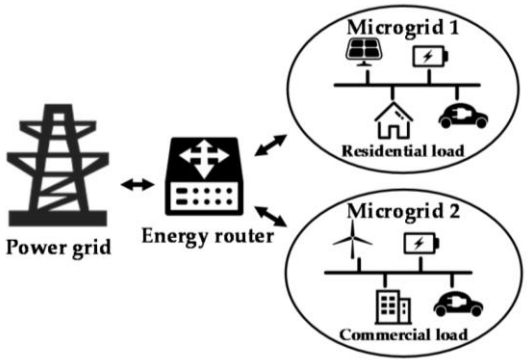

Figure III.8 – ER-based interconnecting framework [93].

In the conventional Internet system, packet routers are the most vital elements as they are responsible for transporting information in the network. Similarly, in the new smart grid – Energy Internet system, the concept of an energy router (ER) is defined for the components that are responsible for managing the transmission and distribution of electricity [94]. Just like packet routers in the Internet network, the energy routers serve as a vital component in the new EI system. An ER-based framework for MG interconnection is demonstrated in Figure III.8. In fact, as a multi-port conversion device with control and communication functions, the ERs are able to carry out power quality regulation, voltage/frequency conversion, reactive power compensation, renewable energy access and power flow control.

III.2.2.a. Benefits of energy routers

ERs are associated with the following benefits [93], [95]:

- The issue of instant energy excess or shortage can be solved with "complementary" energy trade between the adjacent MGs.
- Active control of power flow can be used to eliminate congestion problems.
- Shared DC bus and voltage source converters (VSCs) enable electrical isolation between the MGs.
- The capability of electrical isolation improves power quality and can enhance operation reliability.
- The power system architecture shifts from the conventional framework to a scheme, which is cooperative.

As ERs are used widespread in the grid, they handle a broad range of functions. Similar to the Internet routers, the ERs have different location-dependent tasks, which can be generally classified as the user-level functions and the grid-level functions [94].

1) User-level functions: There are three main categories of users: distributed renewable energy resources, distributed energy storage devices, and loads. These users form a MG, where the ER operates as its central coordinator. Each user in the same MG communicates with the ER for all the energy services. We consider below all the user-level functions required at an ER.

- User Attachment: When a user joins the smart grid via the ER, the ER is in charge of discovering new user attachments and configuring them for precise operations.
- Service Request: When there is a need for a service, the connected user sends a "service request" message to the ER. The ER then responds with a "service acceptance" message back to the user and regulates the energy service.
- Status Update: The user delivers the "status update" message to the ER when the user status changes.
- Service Termination: When the users terminate the service, they transmit the "service termination" message to the ER and then disconnect from it. The ER terminates power exchange with these users.
- User Detachment: When the user disconnects from the grid, the ER detects the disconnection and updates their user interfaces accordingly.

2) Grid-level functions: An ER is not only connected to the energy customers, but it also communicates with the other ERs in the grid system to organize smart energy management. Some typical operational scenarios are discussed below:

- When the PV system is ready, it transmits the energy generation request to the ER. The ER examines the power demand, which includes the current load demand and the energy capacity of the distributed energy storage devices, and then accepts the request of the PV system, which then initiates the solar energy conversion.
- When the PV system stops generating energy, it transmits the "service termination" message to the ER. The ER informs the distributed energy storage devices to start energy supply.
- In the case of light load, the ER begins to charge the plug-in electric vehicles and the distributed energy storage devices.
- The ERs are also able to influence the electricity usage dynamically according to the costs. For example, when the price of electricity is the highest for industrial users, their ERs may schedule the non-urgent tasks at a different time.

III.2.2.b. Design requirements of energy routers

The ER is a technological integration of power electronics, communications and automations. Therefore, its design requirements include these three aspects [94], [96], which are described in the following sections.

1) Power electronic: Power electronics are fundamental ER components because they realize automatic energy distribution and management. Therefore, all power electronics elements must be able to operate fast and stable to guarantee the correct execution of the commands issued by the intelligent management module.

2) Control algorithms: In addition to the power electronics and communications, the ERs must contain the distributed grid intelligence module to participate in decision-making associated with the energy management of the grid. This module utilizes the information collected from the communication module and determines the grid control actions, which are implemented through the ER cooperation.

3) Real–time communications and information processing: The operations of ER depend on the grid status information it collects. The communications between ERS must satisfy three requirements, which are described below:

- Transmission Latency: The communication latency determines the maximum time in which a specific message should reach its destination through a communication network. The messages communicated between ERs may have different network latency requirements relying on the type of events that trigger the messages. The most time-critical messages in the smart grid need a transfer latency as small as 3 milliseconds. Thus, the ERs must have sufficiently fast processing and communication abilities to assure low latency information exchanges.
- Communication Reliability: To enhance the reliability, the ERs need to be developed with the failure possibility minimized and the communication among them must be reliable. In addition, the ERs must have communication failure detection ability to redeliver the lost messages quickly. In case the interface equipment of an ER fails, the remaining ERs should be able to carry on communications through bypassing paths.
- Information Security: The information exchange between ERs includes among others grid operation information. Falsified or impersonated messages will threaten the grid operations. Thus, the ERs must ensure that communications are protected. Properly designed security mechanisms are needed to hinder unauthorized users from reading and altering information, which is exchanged between ERs.

4) Plug-and-play features: The plug-and-play characteristic requires that the ERs have a universal standard interface with both energy exchange and communication functions. Particularly, they are expected to quickly analyze different classes of electrical characteristics and monitor the load, energy storage and power generation equipment. Hence, the automatic access or disconnection with the energy sources corresponds with energy equipment actions correspond to the user's request should be provide by ERs.

5) Satisfaction of users' personalization: EI is designed to support users' personalized energy usage strategy. ERs must present the interactive channels between users and EI with

the consideration of the current energy prices and supply situation that can be automatically regulated to meet users' various needs.

III.2.2.c. Classification of energy routers

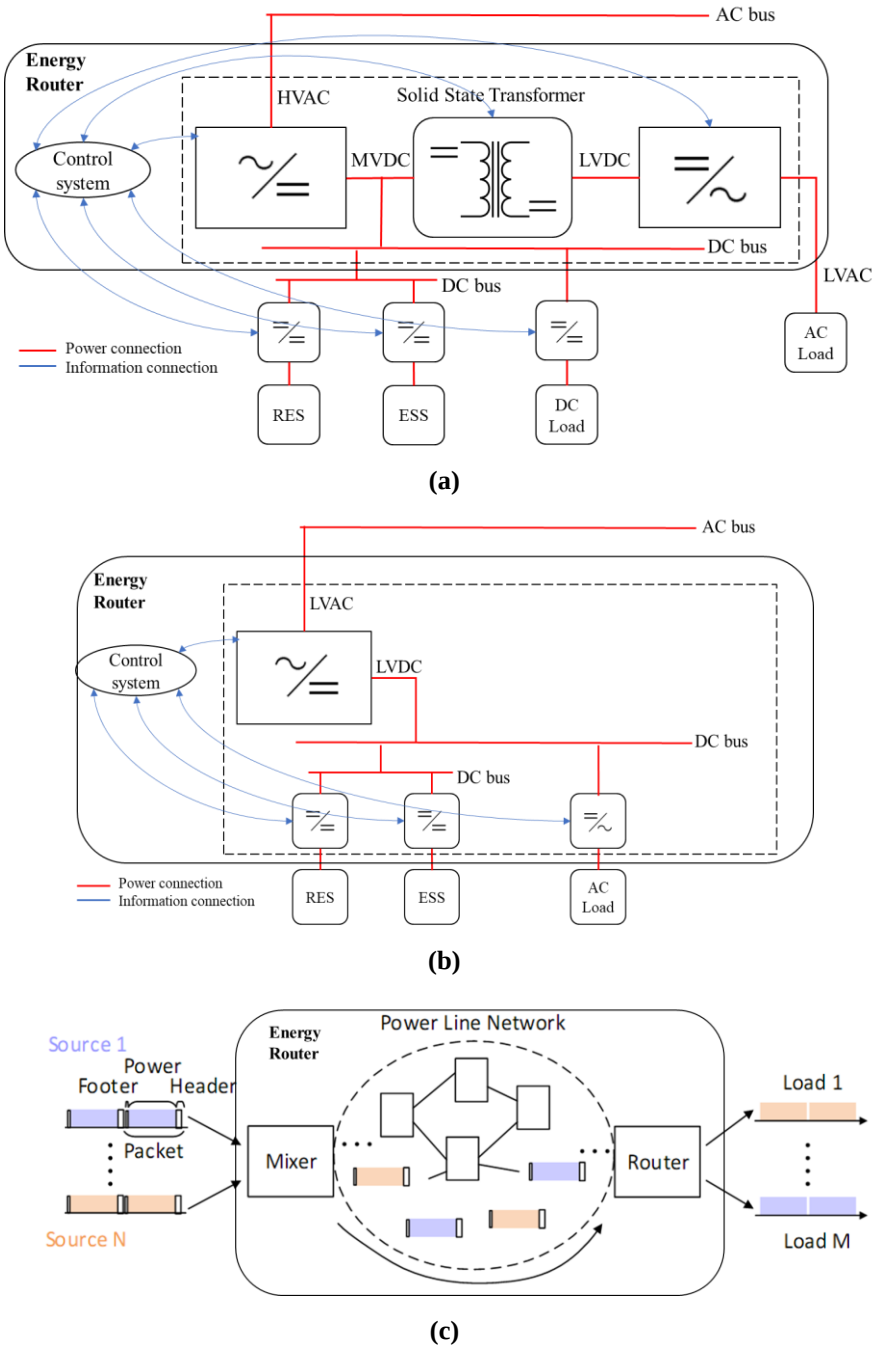

Figure III.9 – Different technologies of energy routers [97]–[100]: (a) an energy router based on Solid State Transformer; (b) an energy router based on Back-to-Back Converter/DC-link; (c) an energy router based on Power Line Communication.

Figure III.9 (a) presents an ER-based solid-state transformer (SST) with a three-stage structure, which has the features of relatively simple control, high functionality and high

reliability. Firstly, the high-voltage AC/DC stage rectifies power frequency high-voltage alternating current (HVAC) into medium-voltage direct current (MVDC), which can be used to connect DC grids. Then the middle DC/DC stage adopts dual active bridge topology to transform the MVDC to a regulated low-voltage direct current (LVDC), which is used to facilitate the DC bus or connect DERs. The employment of a high frequency transformer provides the benefit of both electrical isolation and voltage conversion. Finally, the split-phase DC/AC inverter generates an AC output voltage, which can be used to connect AC grids or loads. Thus, the ER-based SST has multiple plug-and-play interfaces for user access. Each interface may connect multiple energy networks or devices, as long as the total power does not exceed the capacity limits of the connected interface [101]. The above ER-based SST is appropriate for transmission systems with a high voltage and power level.

In contrast, the ER with Back-to-Back (BTB) converter/DC-link technology shown in Figure III.9 (b) is useful for distribution systems, which have a lower voltage and power level. In the literature, this ER technology proved to have a higher degree of reuse and integration compared to the ER-based SST [98]. Without considering the influence of power grids, the proposed BTB converter can provide energy balance among multiple RESs and loads. In case of simple structure and a small number of loads/sources, the system of energy management and control can be executed directly into the controller of BTB converter itself. Through power electronic converters and ICT, the DERs, storage devices and loads are connected to the DC common bus, which is an intermediate link of the energy forwarding. Among those, the storage device can enable the stability of DC bus by means of absorbing or compensating the imbalance power during a short period [101]. The detailed this topology of the ER which is considered in this chapter is discuss in the next section.

Finally, Figure III.9 (c) presents the ER-based power line communication (PLC) technology. The ER-based PLC is able to transmit energy flows and information flows through the same transmission line. The main advantages of this technology are the benefits of simple wiring, reducing device volume and cost. The development of PLC technologies encourages collinear coupled transmissions of energy and information. The major drawback of this architecture is that it is impossible to implement the time-division and multi-path transmission of power flows because the conventional PLC technology carries out power transmission and data communication simultaneously.

III.2.3. Topology of the energy router

As mentioned above, in order to establish a flexible multi-microgrid in the distributed system, an energy router with the DC-link is chosen. The schematic diagram of the chosen energy router is shown in Figure III.10. In this chapter, an energy router with a five-port schematic is investigated. One port of the ER is connected to the main grid and the other four are connected to four adjacent MGs. With this architecture, the ER is made up of five bidirectional voltage source converters (VSC) and a common DC-link. The VSCs can work as rectifier or inverter depending on the direction of power flows in MMG system. The MMG is able to connect or disconnect with the main power system. The ER serves as an interface among MGs in MMG system. The more detail and the mathematical model of the ER topology and controlling system are discussed in the next sections.

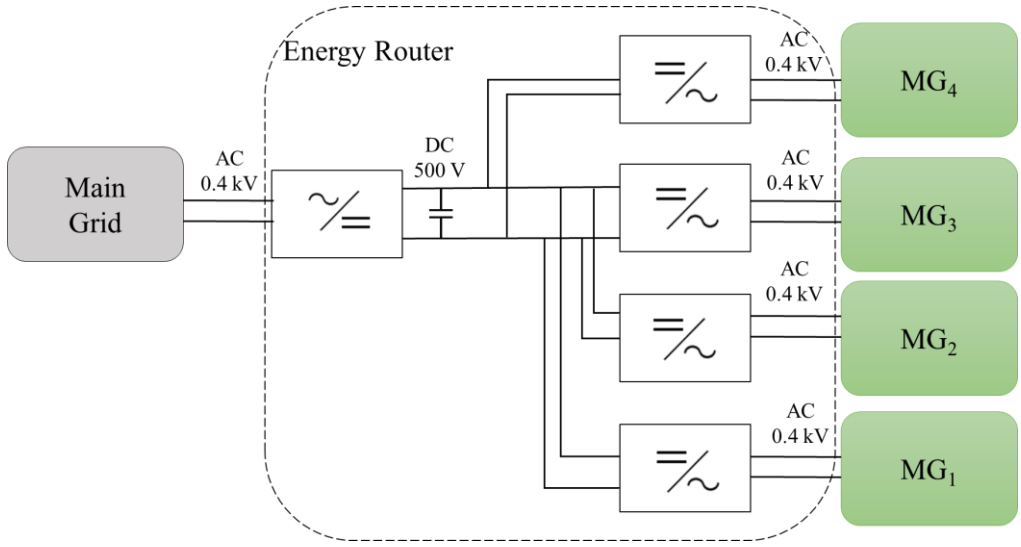

Figure III.10 – Schematic diagram of the chosen energy router topology with a multi-microgrid system.

III.2.3.a. Operation scenarios

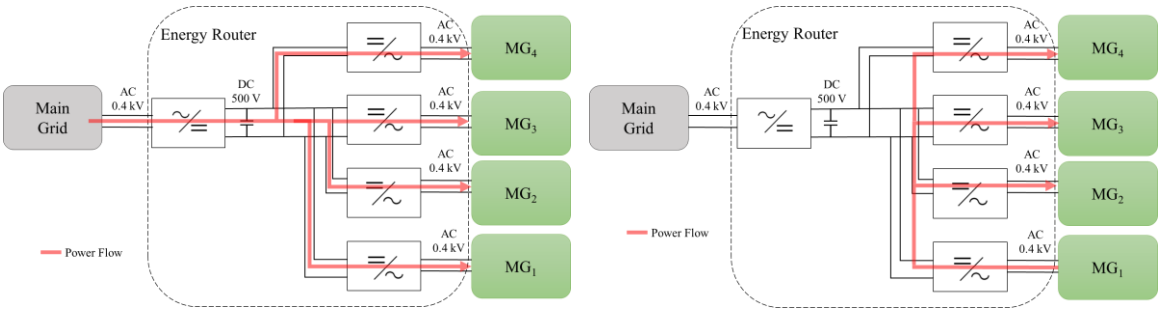

(a) **(b)**

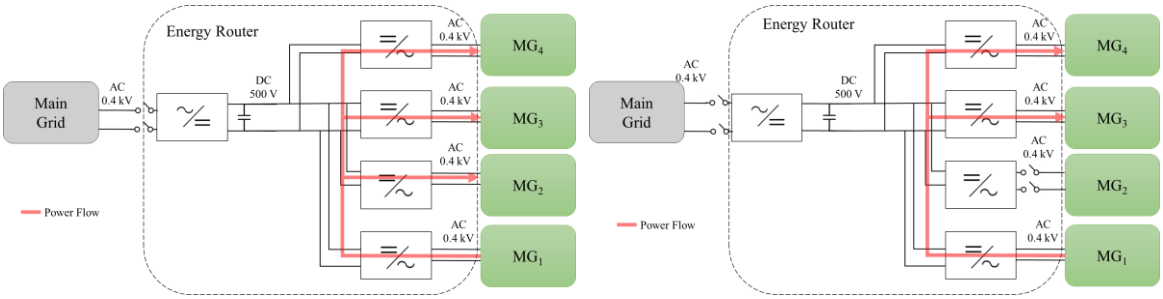

Figure III.11 – Different operation scenarios in multi-microgrid system with the energy router: (a) grid-connected MMG system; (b) grid-connected MMG with parallel MGs; (c) islanded MMG with parallel MGs; (d) islanded MMG with a parallel MG and islanded MGs.

Depending on the energy exchange situation, with the application of the energy router interface, the studied multi-microgrid system is allowed to flexibly operate in various modes which is illustrates in Figure III.11. For example, with the scenario presented in Figure III.11 (a), the MMG system is connected with the main grid and all the loads in MGs are supplied from the main system. Similarity, with the operation case in Figure III.11 (b), the MMG system is still in grid-connected mode but the MG_1 is responsible for supplying energy for the rest of the system with its surplus energy. Despite of the connection with the main system, there is no need for energy exchange with the main grid in this scenario and the voltage of the DC line is still maintained by the main grid. However, the main grid can support MG_1 in this operation scenario if the surplus energy from MG_1 is not enough for the required energy.

On the other hand, in case of power grid faults, the MMG system is also able to work in an isolated mode as shown in Figure III.11 (c) and Figure III.11 (d). With this system configuration, MMG system requires at least one “master” MG for controlling the voltage of the DC common link. With the case presented in Figure III.11 (c), MG_1 is having excess energy and providing energy for four MGs. MG_1 is not only responsible for energy supplying but also for managing the voltage of the DC line. In this situation, the MMG system is working in islanded mode and the MGs in the MMG system are working in “parallel” mode [93]. Furthermore, as in Figure III.11 (d), MGs in islanded MMG can also be disconnected from the MMG system and switch from parallel mode to islanded mode (MG_2 for example).

III.2.3.b. Power circuit structure

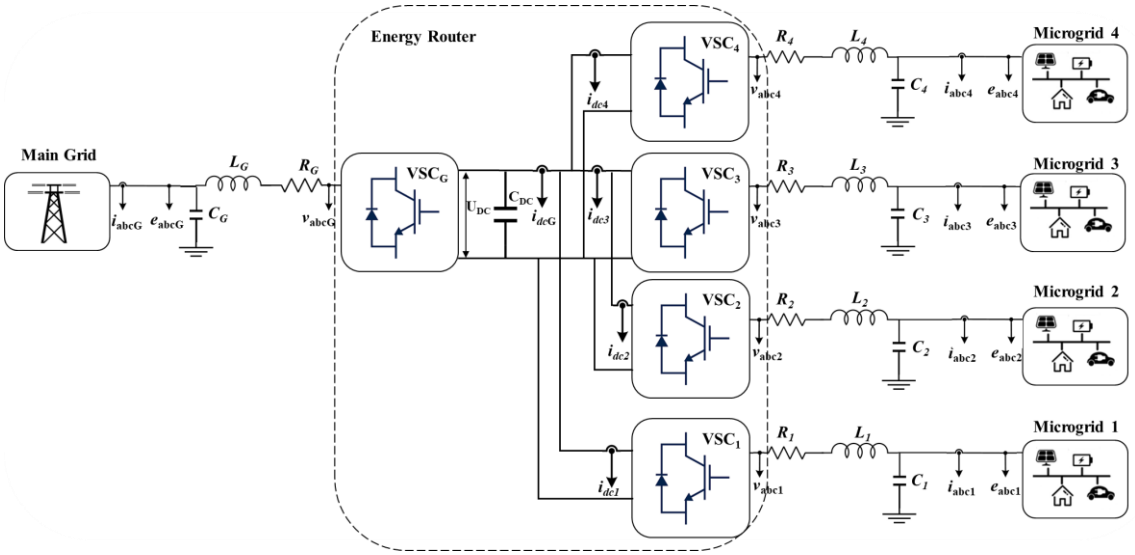

Figure III.12 – The detail topology of the Energy Router with a multi-microgrid application.

The detail topology of the energy router in this chapter is presented in Figure III.12 with a single-line diagram. The ER consists of five voltage source converters (VSC), RLC filters and a common DC – link. With VSC_G is the main grid VSC and VSC_i (i = 1, 2, 3, 4) are the VSCs on the MGs sides. In addition, R_i, L_i and C_i are the resistance, inductance and capacitance respectively of the RLC filters. Furthermore, v_{abci}, e_{abci} and i_{abci} are the AC voltages and the AC currents on the AC sides of the system.

Let i_{dci} and U_{DC} are the DC current flows and DC voltage in the DC sides respectively, and C_{DC} is the capacitance of the DC common link.

III.2.4. Mathematical model of the energy router

Following the same approach in [93], a mathematical model of the energy router presented in Figure III.12 with the selected operation scenarios in Figure III.11 are illustrated in this section.

In this part, a model for the ER with the grid connected MMG operation case shown in Figure III.11 (a) is presented. In this operation scenario, the energy demands of the four MGs are supplied by the main grid. Therefore, VSC_G works as rectifier and VSC_i (i = 1, 2, 3, 4) works as an inverter. By converting the three-phase circuit equations into the *dq* rotating coordinate system, the state-space equations of the VSC_G can be presented:

$$\begin{cases} L_G \dfrac{di_{d_G}}{dt} = -R_G.i_{d_G} + \omega_G.L_G.i_{q_G} + e_{d_G} - U_{DC}.s_{d_G} \\ L_G \dfrac{di_{q_G}}{dt} = -R_G.i_{q_G} - \omega_G.L_G.i_{d_G} + e_{q_G} - U_{DC}.s_{q_G} \end{cases} \quad \text{(III.1)}$$

where i_{d_G}, i_{q_G} and e_{d_G}, e_{q_G} are the components of i_{abc_G} and e_{abc_G} in the *dq* rotating system respectively, ω_G is the angular frequency of the AC main grid system. In addition, s_{d_G} and s_{q_G} are the uni-polar logic switching function in the *dq* rotating system. Similarity, the mathematical models for the rest of the VSCs in MMG system in this operation scenario can also be derived:

$$\begin{cases} L_1 \dfrac{di_{d_1}}{dt} = -R_1.i_{d_1} + \omega_1.L_1.i_{q_1} - e_{d_1} + U_{DC}.s_{d_1} \\ L_1 \dfrac{di_{q_1}}{dt} = -R_1.i_{q_1} - \omega_1.L_1.i_{d_1} - e_{q_1} + U_{DC}.s_{q_1} \end{cases} \quad \text{(III.2)}$$

$$\begin{cases} L_2 \dfrac{di_{d_2}}{dt} = -R_2.i_{d_2} + \omega_2.L_2.i_{q_2} - e_{d_2} + U_{DC}.s_{d_2} \\ L_2 \dfrac{di_{q_2}}{dt} = -R_2.i_{q_2} - \omega_2.L_2.i_{d_2} - e_{q_2} + U_{DC}.s_{q_2} \end{cases} \quad \text{(III.3)}$$

$$\begin{cases} L_3 \dfrac{di_{d_3}}{dt} = -R_3.i_{d_3} + \omega_3.L_3.i_{q_3} - e_{d_3} + U_{DC}.s_{d_3} \\ L_3 \dfrac{di_{q_3}}{dt} = -R_3.i_{q_3} - \omega_3.L_3.i_{d_3} - e_{q_3} + U_{DC}.s_{q_3} \end{cases} \quad \text{(III.4)}$$

$$\begin{cases} L_4 \dfrac{di_{d_4}}{dt} = -R_4.i_{d_4} + \omega_4.L_4.i_{q_4} - e_{d_4} + U_{DC}.s_{d_4} \\ L_4 \dfrac{di_{q_4}}{dt} = -R_4.i_{q_4} - \omega_4.L_4.i_{d_4} - e_{q_4} + U_{DC}.s_{q_4} \end{cases} \quad \text{(III.5)}$$

In addition, the energy storage in the DC – link (W_c) can be defined as:

$$W_c = \frac{1}{2} C_{DC}.{U_{DC}}^2 \quad \text{(III.6)}$$

Thus, by differentiation of equation (III.6), the power stored (P_{DC}) and the current of the DC – link (i_{DC}) can be calculated as:

$$\begin{cases} P_{DC} = \dfrac{1}{2} C_{DC}.\dfrac{d{U_{DC}}^2}{dt} \\ i_{DC} = C_{DC}\dfrac{dU_{DC}}{dt} \end{cases} \quad \text{(III.7)}$$

Furthermore, the power balanced equation of the MMG operation case shown in Figure III.11 (a) in the ER is calculated as:

$$P_{dc_G} - P_{DC} = P_{dc_1} + P_{dc_2} + P_{dc_3} + P_{dc_4} \quad \text{(III.8)}$$

From (III.7) and by differentiation of equation (III.8), the current balance equation of the DC – link in this operation scenario is calculated by:

$$i_{dc_G} - C_{DC}\frac{dU_{DC}}{dt} = i_{dc_1} + i_{dc_2} + i_{dc_3} + i_{dc_4} \quad \text{(III.9)}$$

On the other hand, the current flows through VSCs can be derived:

$$\begin{cases} i_{dc_G} = \frac{3}{2}\left(i_{d_G}.s_{d_G} + i_{q_G}.s_{q_G}\right) \\ i_{dc_1} = \frac{3}{2}\left(i_{d_1}.s_{d_1} + i_{q_1}.s_{q_1}\right) \\ i_{dc_2} = \frac{3}{2}\left(i_{d_2}.s_{d_2} + i_{q_2}.s_{q_2}\right) \\ i_{dc_3} = \frac{3}{2}\left(i_{d_3}.s_{d_3} + i_{q_3}.s_{q_3}\right) \\ i_{dc_4} = \frac{3}{2}\left(i_{d_4}.s_{d_4} + i_{q_4}.s_{q_4}\right) \end{cases} \quad \text{(III.10)}$$

Finally, from equation (III.9) and equation (III.10), the current balance equation can be transformed into:

$$\frac{3}{2}\left(i_{d_G}.s_{d_G} + i_{q_G}.s_{q_G}\right) - C_{DC}\frac{dU_{DC}}{dt} = \frac{3}{2}\sum_{i=1}^{4}\left(i_{d_i}.s_{d_i} + i_{q_i}.s_{q_i}\right) \quad \text{(III.11)}$$

The mathematical model of the energy router in MMG system with the specific operation scenario in Figure III.11 (a) is formulated through equations (III.1) - (III.5) and (III.11). The mathematical models of the energy router for the other MMG system operation scenarios in Figure III.11 can also be presented with the same approach.

III.2.5. Control system structure of the energy router

III.2.5.a. Control functions of voltage source converters

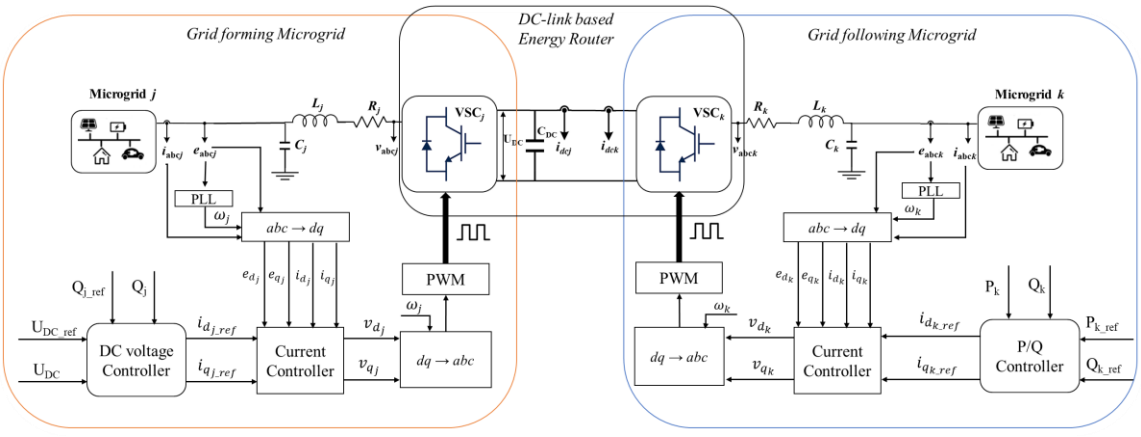

Figure III.13 – The control system of the DC-link based energy router with a grid forming and a grid following units.

For the sake of simplicity, only two typical MG in the studied MMG system are taken into account in this section, which is shown in Figure III.13 (inspired from [93]). With the chosen ER topology, there are two type of MGs: grid forming MGs and grid following MGs. In order to maintain the appropriate operation of the ER, the MMG system requires at least one grid forming MG. The MG with the highest controllable energy in the MMG system is chosen to work as grid forming unit. In this part, it is assumed that MG_j with the corresponding VSC_j works as a grid forming unit and MG_k with the corresponding VSC_k works as a grid following unit. The control functions of the related VSCs in the ER can be described as:

- VSC's function for grid forming MGs: the VSC of the microgrid working in this mode has the responsibility for supplying energy to the other MGs and maintaining the DC voltage in the DC common link in the ER.
- VSC's function for grid following MGs: the VSC of the microgrid working in this mode has the responsibility for following the control signals of the P/Q references from the control system.

III.2.5.b. Control system structure

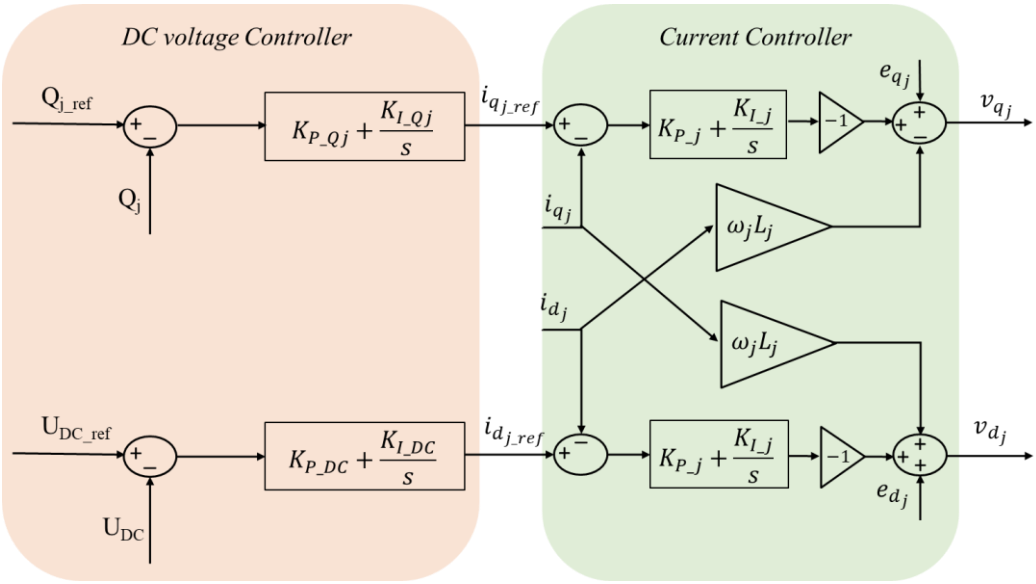

(a) Grid forming unit.

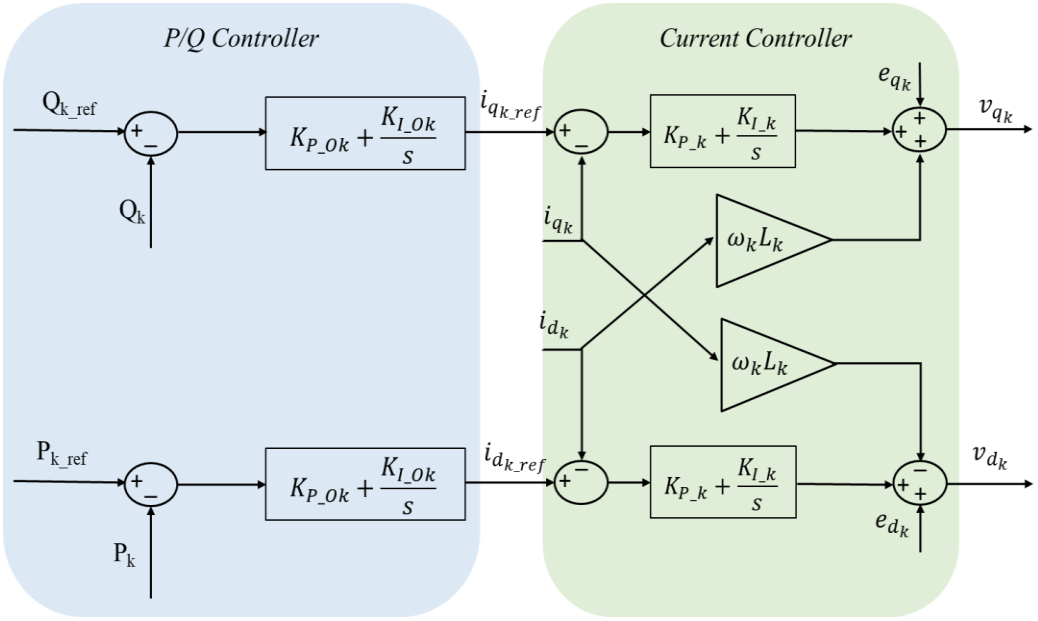

(b) Grid following unit.

Figure III.14 – The diagrams of the VSC control systems.

1) Grid forming microgrid

The microgrid working in this mode has the responsibility for supplying energy to the other MGs and maintaining the DC voltage in the DC common link in the ER. Therefore, as can be seen in Figure III.14 (a) (inspired from [102]), the cascaded control system of the VSC_j consists of an outer-loop with the DC voltage controller for the voltage control loop and a current control loop as an inner loop. The input for the DC voltage block is the reference of the DC voltage for the DC – link (U_{DC_ref}) and the measurement DC voltage of the DC – link (U_{DC}). Through the DC voltage controller, the output current in the *d-axis* of the rotating system can be calculated as:

$$i_{d_{j\_ref}} = K_{P\_DC}\left(U_{DC\_ref} - U_{DC}\right) + K_{I\_DC}\int\left(U_{DC\_ref} - U_{DC}\right)dt \qquad \text{(III.12)}$$

where K_{P_DC} and K_{I_DC} are the proportional and integral regulation gains of the PI controller for *d*-current control in the DC voltage controller block, respectively. On the other hand, the reactive power of MG_j can be regulated by the q component of the current, which can be described as:

$$i_{q_{j\_ref}} = K_{P\_Qj}\left(Q_{j\_ref} - Q_j\right) + K_{I\_Qj}\int\left(Q_{j\_ref} - Q_j\right)dt \qquad \text{(III.13)}$$

where K_{P_Qj} and K_{I_Qj} are the proportional and integral regulation gains of the PI controller for *q*-current control for in the DC voltage controller block, respectively. Q_{j_ref} and Q_j are the reference reactive power and measured reactive power of MG_j respectively.

After that, through the current controller block, with the feed forward control method, the output *dq* voltages of VSC_j working in rectifier mode after Laplace transforms can be derived:

$$v_{d_j} = -\left(K_{P\_j} + \frac{K_{I\_j}}{s}\right)\left(i_{d_{j\_ref}} - i_{d_j}\right) + \omega_j L_j i_{q_j} + e_{d_j} \quad \text{(III.14)}$$

$$v_{q_j} = -\left(K_{P\_j} + \frac{K_{I\_j}}{s}\right)\left(i_{q_{j_{ref}}} - i_{q_j}\right) - \omega_j L_j i_{d_j} + e_{q_j} \quad \text{(III.15)}$$

where K_{P_j} and K_{I_j} are the proportional and integral regulation gains of the PI controller of the inner current controller block of the VSC_j, respectively.

2) Grid following microgrid

The microgrid working in this mode has the responsibility for following the control signals of the P/Q reference. Base on the energy situation of all the MMG members, a central controller of the MMG system is designed to gather all the information and calculate these control signals for all the grid following units. Thus, as can be seen in Figure III.14 (b) , there is a P/Q controller block for the VSC_k as an outer-loop of the grid following unit, with the P/Q reference signals (P_{k_ref} and Q_{k_ref}) as the inputs for comparison with the measurement values of P/Q (P_k and Q_k). The comparison results go through a classical PI controller to estimate the current command value for the current controller block of the control system. This current controller block has the same elements with the grid following unit. The output current in the *dq* rotating system can be calculated as:

$$i_{d_{k\_ref}} = K_{P\_Ok}\left(P_{k\_ref} - P_k\right) + K_{I\_Ok}\int\left(P_{k\_ref} - P_k\right)dt \quad \text{(III.16)}$$

$$i_{q_{k\_ref}} = K_{P\_Ok}\left(Q_{k\_ref} - Q_k\right) + K_{I\_Ok}\int\left(Q_{k\_ref} - Q_k\right)dt \quad \text{(III.17)}$$

where K_{P_Ok} and K_{I_Ok} are the proportional and integral regulation gains of the PI controller in the outer P/Q controller block, respectively. And the output *dq* voltages of VSC_k working in inverter mode after Laplace transform can be derived:

$$v_{d_k} = \left(K_{P\_k} + \frac{K_{I\_k}}{s}\right)\left(i_{d_{k_{ref}}} - i_{d_k}\right) - \omega_k L_k i_{q_k} + e_{d_k} \quad \text{(III.18)}$$

$$v_{q_k} = \left(K_{P\_k} + \frac{K_{I\_k}}{s}\right)\left(i_{q_{k_{ref}}} - i_{q_k}\right) + \omega_k L_k i_{d_k} + e_{q_k} \quad \text{(III.19)}$$

where K_{P_k} and K_{I_k} are the proportional and integral regulation gains of the PI controller of the inner current controller block of the VSC_k, respectively.

III.3. Simulation and discussion

III.3.1. System modelling

In this section of the chapter, a simulation model of the multi-microgrid system with the energy router interface is developed in MATLAB/Simulink 2019a environment. The simulated model includes four microgrids and a main grid, which are separated into five zones by a BTB energy router, which is shown in Figure III.19 (a). For the sake of simplicity and a faster simulation, the AC side in the MMG system is only developed in single phase. The model of the MG member consists of loads and a controllable DG source, which is shown in Figure III.19 (b). Figure III.19 (c) present an example of the detail model of the VSC of the main grid, which is included IGBT components from MATLAB/Simulink library and the developed controlling components. The parameters for the simulation model are presented in Table II-1.

Different simulation scenarios are presented in the next part of this section to investigate the dynamic characteristics of the MMG system in all operation modes defined previously, and to verify the feasibility of the proposed control strategies with energy router application.

Table III-1: Simulation parameters

System parameters	Symbol	Value	Unit
DC-link voltage	U_{DC_ref}	500	V
DC-link capacitor	C_{DC}	6	mF
MGs operating voltage	V_{MG}	0.4	kV
MGs operating frequency	f	50	Hz
Inductance of the filters	L	2	mH
Capacitance of the filters	C	25	µF
Resistance of the filters	r	0.1	Ω
Cut-off frequency	ω_c	5	rad/s
Switching frequency	f_s	10	kHz

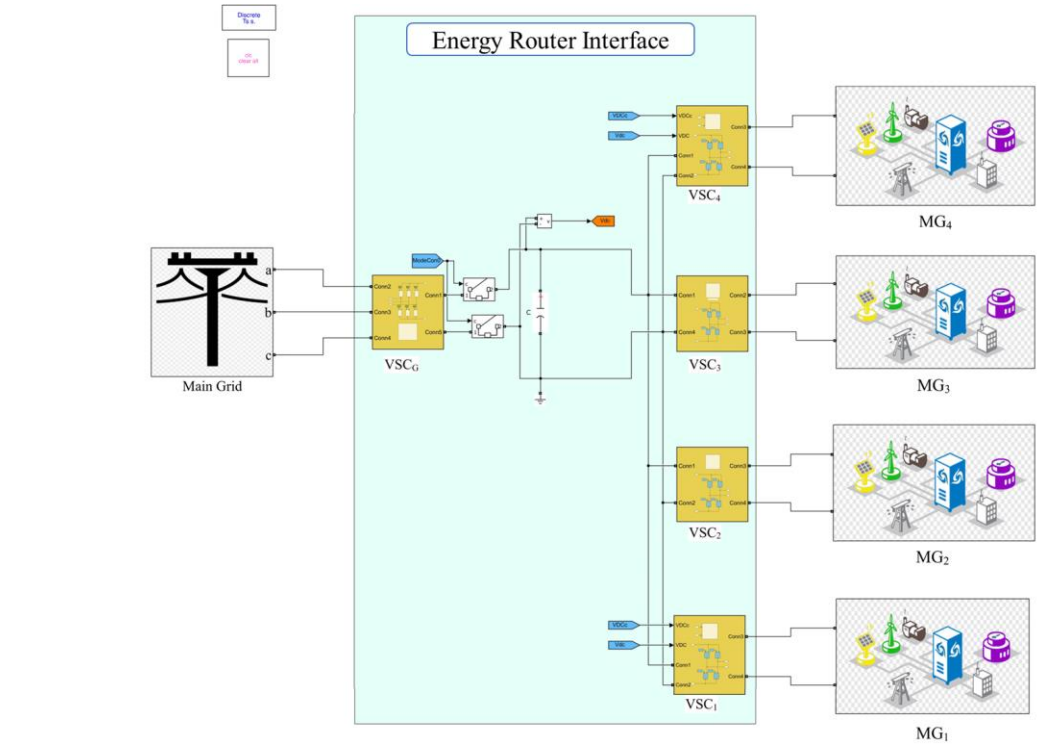

(a)

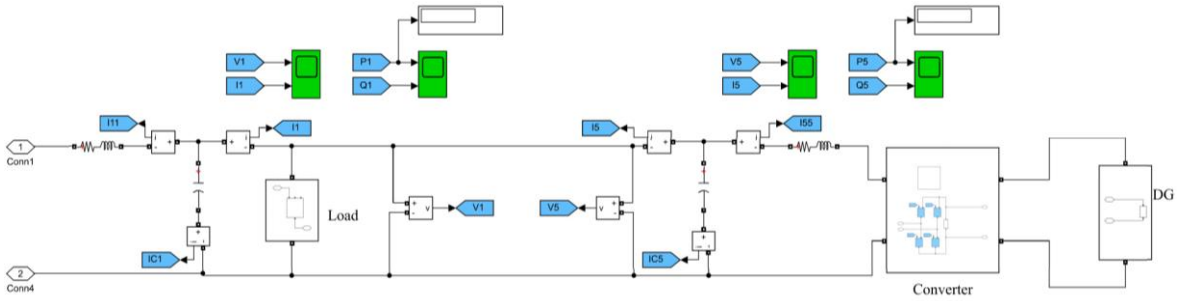

(b)

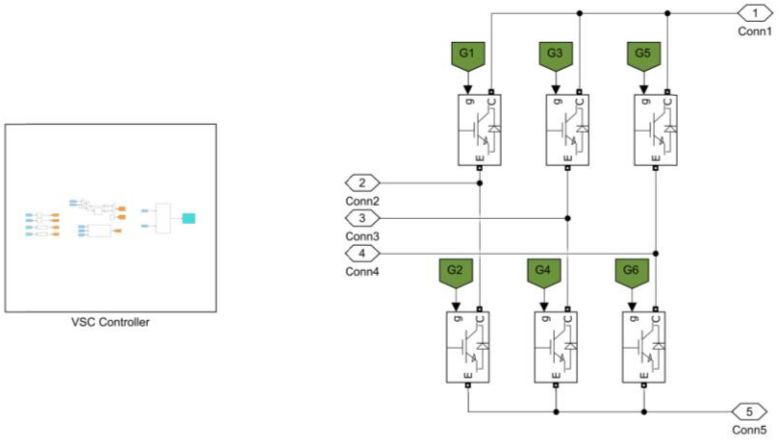

(c)

Figure III.15 – The MATLAB/Simulink simulation model of the multi-microgrid system: (a) overall of the multi-microgrid system; (b) microgrids model; (c) VSC model on main grid side and its controller.

III.3.2. Simulation results and discussion

III.3.2.a. Scenario 1: synchronization

In this first case study, the transition between grid-connected mode and islanded mode of the multi-microgrid system is investigated. When the MMG system works in grid-connected mode, the main grid works as grid forming unit to supply energy and maintain the stability of the DC-link voltage. On the other hand, in isolated mode, the microgrid with the most available surplus of energy works as grid forming unit and the rest of MG members work as grid following unit (parallel mode).

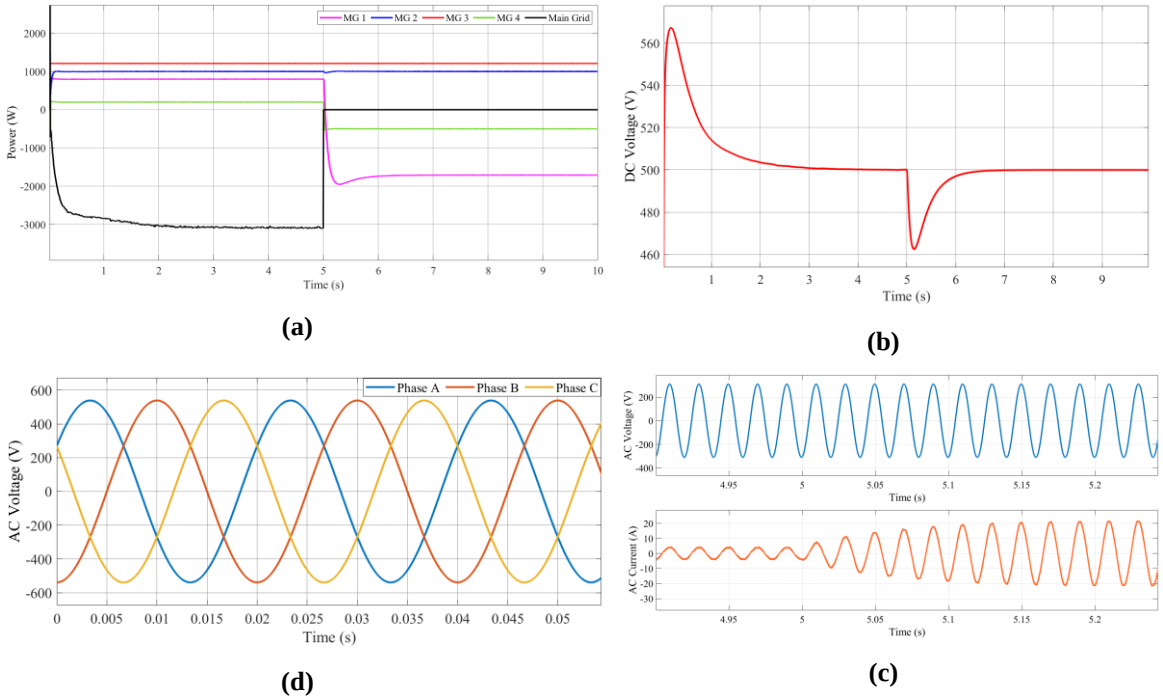

Figure III.16 – Simulation results of scenario 1 – disconnection from the main grid: (a) power exchange scenario; (b) voltage response of the DC-link; (c) AC voltage and current output from the DG of MG_1; (d) AC three phases voltage from the main grid.

Firstly, the transition of the MMG system from grid-connected mode to isolated mode is analyzed. The simulation results for this study case are presented in Figure III.16.

- t = 0 – 5 s

In this period, the MMG system works in grid – connected mode, which is the operation scenario of the ER shown in Figure III.11 (a). Therefore, the main grid is responsible for power balancing in the whole system. As can be seen in Figure III.16 (a), MG_1, MG_2, MG_3 and MG_4 request 0.8 (kW), 1.0 (kW), 1.1 (kW) and 0.2 (kW) respectively. The main grid is able to follow active power demands from all four MGs of the MMG system

in this case. The VSC_G of the ER works as a rectifier and the other VSCs work as inverters. Furthermore, during this stage, the DC – link voltage is also controlled by the main grid. The voltage profile of this DC – link is presented in Figure III.16 (b). There is a fluctuation of this voltage curve from t = 0 – 2.5 s. However**,** it is noteworthy that this fluctuation is come from the developed model itself. With that, this internal fluctuation is ignored for the rest of the simulation results. After that, the model reaches the stable state around t = 2.8 s. The DC – link voltage is maintained stable at U_{DC_ref} (500 (V)) by the main grid in this period. The three-phase line-line voltage of the main grid system is shown in Figure III.16 (c).

- t = 5 – 10 s

In this period, the MMG system works in grid – disconnected mode, which is the operation scenario of the ER shown in Figure III.11 (c). At t = 5 s, the MMG system is isolated from the main grid via a DC switch. The VSC_G of the main grid is disconnected from the ER. It is assumed that the MG_1 has the highest surplus of controllable energy in the MMG community. Therefore, in this period, the role of grid following changes from main grid to MG_1 and MG_1 is responsible for supplying deficit energy and regulating voltage of the DC – link. As can be seen in Figure III.16 (a), there are two MGs with the surplus energy: MG_1 and MG_4. MG_4 in this case works as grid following unit and provides its maximum excess energy. After that, MG_1 provides energy for its own system and for the rest of the deficit energy of the MMG system. After the transition process, there is a slightly decline by 6 (%) in the voltage profile of the DC – link as in Figure III.16 (b). Nevertheless, the DC voltage profile recovers rapidly as the power balance condition in the ER is achieved by MG_1. The AC voltage and current profiles of the DG, which is considered that having highest surplus of energy, in MG_1 are shown in Figure III.16 (d).

In contrast, the transition of MMG system from grid-isolated mode to grid – connected mode is also investigated. The results for this simulation are shown Figure III.17. Similarity with the previous simulation scenario, the transition between the two modes of the MMG system takes place at t = 5 s. Opposite with the disconnection scenario, from t = 0 – 5 s, MG_1 works as grid forming unit and after that, from t = 5 – 10 s, the main grid is reconnected with the MMG system and works as a master unit. As can be seen from Figure III.17 (b), there is a sharp rise by 16 (%) in the DC voltage profile at t = 5 s due to the transition; however, the stable state of the system is restored quickly by the main grid.

The simulation results have verified the feasibility of the ER control scheme in MMG system in both grid – connected, isolated mode and the transition between them.

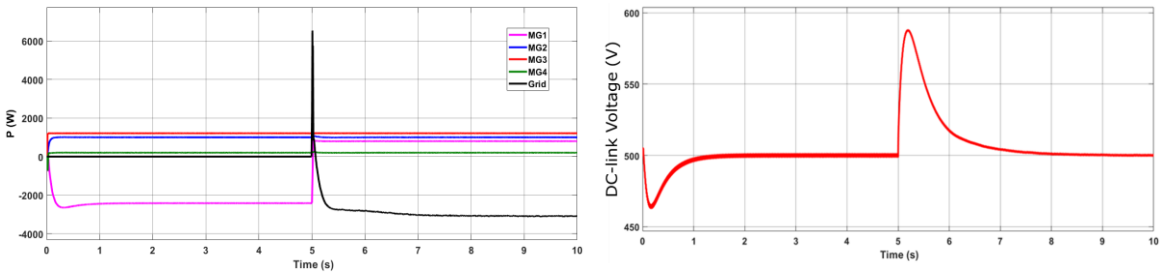

(a) **(b)**

Figure III.17 – Simulation results of scenario 1 – reconnection with the main grid: (a) power exchange scenario; (b) voltage response of the DC-link.

III.3.2.b. Scenario 2: power exchange among MGs

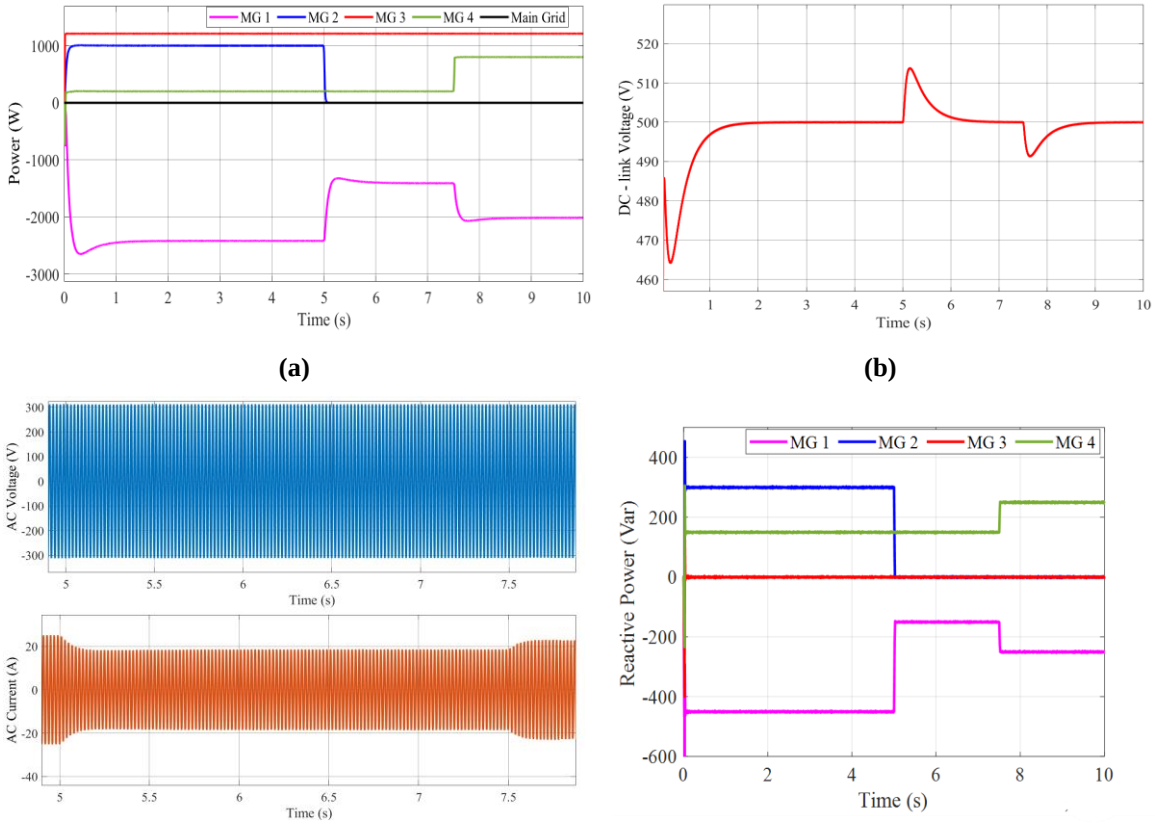

(a) **(b)**

(d) **(c)**

Figure III.18 – Simulation results of scenario 2: (a) active power exchange scenario; (b) voltage response of the DC-link; (c) reactive power exchange scenario; (d) AC voltage and current output from the DG of MG_1.

This scenario demonstrates the process of active and reactive power flow within the interconnected multi-microgrid system. In this case study, the MMG system works in scenario illustrated in Figure III.11 (b). MG_1 is responsible for energy balancing and the rest of MG members work in parallel mode.

The simulation results for active and reactive power exchange scenario in this case are shown in Figure III.18 (a) and (d) respectively. As can be seen in the results, all the grid following units are able to quickly and precisely track their active and reactive power command signals. For example, at t = 5 s, MG_2 is requested to reduce all of its active and reactive power loads from 0.9 kW and 0.3 kVar respectively to 0 and at t = 7.5 s, MG_4 is allowed to increase the active and reactive power from 0.3 kW and 0.175 kVar to 0.7 kW and 0.225 kVar respectively. MG_3 is not involved in the energy exchange in this case so that its active and reactive power profiles follow the power reference setpoints at time t = 0 s. Despite of some fluctuation in voltage profile as in Figure III.18 (b), instant energy and power balances in the MMG system are achieved by MG_1 in this case study, which has confirmed the effectiveness of the proposed control strategies for the ER interface. The voltage variation of the DC – link at the moments of power exchange is negligible and can be neglected.

III.3.2.c. Scenario 3: switching the grid forming unit

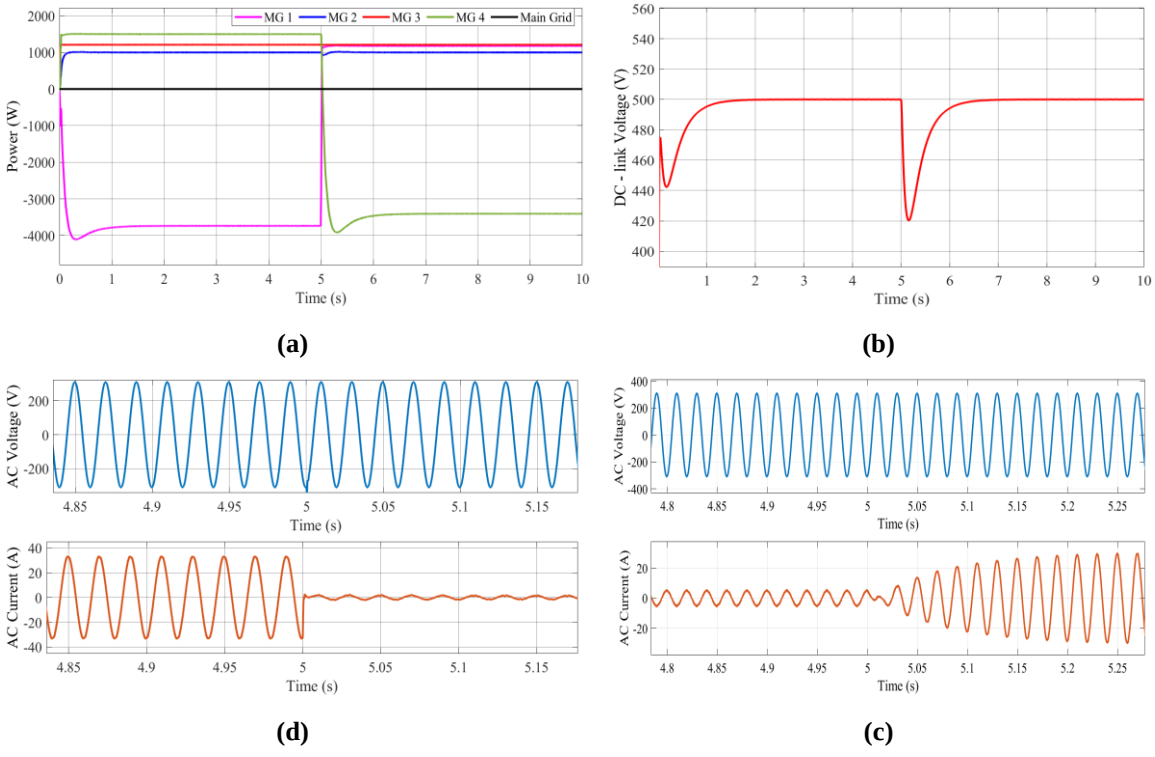

(a) **(b)**

(d) **(c)**

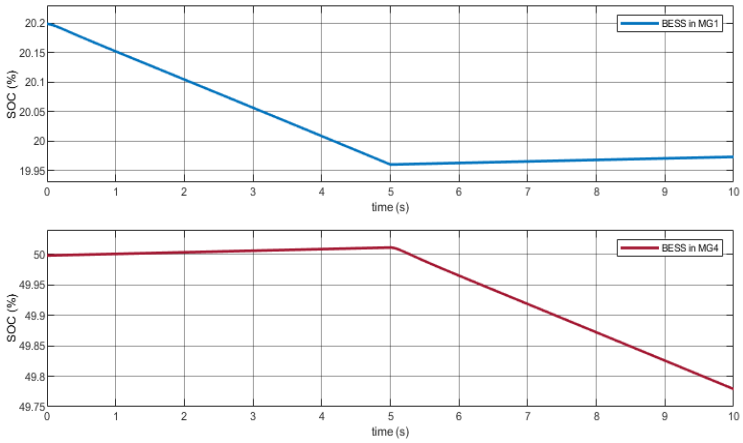

(e)

Figure III.19 – Simulation results of scenario 3: (a) active power exchange scenario; (b) voltage response of the DC-link; (c) AC voltage and current output from the DG of MG_4; (d) AC voltage and current output from the DG of MG_1; (e) state of charge (SOC) of BESS in MGs.

In this chapter, when the MMG system in isolated mode, a grid forming MG in the MMG system with ER interface is defined as a MG having the highest surplus of energy. With this presumption, all the MG members in the MMG community have the possibility to work in this mode, depending on their own energy situation.

Thus, in this case study, it is assumed that the MMG system has to change the grid forming unit during power exchange process because of the MGs constrains. In this simulation scenario, the controllable DGs used in MGs are battery energy storage system (BESS). In addition, to preserve a long lifetime of BESS, the maximum and minimum values of SOCs of BESS in the simulation are 80% and 20%, respectively. The transition of working mode between MG_1 and MG_4 is investigated in this simulation scenario. The BESSs used as DGs for MGs in this case study are Lithium-Ion batteries, which can be found in MATLAB/Simulink 2019b library.

- t = 0 – 5 s

At the beginning of the power exchange scenario shown in Figure III.19 (a), VSC_1 of the MG_1 works in grid forming mode. Therefore, the BESS of MG_1 has to provide energy to regulates the voltage of the DC – link, so the BESS in MG_1 operates in discharging mode to supply the energy for other MGs. Moreover, during this period, the BESS in MG_4 is allowed to charge as long as the upper limit of SOC is not reached.

- t = 5 – 10 s

In this period, at t = 5 s, the SOC of BESS in MG_1 passes its lower limit (20%) as shown in Figure III.19 (e), so this BESS shifts from discharging mode to charging mode and MG_1 works as grid following unit. With that change, the ER needs a new master to control the voltage of DC-link of the MMG system. With the BESS's SOC above 50%, the VSC_4 of MG_4 is considered to have a highest controllable energy source and becomes a new grid forming unit of the system. Therefore, from t = 5 s, MG_4 starts to produce energy from its BESS so that the SOC of the BESS in MG_4 decreases rapidly in the last period of the simulation. The details of outputs current and voltage of the BESS in MG_4 are shown in Figure III.19 (d).

The variation of the voltage profile of the DC – link in the proposed ER for the whole simulation period is illustrated in Figure III.19 (b). There is a significant drop at t = 5 s due to the switching process in the DC voltage profile as the voltage drops to 420 (V). However, after just 1 s, by tracking the reference value, MG_4 has successfully recovered this voltage profile and maintained it stable. The simulation results in this case study have definitely confirmed the efficiency of the control strategies in the islanded MMG system with the exchange of VSCs operation mode in the proposed ER.

III.4. Conclusion

In this chapter, in accordance with Task 4.2 of the m2M-Grid project, an interface among microgrids in a multi-microgrid community is developed. Firstly, the chapter introduces the concept of ER as an interface among MGs, with its characteristics, functionalities and topologies for implementation. A DC bus-based ER topology, which has higher degree of reuse and integration compared to other topologies, is investigated. The control of ERs relies on the VSCs with the grid forming/grid following working mode. The outer-loop controller of the grid forming VSC operates as a DC voltage controller and its objective is to keep a steady and constant DC-link voltage. The rest of the VSCs are the grid following converters, working in the manner of power transfer following up. A mathematical model of the chosen ER architecture is developed, with its detail control system structure.

Secondly, to verify the ER application, a stand-alone multi-microgrid system with the energy router interface is simulated in MATLAB/Simulink environment. A MMG system with four MG members is built and simulated. From the simulation results, in case of transient events in the MMG system such as load variation or disconnection/reconnection with the main grid, the ER is able to keep the DC-link voltage stable. Moreover, MGs are allowed to exchange the energy directly among them via the ER interface, which lessens the dependency on the main grid and enhances the reliability of the whole system. In addition, the roles of VSCs in the ER can be switched among MG members depending on their energy situation. A case study for roles switching when a SOC of the BESS system in grid forming unit reaches its limit is analyzed. Despite of a considerable drop in the voltage of the DC bus during the switching process, the system is able to quickly recover and maintain its stable operation.

Overall, the simulation results achieved by conducting various operation scenario has verified the effective of the energy router for microgrid’s interface. The implementation of the ER is a fundamental step to the future of Energy Internet.

CHAPTER IV : Frequency support in a multi-microgrid system with the energy router interface

Contents

IV.1. Introduction

IV.1.1. Stability situation in the modern grids

In general definition, moment of inertia (J) refers to the resistance of any physical object to change in its rotational motion [103]. In conventional power system, moment of inertia concept represents for the kinetic energy from rotating electrical generators which are part of fossil fuel, hydroelectrical and nuclear power plants. This stored energy can be used for few seconds to give the power grid control system enough time to react in case of power sudden change. Normally, all the generators in the power system are synchronized and connected via electromagnetic force. Therefore, all the generators can contribute and support to grid inertia. In power systems, it is common to express inertia constant (H) instead of J [kg.m2], H [s] can be calculated as in [104]:

$$H = \frac{1}{2}\frac{J.\omega_r^2}{S_r} \tag{IV.1}$$

where S_r [MVA] and ω_r [rad.s] are the rated power and the rated rotational angular speed of the synchronous generator respectively. The average value of H in conventional power plants vary between 2 and 10 s [105]. Considering small variations around the steady state, the *swing equation* in the power system can be written as [106]:

$$2H\frac{d\Delta\omega_r}{dt} = \Delta P_m - (\Delta P_L + D.\Delta\omega_r) \tag{IV.2}$$

where ΔP_m and ΔP_L are the power change of mechanical power and those loads independent from frequency deviations, with D is the damping factor (load-frequency response). The term $\frac{d\Delta\omega_r}{dt}$ or $\frac{d\Delta f}{dt}$ refers to the rate of change of frequency (ROCOF) of the AC system.

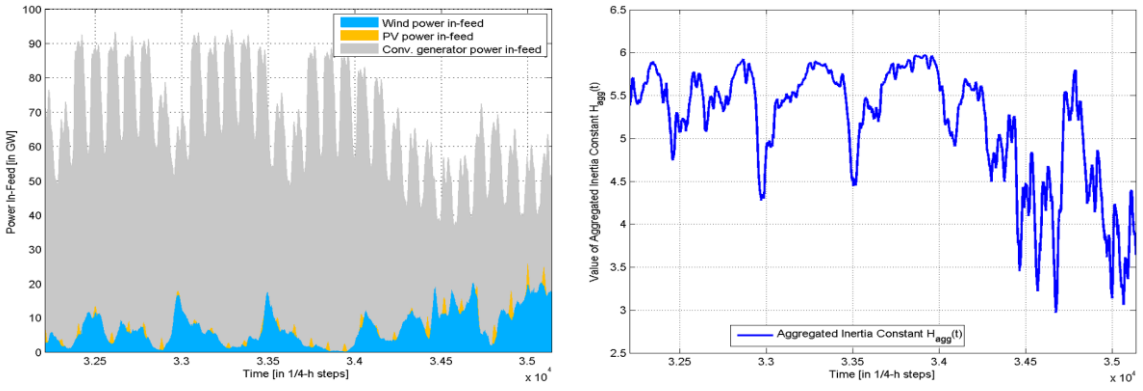

(a) (b)

Figure IV.1: German Power System situation in 2012 [107]: (a) Power Dispatch ; (b) Aggregated Rotational Inertia.

Nowadays, with the large penetration of inverter-based RES, the number of synchronous generators connected to the grid reduces rapidly. The replacement of this inverter units decreases the level of rotational inertia in power systems, which makes frequency dynamic of the system become faster and unstable. An example of German power system for this phenomenon is illustrated in Figure IV.1. It shows that the inertia constant of the system is highly fluctuation and time – variation due to the penetration of wind and solar generation. As can be seen from the figure that the lowest level of inertia constant of 3 s was reached around December in which the wind power in-feed level was high. With reduced inertia, the ROCOF of the system increases which causes larger changes in frequency of the system in the same time-frame.

IV.1.2. Potential options to improve frequency stability in the modern grids

In [108], the system stability can be improved by maintaining the inertia via operating the grid to ensure the mix of conventional generators online exceeds critical inertia levels. With this strategy, a certain number of generators are always online to maintain a predefine inertia level which is actively monitor by the grid operator. However, this method reduces the efficiency of the generators and has negative impact on the environment due to the existed of the conventional generators. On the other hand, there are synchronous condensers, which are non – generation units, to support system stability by providing inertia. These devices are mostly generators or motors which take energy from the grid system for maintaining their spinning mass and send back into the grid in case of power unbalance. This method is a potential solution to preserve a minimum level of inertia in the modern grids [109].

Another potential solution is demand response (DR) approach. This DR technique manages the power demand from the load side of the power flow. In case of generation – load imbalance, the provision of active non-critical loads response from the demand side can assist in tackling some of the problems of frequency. With the most generators, primary frequency response (PFR) solution responses 2% per second of a target power. However, the load resources can drop 100% of a targeted load in less than half a second [110]. Therefore, it could be less expensive to encourage proactively participating consumers to drop their non-critical loads infrequently, as opposed to continuously providing PFR from the generators. The use of frequency response from loads has been one of the major factors that

has allowed and continues to allow Electric Reliability Council of Texas to develop its wind penetration, which has reached 58% on an instantaneous basis despite the associated decline in inertia [108]. For example, a large cooling equipment in an industrial consumer can be considered as a non – critical load and might be drop for few minutes without any crucial impact on the temperature in a large cold – storage facility [108]. This method depends on consumers constrains and requires their data and communication, which may increase the cost for system-wide deployment.

The stability of the power system can also be improved by the responses from inverter – based resources. With solar and wind system, these sources can reduce their maximum output powers so that they can quickly release these "reserve" powers to provide frequency support services. As mention in [111], this approach can also be describe as "synthetic inertia" method. To apply this strategy, the output power of the wind system can be controlled by regulating the blade pitch angle while the output power of the solar system can be adjusted by using power electronics [108]. However, there is a tradeoff between producing maximum energy and providing the ability to power respond. Moreover, recently, energy storage system (ESS) such as batteries, compressed air system, flywheel or supercapacitors are playing a more important role in supporting frequency stability in low inertia grid [112]. ESS can be integrated into ancillary services and activated rapidly to reduce rate of change of frequency (ROCOF) during transient event. A major drawback of ESS is the high investment cost. A typical application of ESS in frequency supporting is virtual synchronous generator (VSG).

IV.1.3. Multi – microgrid system frequency control scheme

In stand-alone multi – microgrid (MMG) system, the reliability can be improved by cooperative operation. With the interconnected of microgrids, not only the system stability but also the penetration of RES can be increased as in [82]. In [113], the frequency in an isolated AC multi – microgrid system is supported by tuning the parameters of the PID controller with grey wolf optimization. The proposed control strategy has reduced the frequency deviation and power exchange between MGs. Similarity, the frequency control in an AC stand – alone MMG system is enhanced by using an imperialist competitive algorithm for tunning the dual-stage fractional order PID controller gains. The effectiveness of the proposed method has been verified through a transfer function model in MATLAB/Simulink environment.

Recently, a multi – microgrid system with a flexible frequency operation control strategy has gained attention [82], [102], [114], [115]. The idea behind this approach is to separate the MG with sensitive loads and MG with general loads as only the sensitive loads require high frequency quality [116]. With that, each MG in the MMG system is able to work in different frequency ranges. This approach adds more flexible for frequency control and reduces the need of ancillary services cost for MGs. By contrast with the previous AC tied line MMG system, MMG with the flexible frequency operation has a DC interface among MGs. In [82], an example of the MMG system in Korea power system with Back-to-Back HVDC interface is introduced. With the use of HVDC and flexible range of frequency, the swing equation is modified and the simulation results have confirmed that the flexible frequency operation makes Korean power system economical for more RES penetration, without extra governor response, and it can also reduce the cost for ancillary service. Moreover, a DC isolation with Back-to-Back voltage source converters is also utilized in [114] for frequency control improvement in MMG system.

Overall, the previous references have recommended that the DC connection among MGs in MMG community could reduce the complexity compared to the AC connection. However, more control strategy for frequency enhancement in this MMG system is still needed to be investigated. Therefore, in this chapter, the application of the ER for various frequency control methods for MMG system with an DC-link based energy router interface is developed and validated with simulation results.

IV.2. Frequency support strategies with energy routers application

IV.2.1. Strengthen the “inertia” of the system

Thanks to the existence of the DC-link in the structure of the chosen ER topology, the stability of the overall MMG system can be improve by increasing the “inertia” of this DC-link. The virtual “inertia” method for stability and the analogy with the AC system of the DC system is deeply discussed in [117]. With an AC system, the inertia indicates the capability to maintain the stability of frequency with the sudden change of active power. For a MMG system with a DC link, the inertia can also indicate the ability to restrict the sudden changes of the DC bus voltage. For the AC system, the inertia is related to the kinetic energy

W_r saved in the rotor of the synchronous generator whereas in the DC interconnected network, the inertia is related to the electrical energy W_c saved in the capacitors connected in the DC-link. These energies can quickly provide active power support when the system suffers from disturbance. These storage energies are defined as:

$$\begin{cases} W_r = \frac{1}{2} J \omega^2 \\ W_c = \frac{1}{2} C {U_{dc}}^2 \end{cases} \quad \text{(IV.3)}$$

As can be seen in equation (IV.3), the value C is analog with J in term of "inertia" unit. The analogy between the AC and DC system is summarized in Table IV-1.

Table IV-1: Analogy between AC and DC system

Variable	AC system	DC system
Inertia	J	C
Stored Energy	W_r	W_c
Stability indicator	f/ω	U_{dc}
Output control	P	i_{dc}

Furthermore, the current balance equation in the DC-link in the MMG system is formulated as:

$$C_{DC} U_{DC} \frac{dU_{DC}}{dt} = \Delta i \quad \text{(IV.4)}$$

From the equation above, the term $\frac{dU_{DC}}{dt}$ is similar to ROCOF in the AC domain and can be consider as a rate of change of voltage (ROCOV). It is obvious that the simplest solution for improving the stability of the MMG system is to improve the ROCOV by increasing the capacity of the capacitor connected to the DC-link. This solution is easy to apply and doesn't require any information from MMG members. However, the cost of increasing size for capacitors need to be considered in real implementation.

IV.2.2. Virtual synchronous generator approach

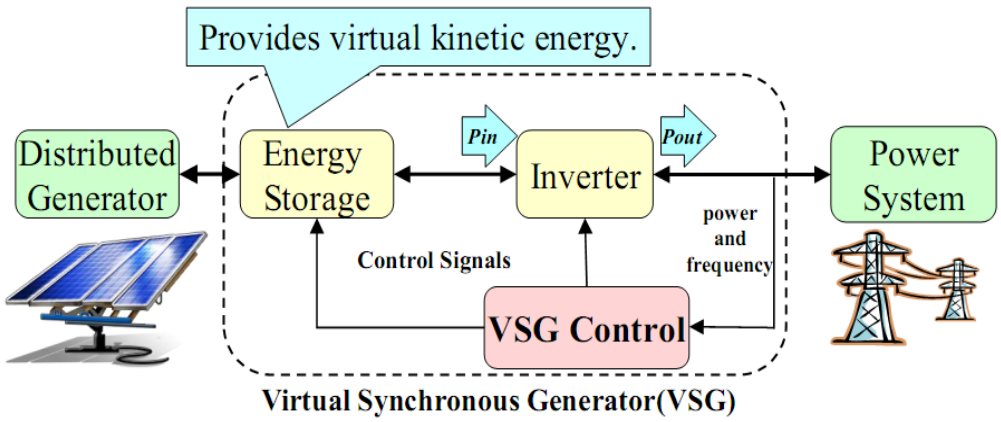

(a)

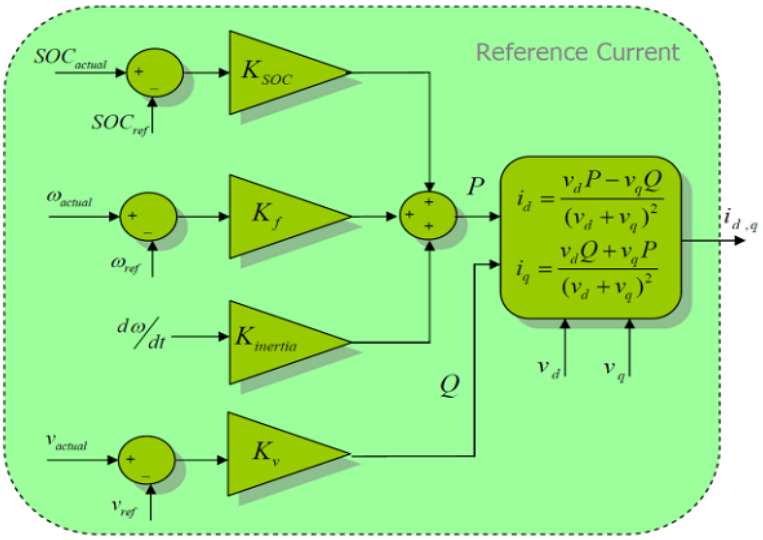

(b)

Figure IV.2: (a) The concept of VSG [118]; (b) The VSG control scheme developed by VSYNC project [119].

Another potential solution for enhancing the stability of the studied MMG system is to apply VSG concept, which is shown in Figure IV.2. VSG solution is widely employed for adding virtual inertia of the AC system [120]. VSG can be used as current source as in VSYNC project or voltage source developed by Ise Laboratory [119]. However, at the present, the use of VSG concept for inertia support in islanded hybrid MMG system is not considered in the existing literatures. For the sake of simplicity, a current source VSG technology, that is developed by the VSYNC project, is chosen in this chapter.

It is assumed that, in the studied system, at least one energy storage system (ESS) of MGs in MMG system is reserved for this VSG application. The VSG topology applied in this paper is a frequency-power response base topology, which takes frequency and rate of change of frequency (ROCOF) response as inputs. Firstly, in term of AC domain, the output power of VSG (P_{VSG}) is calculated as [120]:

$$P_{VSG} = K_D.\Delta\omega + K_I.\frac{d\Delta\omega}{dt} \quad \text{(IV.5)}$$

where, $\Delta\omega$ and $\frac{d\Delta\omega}{dt}$ represent the change in angular frequency and the corresponding ROCOF. K_D and K_I represent the damping and the inertial constant, respectively. Similarity with the concept of VSG in the AC system, the output of VSG power for supporting virtual inertia in DC domain can be written as

$$P_{VSG} = K_D.\Delta V_{DC} + K_I.\frac{dV_{DC}}{dt} \quad \text{(IV.6)}$$

where ΔV_{DC} and $\frac{dV_{DC}}{dt}$ represent the change in voltage of DC-link in the ER of MMG system and the corresponding rate of change of DC-link voltage (ROCOV). K_D and K_I can be estimated with the same approach with AC domain in [121] and it can be estimated as

$$K_I = \frac{P_{VSG\_nominal}}{\left(\frac{d\Delta V_{DC}}{dt}\right)max} \quad \text{(IV.7)}$$

$$K_D = \frac{P_{VSG\_nominal}}{\Delta V_{DC}\ max} \quad \text{(IV.8)}$$

where $P_{VSG\_nominal}$ is the nominal value of VSG power, $\left(\frac{d\Delta V_{DC}}{dt}\right)max$ is the maximum allowed value of ROCOV of DC-link voltage, $\Delta V_{DC}\ max$ is the maximum value of the deviation of DC-link voltage. There hasn't had any standard for the deviation of DC voltage and ROCOV for the studied MMG system. Thus, these values should be chosen based on the specific configuration of MMG, which should be related the standard of ROCOF in the AC domain of the MGs system. The only input for this proposed approach is the voltage value of the DC-link in the ER interface, which doesn't require any privacy information from MGs in MMG system.

IV.2.3. Frequencies droop approach

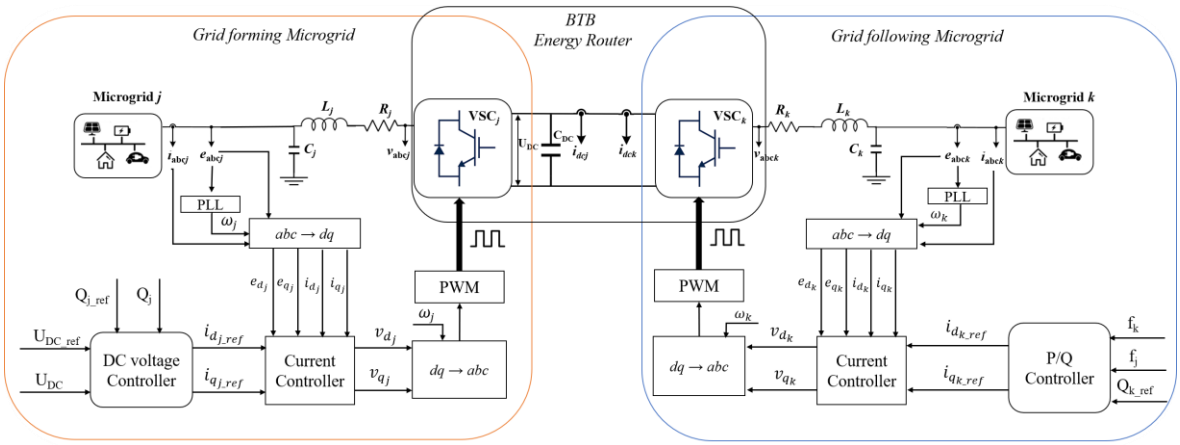

Figure IV.3: The control system of the energy router with a grid forming and a grid following units with frequency droop approach.

The frequency performance of the MMG system can be improved by designing a suitable controller of the ERs with a DC-link based energy router [102]. A MMG control system is shown in Figure IV.3, where a back-to-back converter is used for interconnecting two adjacent MGs. In this configuration, MG_j is responsible for the regulation of the dc-link voltage whereas MG_k is utilized for regulating the frequencies of the two adjacent MGs.

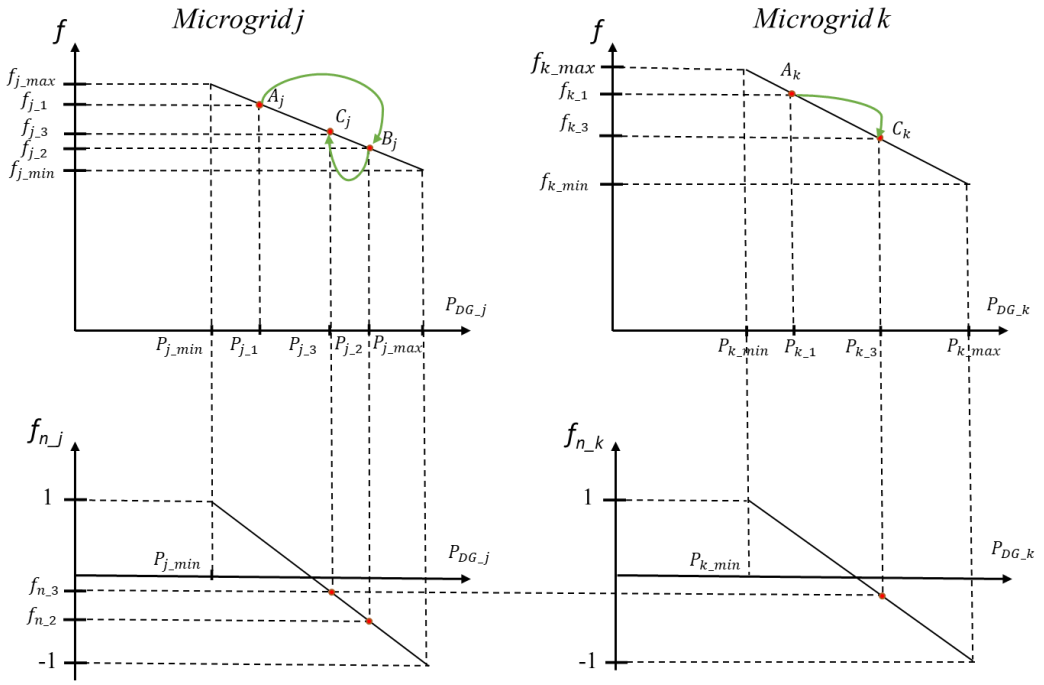

Figure IV.4: The frequency droop characteristic between two adjacent microgrids

The MMG multi-frequency regulation strategy is based on a droop frequency control characteristic [102], which is presented in Figure IV.4. In this case, MG_j are responsible for

regulating the DC voltage and its frequency is supported by MG_k. Normally, the working frequency of MG_j and MG_k are A_j and A_k, respectively. After a load variation in MG_j, the new working point of MG_j is dropped to B_j via its droop characteristic. With the ER interface, MG_k can share this increasing load by transferring energy to MG_j through the BTB converter. The transferred power is estimated with Equation (IV.9). Consequently, the frequency of MG_j recovers from point B_j to C_j but the frequency of MG_k decreases from A_k to C_k. This is a tradeoff in this method. The system frequencies of the two MGs are stable at new steady state values (C_j and C_k) when the normalized frequencies (f_{n_j} and f_{n_k}) of the two MGs are equal.

The control diagram of the grid forming converter unit in this chapter is the same with the one presented in section III.2.5.b. The control diagram of the grid following converter in this part is shown in Figure IV.5, which includes the P/Q controller with the multi-microgrid frequency function and the current controller. The reference real power (P_f) is given by the outer multi-frequency controller can be calculated as:

$$P_f = K_{P\_f}\left(f_{n\_j} - f_{n\_k}\right) + K_{I\_f}\int (f_{n1} - f_{n2})dt \tag{IV.9}$$

where f_{n_j} and f_{n_k} are the normalized frequencies of MG_j and MG_k, respectively and K_{P_f} and K_{I_f} are the parameters of PI controller of the multi-frequency controller. The frequency of each MG is normalized to obtain the value of frequency deviation, which can be calculated as [102]:

$$f_{n\_i} = \begin{cases} \dfrac{(f_i - f_{i,rated})}{(f_{i,max} - f_{i,rated})}, (f_i > f_{i,rated}) \\ \dfrac{(f_i - f_{i,rated})}{f_{i,rated} - f_{i,min})}, (f_{i,rated} > f_i) \end{cases} \tag{IV.10}$$

where, f_i represents the measured frequency of MG_i; $f_{i,rated}$ is the rated frequency of MG_i; $f_{i,max}$ and $f_{i,min}$ are the maximum and minimum frequency deviations, respectively; f_{n_i} is the normalized frequency of MG_i. Finally, the reference currents for the current control loop of the grid following converter are given by:

$$\begin{cases} i_{q_{k\_ref}} = \dfrac{\frac{2}{3}\left(e_{q\_k}P_f - e_{d\_k}Q_{k\_ref}\right)}{e_{d\_k}^2 + e_{q\_k}^2} \\ i_{d_{k\_ref}} = \dfrac{\frac{2}{3}\left(e_{d\_k}P_f + e_{q\_k}Q_{k\_ref}\right)}{e_{d\_k}^2 + e_{q\_k}^2} \end{cases} \tag{IV.11}$$

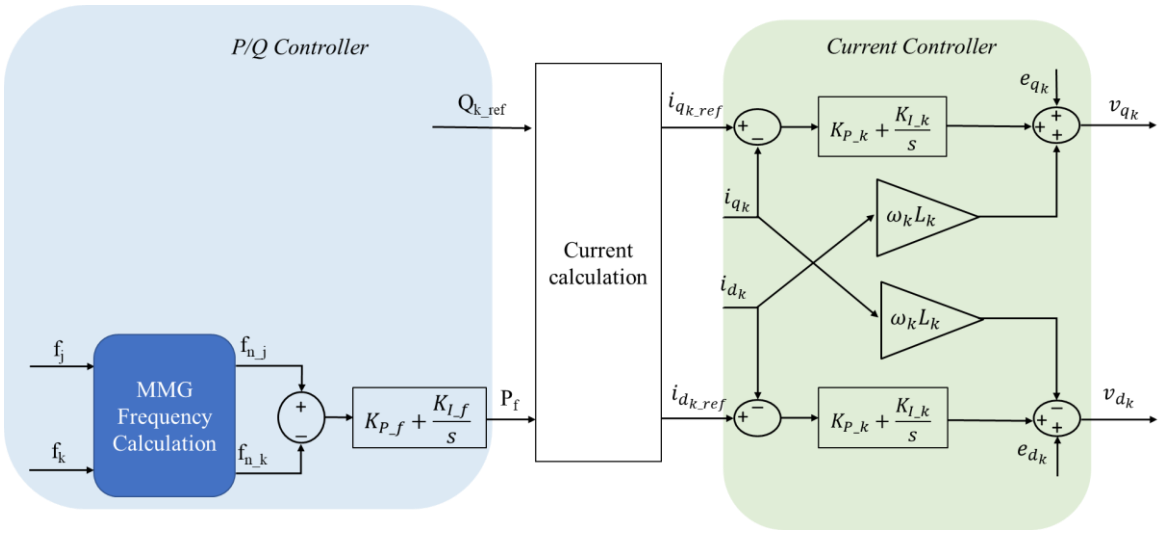

Figure IV.5: The control diagram of the grid following microgrid for multi-frequency control.

IV.3. Simulations and discussion

In this section, a simulation model is built in MATLAB/Simulink environment to verify the efficiency of the presented solutions in the previous section. The detail of the model is shown in Figure IV.6. The simulated MMG system consist of four AC MGs which are able to connect or disconnect from the main grid. A DC-link with a capacitor is used to connect all the MGs. The simulation parameters are listed in Table IV-2. In the simulation, the MG_1 is chosen as a gridf orming MG, the other three MGs work in grid-following mode. The MMG is disconnected from the main grid in all simulations.

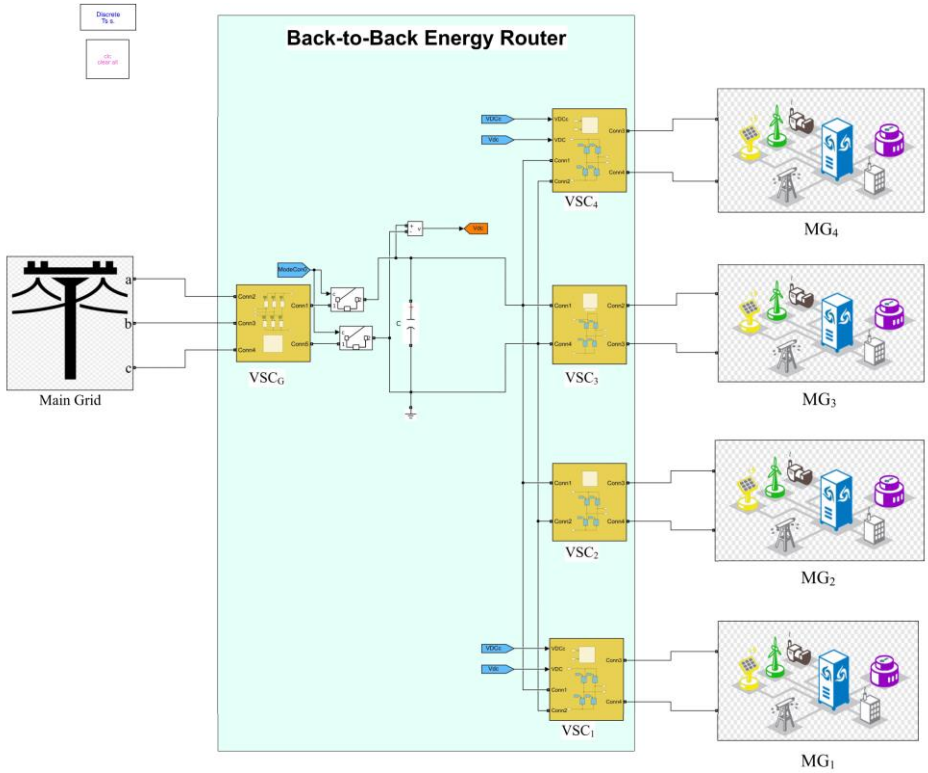

Figure IV.6: The developed model of the multi-microgrid system in MATLAB/Simulink.

Table IV-2: Simulation parameters

The power exchange scenario for this simulation is presented in Figure IV.7, where MG_1

System parameters	Symbol	Value
DC-link voltage	V_{DC}	500 V
DC-link capacitor	C_{DC}	6 mF
MGs operating voltage	V_{MG}/f	220 V, 50 Hz
LC filter	$L/r_L/C$	2 mH/0.1 Ω/25 µF
Cut-off frequency	ω_c	5 rad/s
Switching frequency	f_s	10 kHz

IV.3.1. Strengthen the “inertia” of the system

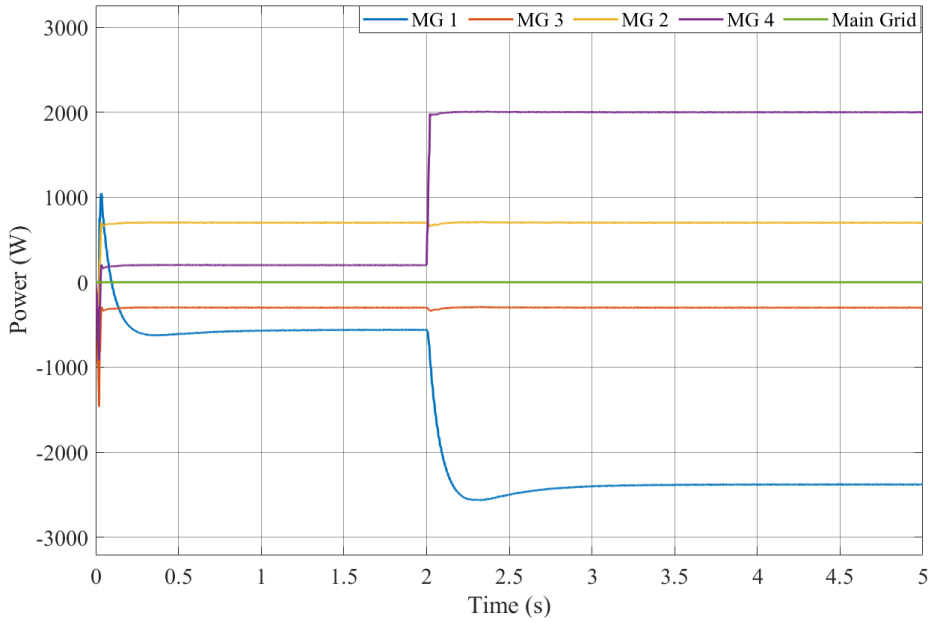

Figure IV.7: Power exchange scenario in the studied MMG system

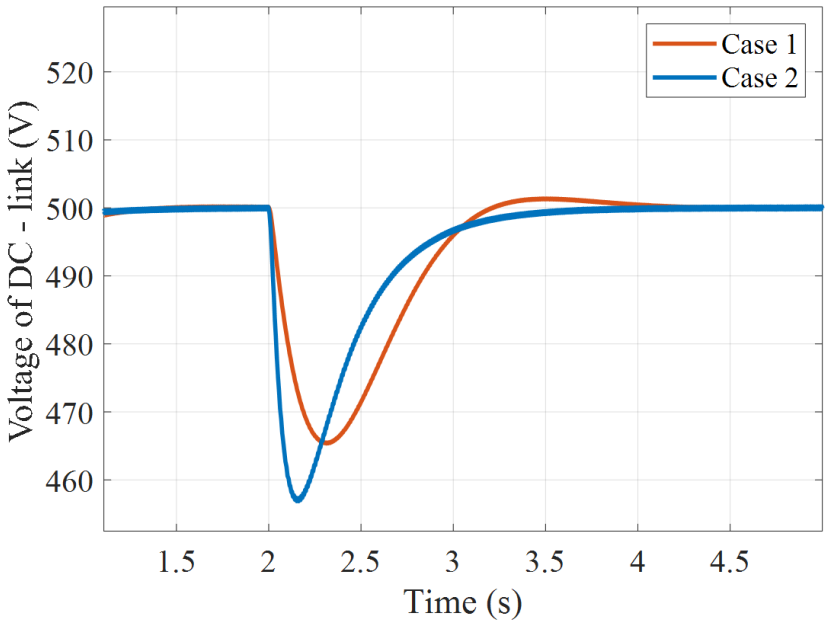

(a)

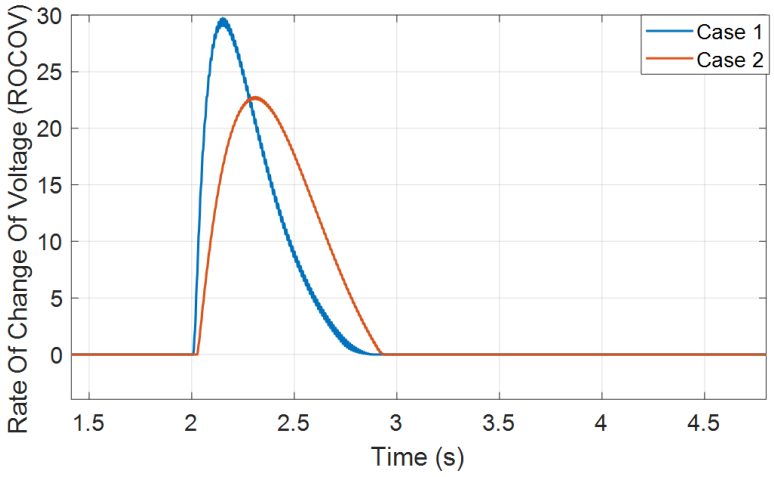

(b)

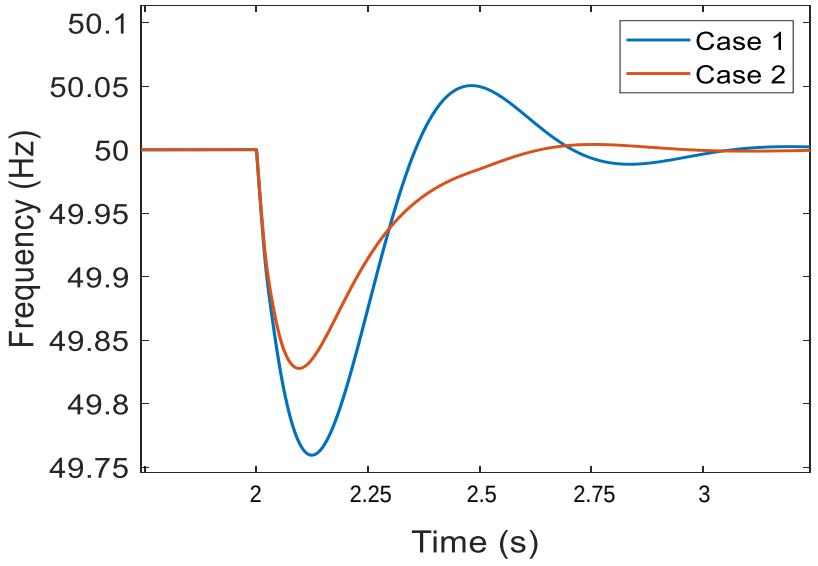

(c)

Figure IV.8: Strengthen the inertia of the system: (a) Voltage response of the DC-link; (b) ROCOV of the DC-link; (c) Frequency response from MG_1.

The power exchange scenario for this simulation is presented in Figure IV.7, where MG_1 is responsible for energy balance in the MMG system. At t = 2s, the power demand in MG_4 increases sharply, the power from other MGs remain constant in this period.

With the first simulation, in case 1, the capacity of the capacitor of the DC-link is kept the same value as in Table IV-2. In case 2, to increase the inertia of the DC-link, the capacity of this capacitor is increased 40%. The simulation results for the first approach is shown in Figure IV.8. As, can be seen, at t = 2s, due to the increasing of load demand from MG_4, the voltage of the DC-link drops and the ROCOV rises significantly in case 1. However, by

increasing the capacity of capacitor in case 2, the voltage of DC-link returns to the nominal value slower than case 1 but the DC voltage nadir and the peak of ROCOV have decreased considerably. In addition, as can be seen from Figure IV.8 (c), the frequency of MG_1 is also improved when the voltage response of DC-link is improved, which proves that the solution has brought benefit for not only the "inertia" of MMG system but also for the stability of the grid-forming MG.

IV.3.2. Virtual synchronous generator approach

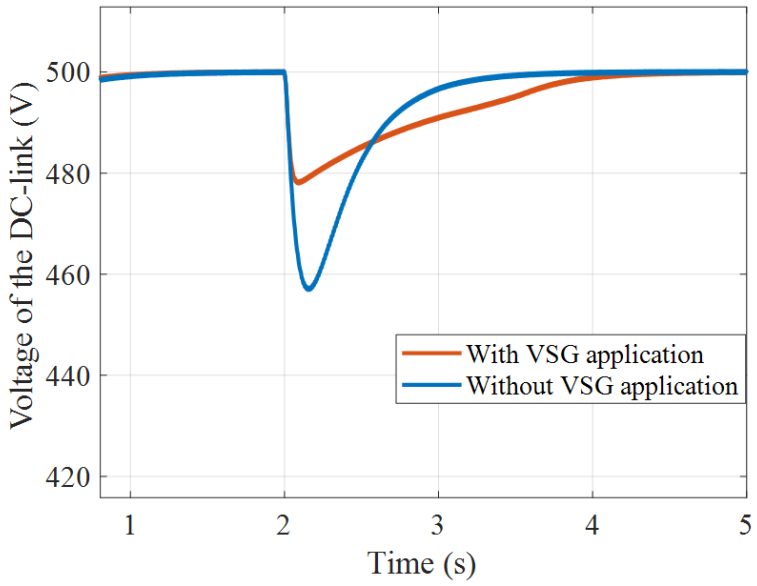

(a)

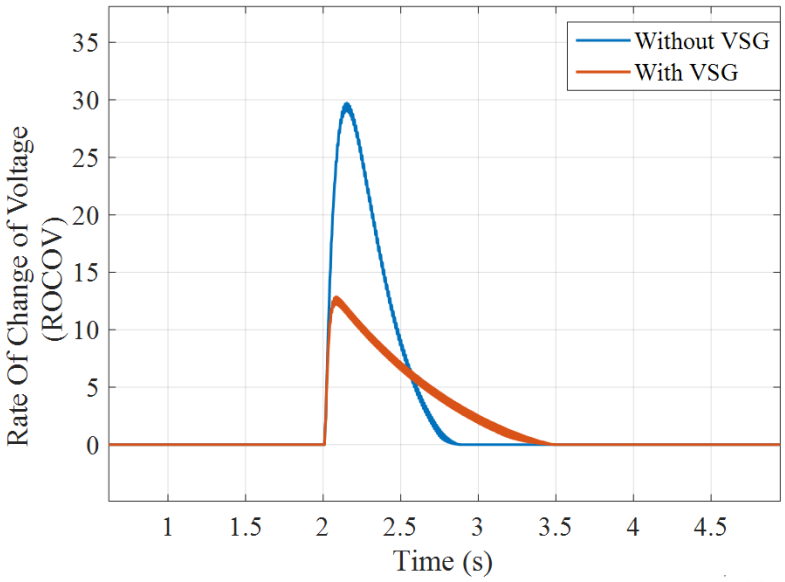

(b)

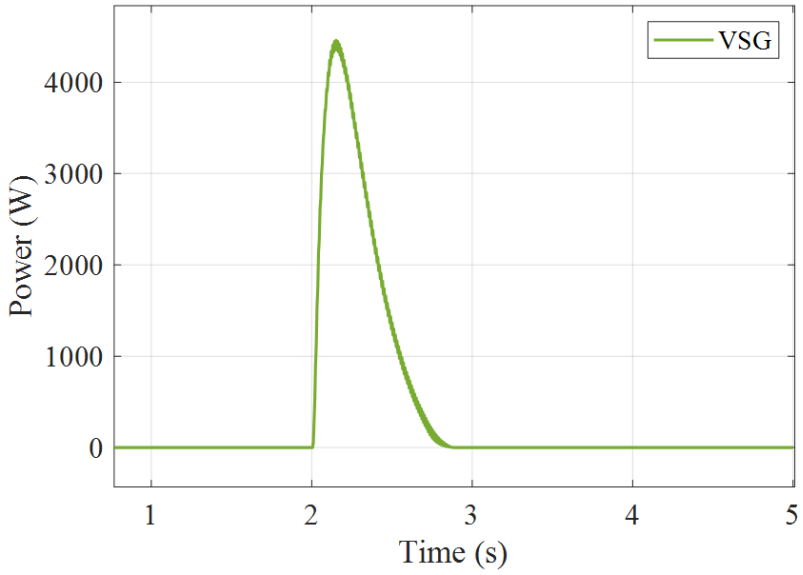

(c)

Figure IV.9: VSG approach: (a) Voltage response of DC-link, (b) ROCOV of DC-link, (c) Power from VSG.

In this simulation, the same power exchange scenario from as in Figure IV.7 is applied. The BESS of MG_2 in the MMG system has been utilized for VSG application.

The simulation results in this case study are shown in Figure IV.9. As can be seen in Figure IV.9 (c), the VSG system has provided power as soon as it detects the variation of the ROCOV values. After 1 second of supplying energy, the VSG system can be rested for the next transition even. By applying this method, similar with the previous simulation scenario, DC voltage nadir and the peak of ROCOV have been reduced, the stability of the whole system is significantly improved.

IV.3.3. Frequencies droop approach

In this case study, only MG_1 and MG_4 are taken into account. MG_1 still control the DC-link and MG_4 still work in P/Q mode. However, it is assumed that, in order to maintain the voltage of DC-link, the MG_1 has reached it limitation, its frequency has fallen into critical value and cannot come back to the standard value. There are two possible solutions: selective frequency droop solution and autonomous frequency droop solution.

With the first approach, by sharing the grid information with MG_4, MG_4 only activate the frequency coordination mode when the frequency of MG_1 drops to a critical value and the input for active power of MG_4 is calculated as in equation (IV.9). In the first case study, the

minimum and maximum values of the frequencies between the two MGs are equal: $f_{1,max}$ = $f_{4,max}$ = 50.2 Hz; $f_{1,min}$=$f_{4,min}$= 49.8 Hz.

The first simulation results are presented in Figure IV.11. At t = 2.5 s and t = 3.5 s, more loads are added into the MG_1, respectively. Thanks to the isolation of DC-link, the disturbances of frequency of MG_1 are not affected to MG_4 in the MMG system. Only when the frequency of MG_1 drop to 49.8 Hz at t = 3.5 s, the frequency coordination mode is activated. Therefore, the load in MG_1 is recognized and shared with MG_4 through ER interface so that the frequency of MG_1 is recovered to an acceptable value.

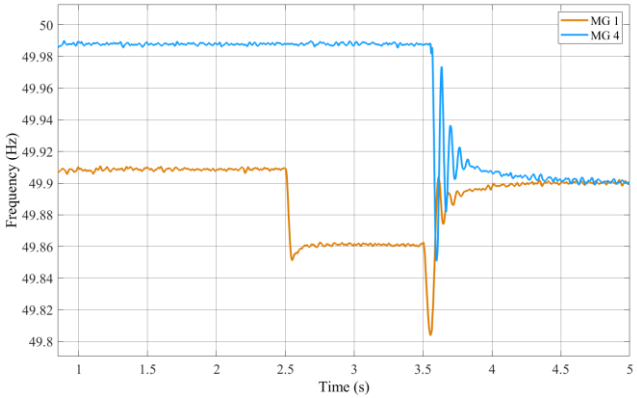

(a)

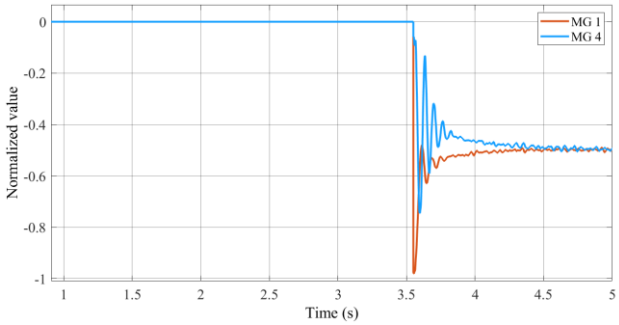

(b)

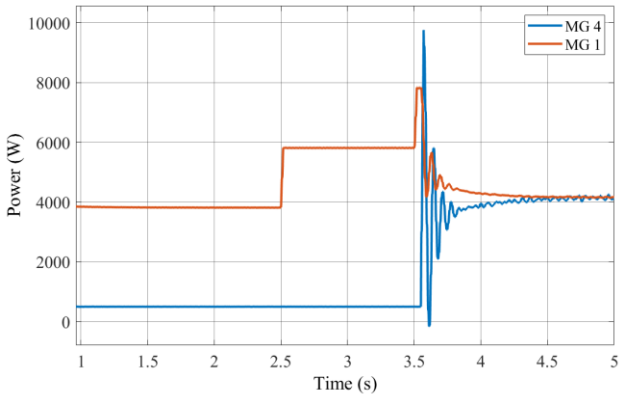

(c)

Figure IV.10: Simulation results with frequency droop method: (a) Frequencies response; (b) Frequency normalized values; (c) Output power of DGs in MGs.

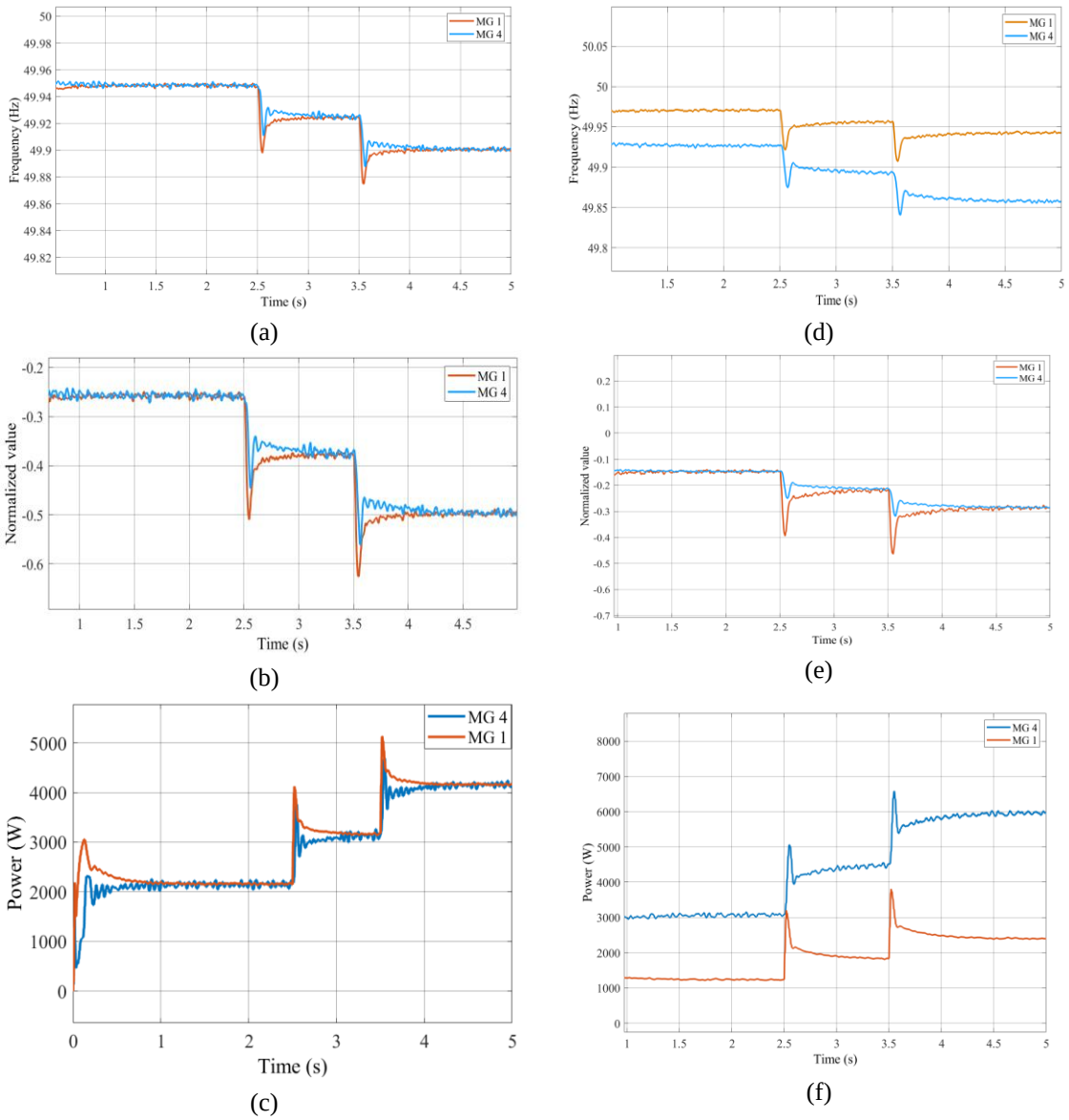

Figure IV.11: Simulation results with autonomous frequency droop method: (a) (d) Frequencies response; (b) (e) Frequency normalized values; (c) (f) Output power of DGs in MGs.

With the autonomous approach, without any communication, the multi-frequency method is automatically applied through the ER interface when there is a variation of frequency in MG_1. Similarity with the previous case study, a 2 kW of load are consecutively added into MG_1 at 2.5 s and 3.5 s.

First of all, the minimum and maximum values of the frequencies between the two MGs are set at the same values. The simulation results for this case are presented in Figure IV.11 (a); (b) and (c). The loads connection in MG_1 results in the decrease of the frequency in both MGs. However, compared to the normal frequency control in MG_1 shown in Figure IV.11 (a), the frequency deviation of MG_1 at t = 2.5 s is much smaller thank to the proposed method. The frequency of the both MGs reaches an equilibrium state when their normalized

values of frequency are equal as in Figure IV.11 (b). Because of the same frequency limitations, the output power of the DGs in both MGs are also equal as in Figure IV.11 (c). This scenario is appropriate in case MG_1 and MG_4 require a same quality of working frequency.

After that, in the next case study, different ranges of frequency are analyzed with this method. The minimum and maximum values of frequency in MG_1 are 49.8 Hz and 50.2 Hz respectively while the minimum and maximum values of frequency in MG_4 are set at 49.5 Hz and 50.5 Hz. The simulation results for this case are presented in Figure IV.11 (d); (e) and (f). In this scenario, only the normalized values of frequency are equal as in Figure IV.11 (e). Due to a more flexible range of frequency, the variation of frequency in MG_4 is higher than MG_1 as in Figure IV.11 (d). Furthermore, the DG in MG_4 is also allowed to provide more power than MG_1 as in Figure IV.11 (f). This scenario is very suitable in case MG_1 require a higher frequency quality than MG_4.

IV.4. Conclusion

In this chapter, an islanded multi-microgrid system with the use of a DC-link based energy router for interconnecting the adjacent microgrid has been presented for stability enhancement analysis. Several approaches have been proposed for supporting the frequencies of multiple MGs. The overall stability of the studied MMG system is presented by the voltage of the DC link. Firstly, it is proved that, with the chosen ER topology, the energy storage in DC-link can be useful in case of power transition. The energy stored in the capacitor of the DC link can contribute to system stability in the same way that the kinetic energy stored in the conventional generator. Furthermore, the concept of VSG in AC domain can be used in DC application for stability support as well. A current source VSG topology is chosen so that the storage system only participates when there is a power fluctuation, which is a benefit for the lifespan of the storage unit. With the AC system, the input signal for the VSG is ROCOF whereas with the DC link, the input signal is ROCOV. Finally, a multi-frequency control approach has been presented for supporting and managing the frequencies in the MMG system. Normally, with the DC interface, the AC MGs in the MMG are isolated with their own frequencies. However, in case of frequency violation, the grid forming unit must be supported and shared the loads. With the ER interface, the frequency deviations of all MG system can be achieved equally with the use of the frequency droop

control strategy. The proposed multi-frequency control has addressed the disadvantage of the single frequency control by compensating for power variation in all MGs. All the presented strategies have been tested with a stand-alone MMG system in MATLAB/Simulink environment. The simulation results have verified the effectiveness of the proposed methods.

CHAPTER V : Graph-based routing algorithm application for energy routers in multi-microgrid system

Contents

V.1. Introduction

The work in this chapter has been published in IEEE Transactions on Industrial Informatics journal since 2020 [122]: "R. Razi, **M. -C. Pham**, A. Hably, S. Bacha, Q. -T. Tran and H. Iman-Eini, "A Novel Graph-Based Routing Algorithm in Residential Multi-microgrid Systems," in *IEEE Transactions on Industrial Informatics*, vol. 17, no. 3, pp. 1774-1784, March 2021, doi: 10.1109/TII.2020.2997516" and it is re-presented in this chapter.

The complementary energy exchange between residential microgrids aims at decreasing the dependence on the main grid, reducing the size and cost of the energy storage units, and increasing energy efficiency. In this regard, the use of an energy router interface to connect the microgrids to the power system is necessary for controlling bidirectional power and data flow, which will build the core of the future Energy Internet (EI). In fact, an energy router is served as an energy exchange center that enables energy flow between microgrids. One of the most important factors in determining multi-microgrid system performance is the energy routing algorithm strategy. Therefore, in this chapter, a new routing algorithm is proposed based on the graph theory. The objective of proposed algorithm is to minimize the overall power losses with respect to congestion and reliability. The best set of loads, optimal sources, and no-congestion minimum loss paths are determined. Various analysis cases have been investigated to confirm the performance and flexibility of the proposed algorithm. A novel case study with multi-sources and multi-loads is addressed, which has not been previously analyzed with the application of energy routers. In addition, the developed algorithm is compared with other existing algorithms in terms of power loss minimization, different scenarios, congestion management, computation time and complexity.

In this chapter, each MG in the MMG system must decide on its strategy to interact with the rest of the system. In this regard, depending on the energy situation, MGs can act as a customer (load) or producer (source) to maintain the energy balance more efficiently in the whole of MMG system. Peer-to-Peer (P2P) energy trading in MMG structure is similar to the information exchange in the internet platform and therefore, it is usually known as the Energy Internet [123]–[125] . In other words, the concept of EI promotes a new revolution of energy trading, which attempts to increase the efficiency of energy dispatch between sources and consumers. The energy router is the key element of the EI [126]. All MGs and

main grid are connected to the MMG system by an energy router interface in order to provide bidirectional power and information flows. The interaction among energy routers can be established with P2P technology based on the multi-agent system (MAS) framework, which can implement distributed energy management in smart grids [127]. An example of an MMG system with ER application for P2P energy trading is shown in Figure V.1. In this structure, the MGs are connected to each other and the main grid through ERs and power lines.

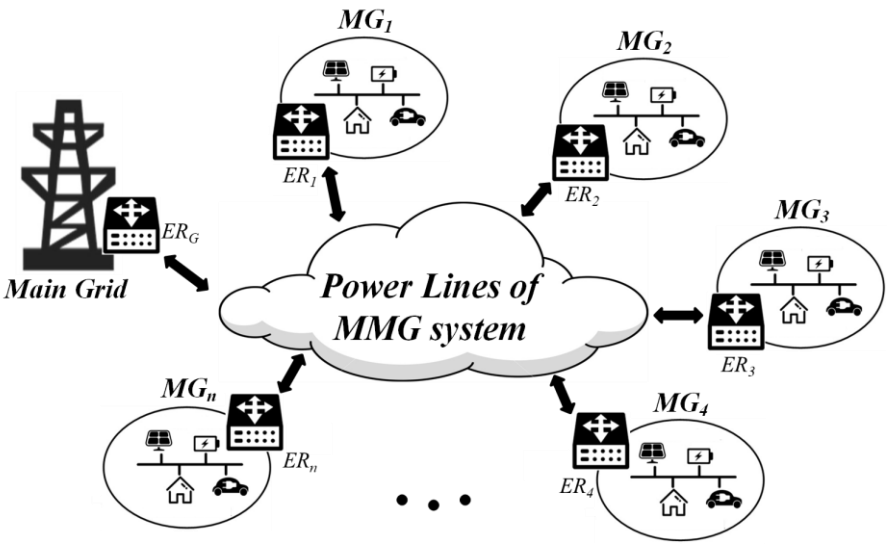

Figure V.1: Overall structure of the MMG system with energy routers [93]

It should be noted that P2P communication links are used between adjacent power routers so that the structure of the communication links is similar to the structure of the power lines. As a result, all power routers get the whole system information through communication links. This information includes the general status of MGs, power lines and energy routers. Noted that each load or source must be considered either as an MG or as part of another MG so that the power lines of the system are free of any other elements. This kind of structure can bring several benefits such as:

- Decrease dependency on the main grid,
- Reduce the cost and size of energy storage units,
- Increase energy efficiency (loss reduction) with an appropriate energy routing algorithm.

The control of the MMG system can be centralized [128], [129] or distributed [130], [131], where each method has its own advantages and disadvantages. However, in most of the existing literature, the key element of MMG systems, i.e. the ERs, has not been considered, which alters the overall topic. Besides, an important method to keep the energy

trading process in MMG stable is the energy routing algorithm strategy, which has attracted much attention in recent years [90], [132]–[140]. In other words, routing is finding efficient transmission paths and it is very critical because it makes the system work well with high stability and efficiency. In [132]–[135], routing algorithms are proposed for electric vehicles (EVs) based EI. In this structure, EVs and charging stations, instead of power lines, are used to exchange energy between MGs [141]–[143]. However, EVs based EI has some obvious limitations such as long time to transfer power and the need for more energy storage units that violate the benefits described earlier.

At present, existing literature shows that routing algorithms are typically designed based on graph theory [90], [136] , [139], [140] or game theory [137], [138]. The objective of graph-based methods is to find the optimal path based on the network graph. In [90] and [139], the lowest-cost path is determined for heavy loads in the energy local area network (e-LAN). In these references, sources and power lines that do not meet the load power are eliminated before the graph traversal, which is the main disadvantage of these methods. In fact, although this technique is used to prevent overflow, the optimal paths may be removed and congestion management is not achieved automatically. In [140], which is implemented by adapting the method of [90], the solution to the congestion problem is to transmit power in pockets. In other words, the remaining power will be transmitted through the sub-optimal minimum loss routing. However, in the mentioned algorithms, the load address is assumed directly, which is not optimized in the presence of different loads simultaneously. In [136], secure energy routing mechanism is designed to defend against cyber-attacks and to transmit information securely, rather than energy losses. Meanwhile, many details are not considered, such as the capacity of ERs and power lines, network topology modification, and power quality issues.

On the other hand, routing algorithms are based on game theory, which mainly addresses subscriber-matching issues [137]. The authors in [137], proposed a two-step method that price based subscriber matching is followed by optimal transmission path calculation. The most significant disadvantage of this method is the need for a central controller that reduces the reliability of the system. An optimal power dispatching is also proposed in [138] that divides the operation of the central energy router into three different functions in a local area packetized-power network (LAPPN). This method, despite the deployment of a suitable subscriber-matching algorithm, does not take into account the cost and it has high complexity.

Motivated by the aforementioned challenges, this chapter develops a new energy routing algorithm with a minimum power losses approach based on graph theory. This work focuses on the multi-sources and multi-loads scenario, which has not been previously addressed in the power management with the application of ERs. In fact, the source refers to a microgrid that has surplus energy and the load is a microgrid with energy shortage. In multi-sources and multi-loads scenario, multiple sources and multiple loads are present simultaneously in the energy routing algorithm. The proposed algorithm can effectively determine the optimal transmission path based on the desired power and capacity of the MGs and network information such as lines availability and their capacity. Furthermore, the algorithm can be easily implemented in any variable structure grid. The main contributions of this chapter can be resumed as follows:

- Implementation of the power loss minimization and congestion management optimally and automatically,
- Considering all sources and loads at the same time to find the minimum loss paths (multi-sources and multi-loads scenario),
- More in-depth analysis and comparison of the performance of the proposed method with other methods.

V.2. Residential multi-microgrid system topology

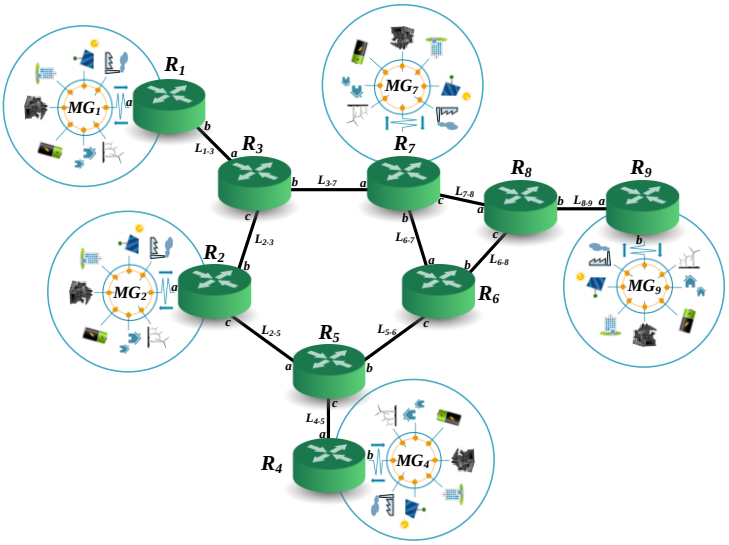

(a)

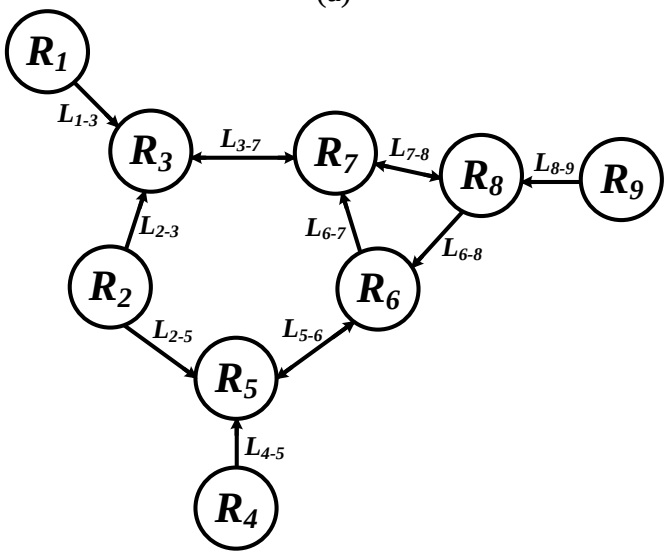

(b)

Figure V.2: (a) Desired structure of the MMG system, (b) Equivalent digraph of the MMG system.

In this chapter, a group of nine residential MGs in a stand-alone MMG system are connected through nine ERs and ten power lines. In fact, each ER represents one MG, which can play a role in power transmission even in the absence of the respective MG. As shown in Figure V.2 (a), the structure of the MMG system shows the position of the ERs, the MGs, and the power lines between them. The shared information, including the detail of the MMG structure and the power output of each microgrid, is stored in the ERs. As soon as the information change is detected, the ER sends them to the adjacent ERs.

At first, a similar structure with [90] is used, so that the proposed algorithm can be compared fairly with other existing algorithms. Table II-1, Table V-2 and Table V-3 list the

MMG system information, which present the power capacity of the elements, the efficiency of the devices, and the impedance of the power lines. In addition, the voltage level in the power lines are assumed 400 VDC. This is a reasonable assumption due to the flexible structure of the ER. Moreover, as the energy situation assumption in MGs in Table II-1, the corresponding energy direction of the DC transmission lines are deduced in Table V-3.

The equivalent digraph of the desired structure or the corresponding communication topology is shown in Figure V.2 (b). As can be seen, the structure model is described using a graph G (u, v). The ERs form the nodes set u = {R_1, R_2, … R_n} and power lines form the edges set v = {L_{i-j}, …}; where L_{i-j} is the power line between R_i and R_j. Two nodes i and j are adjacent if $L_{i-j} \in v$.

According to Table II-1, MG_7 requires 22 kW, while there are four different sources. Using the graph model, it is seen in Figure V.3 that there is only one path from MG_1 and MG_4 to the MG_7, while two optional paths are found for MG_2 and MG_9.

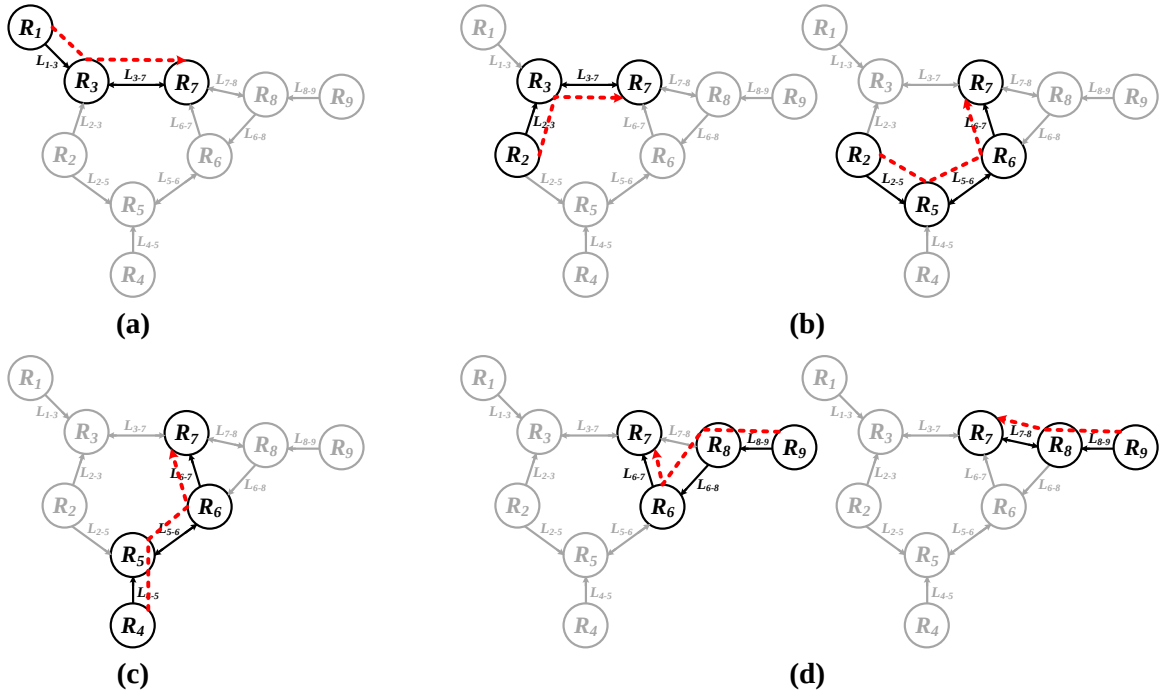

Figure V.3: Different paths to MG_7 from (a) MG_1, (b) MG_2, (c) MG_4, (d) MG_9.

Table V-1: Multi – microgrid system parameters

Microgrid	Energy situation	Total power (kW)	Available power (kW)	Efficiency (%)
MG_1	Surplus	6.0	5.5	96
MG_2	Surplus	12.0	9.2	95
MG_4	Surplus	5.0	4.0	100

MG_7	Deficit	22.0	22.0	100
MG_9	Surplus	14.0	10.9	96

Table V-2: Energy routers parameters

Energy router	Port	Total power (kW)	Available power (kW)	Efficiency (%)
R_1	a	20	19.5	100
	b	15	9	98
R_2	a	15	12.2	97
	b	15	14	98
	c	15	13	98
R_3	a	18	12	100
	b	15	14	98
	c	15	15	100
R_4	a	15	9	98
	b	10	9	100
R_5	a	15	13	100
	b	18	12	98
	c	15	15	100
R_6	a	20	20	98
	b	20	20	100
	c	18	18	100
R_7	a	25	25	100
	b	20	20	100
	c	25	23	100
	d	25	25	100
R_8	a	20	18	98
	b	20	20	100
	c	18	12	98
R_9	a	20	14	98
	b	20	16.9	100

Table V-3: Multi – microgrid DC transmission lines parameters

Transmission line	Direction	Total power (kW)	Available power (kW)	r (Ω)
L_{1-3}	unidirectional	30	24	0.6
L_{2-3}	unidirectional	20	19	0.64
L_{2-5}	unidirectional	20	20	0.51
L_{3-7}	bidirectional	45	45	0.94
L_{4-5}	unidirectional	24	18	0.19
L_{5-6}	bidirectional	20	20	0.45
L_{6-7}	unidirectional	40	40	0.24
L_{6-8}	unidirectional	30	30	0.21

L_{7-8}	bidirectional	30	30	0.21
L_{8-9}	unidirectional	32	26	0.60

V.3. Proposed routing algorithm for energy routers

Obviously, applying a distributed energy routing algorithm based on ER is necessary for MMG system topology [144]. Due to the structure of the MMG system, certain requirements must be considered in the routing algorithm [145]. For example, the dynamic routing protocol must ensure the balance between producer and consumer actors, even in the case of the network structure change. In addition, for a certain load, the specific number of sources is not defined, but it is better to have the lowest possible number of involved sources to improve energy security and system reliability [146]. In fact, fewer elements in energy routing can reduce the possibility of error or threat. The rest of sources are reserved in the system. Assuming this strategy, the set with the lowest number of sources is chosen in the proposed algorithm, even though it has more losses. In such systems, the hierarchical control methods are typically used including primary, secondary and tertiary control levels that differ in the response time scale. Energy management for loss reduction, cost optimization or environmental benefits is accomplished in tertiary level, which has a very slow time response (about a few minutes). Also, it is assumed that a real-time transaction based on matchmaking tradeoff competition mechanism is performed, as a result, the most economical set of loads and resources are selected [147].

In this chapter, the focus of the proposed routing algorithm is to minimize power losses with respect to the number of involved sources. In other words, the optimal path for power transmission is determined by the minimum power losses index, and as long as one source has production capacity, another source is not included in the routing algorithm unless it is restricted by another constraint. As mentioned earlier, some studies with similar goals have proposed different routing algorithms but proposed solutions are not optimal (minimum loss) and not general (different scenarios).

Firstly, power losses in an MMG system consist of two major components, including ERs losses (W_i) and power lines losses (W_{i-j}). The loss of ERs depends on the transferred power from each router. For simplicity, the efficiency of power electronic converters is measured in nominal power and it is assumed constant. As a result, the total loss of an ER is a linear function of the transferred power:

$$W_i = \left[(1 - eff_{i-port}) + (1 - eff_{o-port})\right] \times P_i \quad \text{(V.1)}$$

where $eff_{i\text{-}port}$, $eff_{o\text{-}port}$ and P_i indicate the input port efficiency, the output port efficiency, and the transferred power of the ER (R_i), respectively.

On the other hand, the power line losses are only related to the active power in dc or low-voltage ac lines structure. So, the power line losses are calculated as follows:

$$W_{i-j} = \left(\frac{r_{i-j}}{V_{i-j}^2}\right) \times P_{i-j}^2 \quad \text{(V.2)}$$

where $r_{i\text{-}j}$, $V_{i\text{-}j}$ and $P_{i\text{-}j}$ are impedance, voltage and transferred power of power line $L_{i\text{-}j}$, respectively. As can be seen in Equation (V.2), power line losses have a nonlinear relation with transferred power. In fact, the above is not valid for lines with an occupied capacity. Therefore, this equation can be improved as follows:

$$\Delta W_{i-j} = \frac{r_{i-j}}{V_{i-j}^2} \times \left((\Delta P_{i-j} + P_{i-j}^{old})^2 - (P_{i-j}^{old})^2\right) \quad \text{(V.3)}$$

where $\Delta P_{i\text{-}j}$ and P_{i-j}^{old} are added transmitting power and already existing power, respectively. Therefore, the total losses of a route between a specified pair of source and load can be defined as the total losses of ERs and power lines along the transmission paths:

$$W_{total} = \sum_{R_i \in path} \Delta W_i + \sum_{L_{i-j} \in path} \Delta W_{i-j} \quad \text{(V.4)}$$

However, there may be multiple sources, multiple loads, or even different paths at the same time. Consequently, the objective function C, which is described Equation (V.5), will try to minimize the losses of the system under constraints Equation (V.6)-(V.9):

$$min\, C = \sum_{P \in paths} W_{total}^P \quad \text{(V.5)}$$

$$\sum P_{Load} = \sum P_{Source} \quad \text{(V.6)}$$

$$P_{exchange} \leq P_{lines(S \to L)}^{available} \quad \text{(V.7)}$$

$$P_{exchange} \leq P_{source}^{available} \quad \text{(V.8)}$$

$$P_{exchange} \geq W_{total} \quad \text{(V.9)}$$

$$V_{i-min} \leq V_i \leq V_{i-max} \quad \text{(V.10)}$$

where $P_{exchange}$, $P_{lines}^{available}$ and $P_{source}^{available}$ represent the power exchanged between a specified source-load pair in the system, the available capacity of the lines and the available capacity of the source, respectively. So, the losses cost is formulated as a function of the physical characteristics of the MMG system. It should be noted that power losses should also be included in Equation (V.6). In this case, due to the uncertainty of the power losses initially, the energy routing equations can only be solved recursively, which increases the complexity and volume of the calculations substantially. The literature has simply gone from considering losses into the power equilibrium equations.

Following that, in the next stage, the objective function is implemented using the proposed routing algorithm, which its flowchart with the example shown in Figure V.4. In this algorithm, the MGs with surplus energy are considered as sources and others with deficit energy are regarded as loads. The rest of the MGs operate separately from the MMG and do not have any energy exchanges with the system. The algorithm in accordance with Figure V.4 consists of ten steps that are presented below:

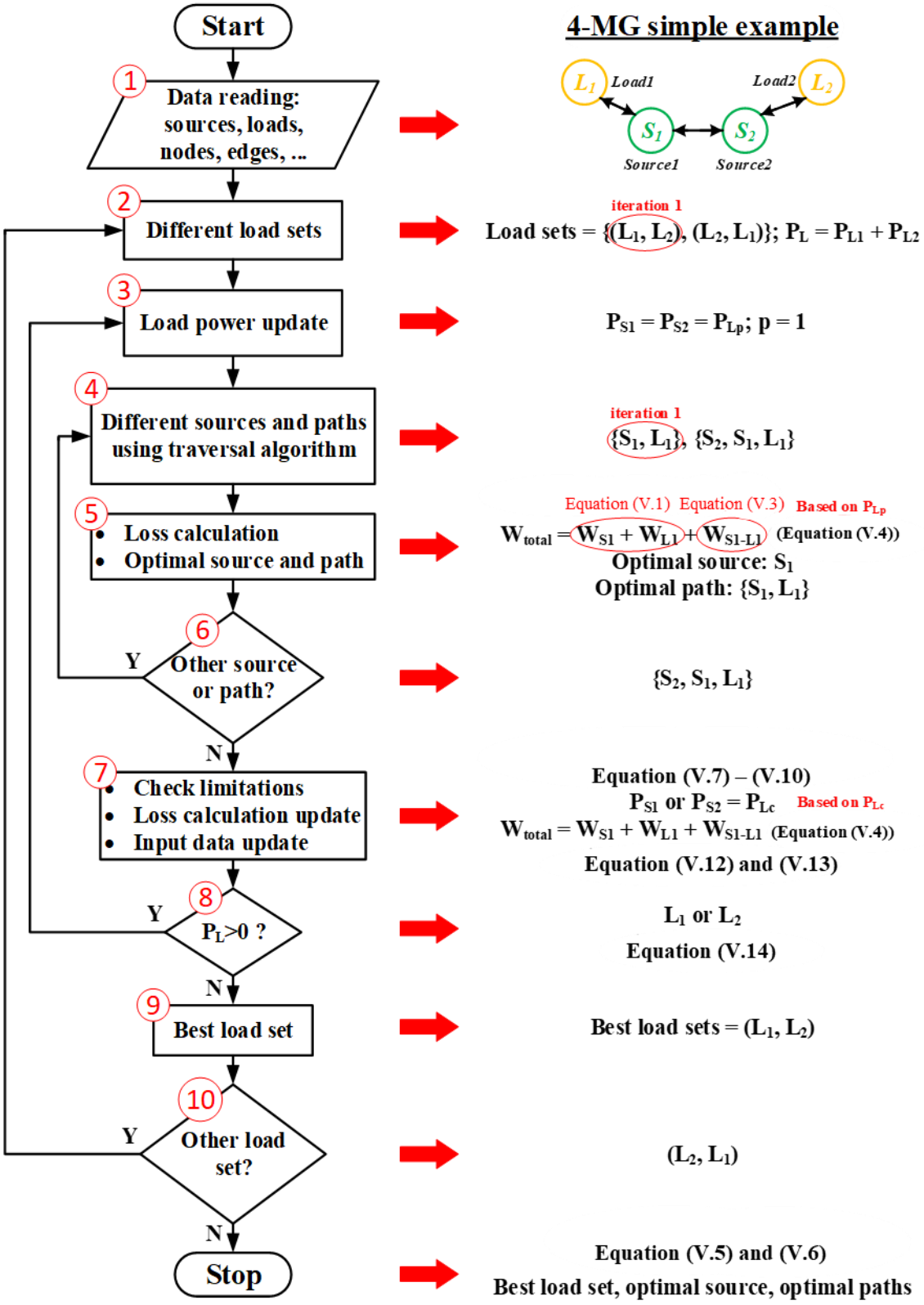

Figure V.4: Flow chart of the proposed routing algorithm for energy routers application.

Step 1. Firstly, ERs perform reading and storing data. In fact, the amount of shortage or excess power of each MG and the MMG system information from Table II-1,Table

V-2 and Table V-3 are sent to all ERs by using the P2P communication links of adjacent routers.

Step 2. With *N* different loads in the MMG system, the number of load sets with the assuming specific priorities is:

$$Q_{load} = N! \tag{V.11}$$

The routing algorithm should feed all loads but priority of loads can affect power line losses or problem constraints. Thus, all sets are analyzed so that one set is selected each time this step is repeated (only in multi-loads scenarios).

Step 3. In the load set, which is selected in the previous step, the load with the highest priority (P_{Lp}) is assumed as the output power of all sources. In fact, an equal amount of power is defined for all sources to be a proper criterion for comparing them.

Step 4. All the possible power transmission paths between the available sources and the high priority load are obtained using depth-first search traversal algorithm; in which one of paths is considered.

Step 5. Next, by using Equations (V.1) and Equations (V.3), power losses are calculated for the chosen source and path. Then, the optimal source and path are updated if the power losses of desired state are lower than the previous value.

Step 6. If there is another source or path in step 4, the algorithm will return to **Step 4**. In fact, checking all the sources and paths will continue to obtain the minimum power losses in the presence of high priority load.

Step 7. All constraints of the selected source and path, such as the capacity of source, ERs, and power lines, are checked up to prevent the MMG system from congestion and failures. If any of the constraint is activated, the relevant losses and system information will be updated with new transmission power (P_{LC}). Then, the input information of the sources and lines are also updated according to total pre-existing power as follows:

$$P_{lines(S\to L)}^{available} = P_{lines(S\to L)}^{available} - min(P_{Lp}, P_{Lc}) \tag{V.12}$$

$$P_{source}^{available} = P_{source}^{available} - min(P_{Lp}, P_{Lc}) \tag{V.13}$$

Step 8. If the selected source and path does not meet the total load, the load power (P_L) is updated and goes back to **Step 3** again. This process continues until the total load power is satisfied.

$$P_L = P_L - min(P_{Lp}, P_{Lc}) \quad \text{(V.14)}$$

Step 9. By comparing the result of the current load set with the previous ones, the best load set is updated with the lowest total cost (only in multi-loads scenarios).

Step 10. Lastly, if there is another load set, the algorithm returns to **Step 2**. Otherwise, the optimal path and sources are presented in this final step (Equations (V.5) is obtained).

Therefore, the appropriate match between suppliers and consumers with the best load set, the best sources and no-congestion minimum loss paths for power transmission are determined. In addition, the limitations of power transfer from source to load are considered. Also, in this algorithm, unlike data packet routing, a single source can simultaneously transmit power to multiple loads and a single load can receive power from multiple sources at the same time (many-to-many scenario). A detailed analysis of these issues is presented in the next section.

V.4. Simulation and discussion

In this section, several analysis cases based on MATLAB software are carried out to confirm the performance of the proposed routing algorithm. Also, a comparison with existing routing algorithms is conducted to verify the superiority of the proposed algorithm.

V.4.1. Small microgrids system structure

In the first part of this section, a MMG system with 9 MGs shown in Figure V.2 is utilized for validating the proposed routing method.

V.4.1.a. Case analysis 1: Heavy load feeding

According to Table II-1, in this case, it is assumed that there are four surplus-energy MGs that must supply 22 kW power demand by MG_7. In fact, the EV power charger can be up to 22 kW according to the European EV charging standard IEC 61851 [148]. In this case, MG_7 requests the required power from other MGs by the ER R_7. A MG with surplus energy can be considered as a “source” and a MG with deficit energy can be considered as a “load”. The other MGs not participating in energy exchange scenario are considered to be working in virtual islanded mode.

Different optional paths from other MGs to the microgrid MG_7 are found out after graph traversal in simulation as shown in Figure V.5:

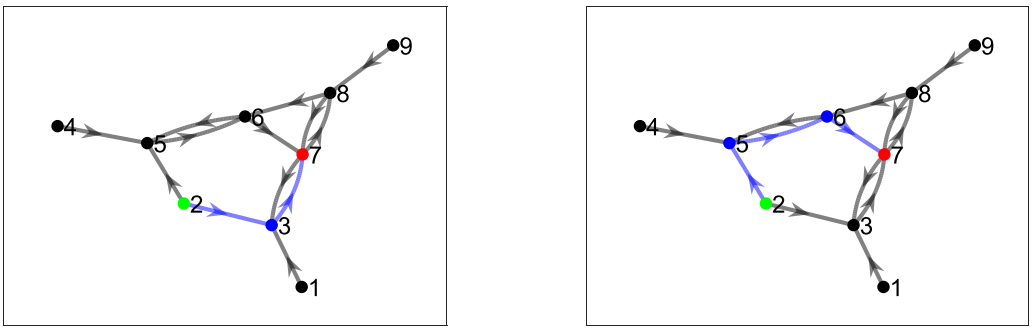

(a) Energy paths from source 2

$$path\ 1\ (MG_2 \longmapsto MG_7) \coloneqq MG_2 \equiv R_2, R_3, R_7 \equiv MG_7$$

$$path\ 2\ (MG_2 \longmapsto MG_7) \coloneqq MG_2 \equiv R_2, R_5, R_6, R_7 \equiv MG_7$$

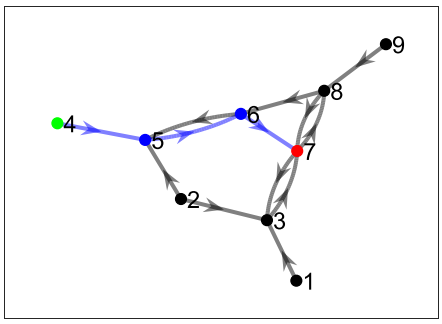

(b) Energy path from source 4

$$path\ 1\ (MG_4 \longmapsto MG_7) \coloneqq MG_4 \equiv R_4, R_5, R_6, R_7 \equiv MG_7$$

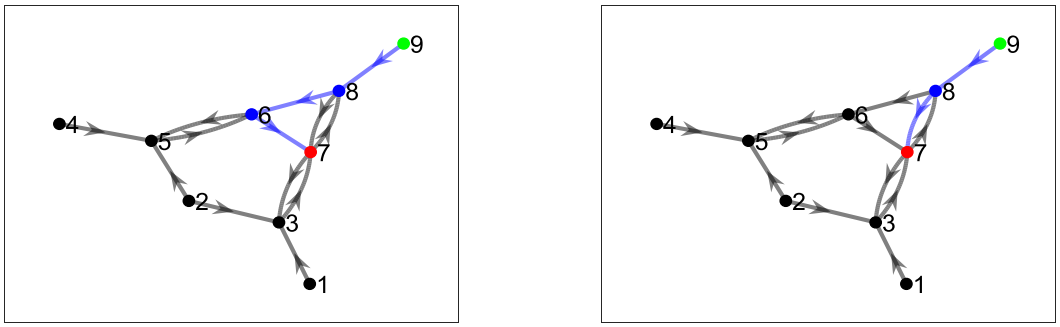

(c) Energy paths from source 9

$$path\ 1\ (MG_9 \longmapsto MG_7) \coloneqq MG_9 \equiv R_9, R_8, R_6, R_7 \equiv MG_7$$

$$path\ 2\ (MG_9 \longmapsto MG_7) \coloneqq MG_9 \equiv R_9, R_8, R_7 \equiv MG_7$$

Figure V.5: Different paths from MGs with surplus energy to MG$_7$ with deficit energy from MATLAB simulation results.

By applying the proposed routing algorithm, the calculation results including selected sources and paths, transmission power and power losses are shown in Table V-4 and Figure V.6.

Table V-4: Simulation results for case analysis 1 (Heavy load feeding)

Priority	Source	Path (num.)	Power (kW)	Node loss (kW)	Edge loss (kW)	Total loss (kW)
1	MG_4	4, 5, 6, 7 (1)	4.0	0.240	0.145	0.385
2	MG_9	9, 8, 7 (2)	10.9	0.436	0.1092	0.1528
3	MG_2	2, 3, 7 (1)	7.1	0.497	0.5546	0.10516
Total			22	1.173	1.17916	2.9646

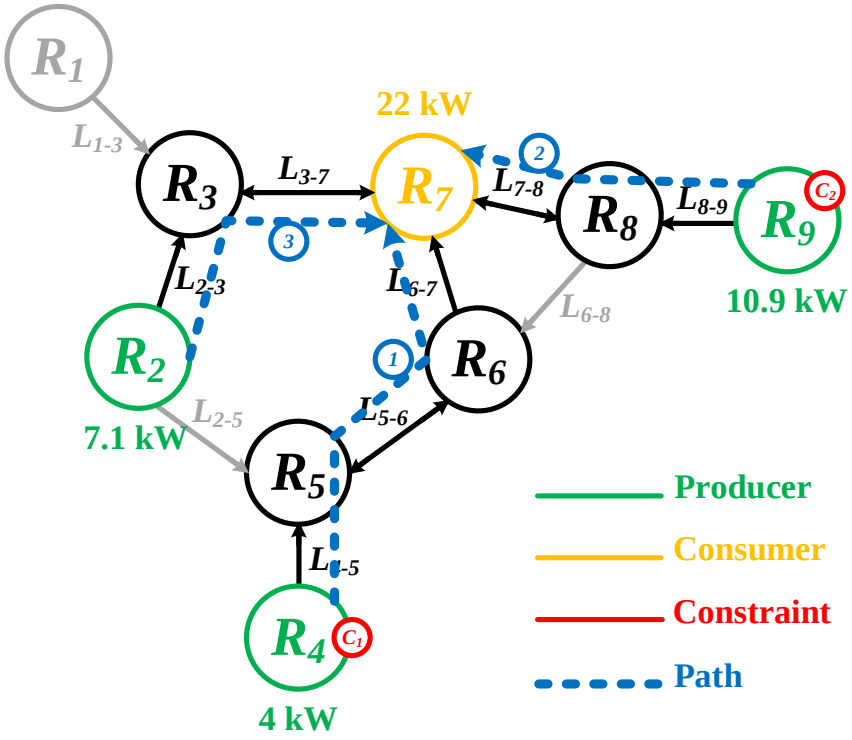

Figure V.6: Simulation results of case analysis 1.

From this table, it is concluded that for 22 kW load in MG_7, the only available path between MG_4 and MG_7, {R_4, R_5, R_6, R_7}, has the lowest cost. After that, the second path from MG_9, {R_9, R_8, R_7}, is the second priority. Finally, the remaining load capacity is provided by the first path of MG_2, {R_2, R_3, R_7}.

Here, MG_4 and MG_9 are limited to their maximum production. The total loss, in this case, is 2.9646 kW. In accordance with the energy routing algorithms in [90] and [136], with similar parameters, the power losses are 3.452 kW and 3.821 kW, respectively, which are about 16% and 29% higher than the proposed routing algorithm.

V.4.1.b. Case analysis 2: Congestion management

In high-power conditions, overflow may occur in some critical power lines, which results in serious consequences. As another simulation case, it is assumed that the capacity of power lines $L_{7\text{-}8}$ and $L_{6\text{-}7}$ is limited to 5 kW and 7.5 kW, respectively. By applying the proposed algorithm to the desired structure, Table V-5 and Figure V.7 show the calculation results for this case.

Table V-5: Simulation results for case analysis 2 (Congestion management)

Priority	Source	Path (num.)	Power (kW)	Node loss (kW)	Edge loss (kW)	Total loss (kW)
1	MG_4	4, 5, 6, 7 (1)	4.0	0.240	0.145	0.385
2	MG_9	9, 8, 7 (2)	5.0	0.200	0.3516	0.5516
3	MG_2	2, 3, 7 (1)	9.2	0.644	0.9094	1.5534
4	MG_9	9, 8, 6, 7 (1)	3.5	0.410	0.7627	1.1727
5	MG_1	1, 3, 7 (1)	0.3	0.012	0.0468	0.0588
Total			22	1.506	2.2155	3.7215

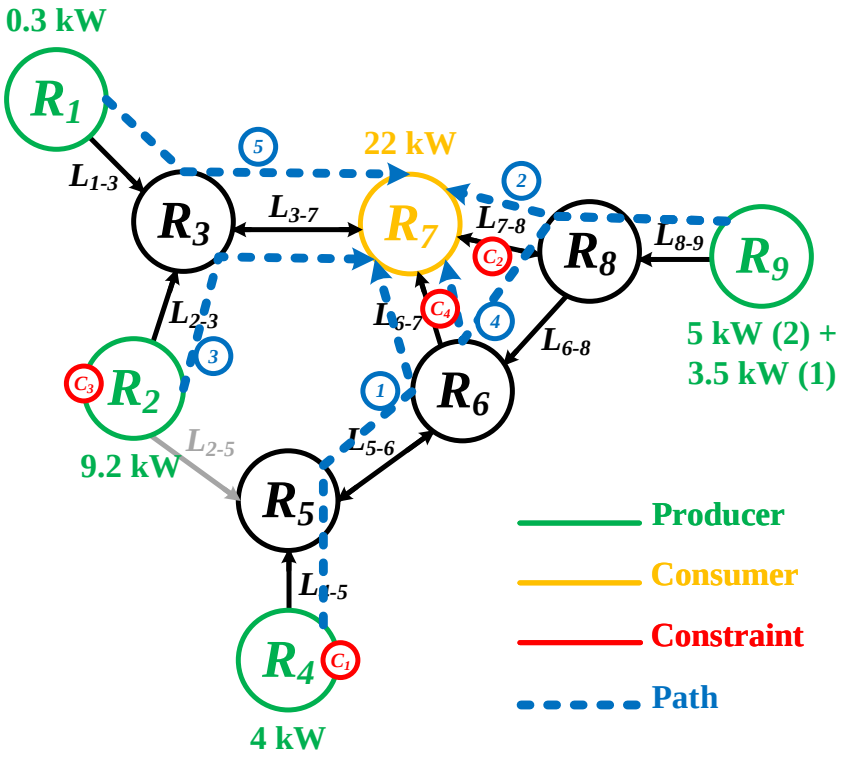

Figure V.7: Simulation result of case analysis 2.

Compared to the previous case analysis, it can be found that although the load power does not change, the capacity of the power lines $L_{7\text{-}8}$ and $L_{6\text{-}7}$ reach their maximum. Therefore, other paths with more losses replace them, and as a result, the total cost of the

system has increased. The best path from MG_4 is being used without any changes, but the second priority is capped by capacity limitation of power line L_{7-8}. Also, in the fourth priority, power line L_{6-7} reaches its maximum, and inevitably the MG_1 also enters the routing.

However, to avoid overflow as in [90], a screening process is performed. In this regard, elements that do not meet the power demand rate are eliminated from the algorithm, resulting in more losses and calculations.

V.4.1.c. Case analysis 3: Multi-sources and multi-loads (MSML)

Unlike other existing algorithms, the proposed routing algorithm is valid to manage power transmission for more than a single load. In other words, the MSML scenario can be divided into several multi-sources and single-load (MSSL) or single-source and multi-loads (SSML) scenarios. Nevertheless, the response of routing algorithm to the MSML scenario can be better than the sum of other scenarios because it covers more states. In fact, in the case of MSML scenario, there are other steps in the proposed routing algorithm, which determine each source should feed what loads and from what paths to minimize the power losses of system. In this case, the imaginary priority of loads is important for calculating power losses and choosing the best paths. In this regard, as stated earlier, all sets of loads priority are considered and the set with the least losses will be selected. For this study, three MGs, i.e. MG_3, MG_6 and MG_7 are considered with power demands of 2 kW, 5 kW and 8 kW, respectively. Following Equation (V.11), there are six different priority sets for loads as {(7-6-3), (7-3-6), (6-7-3), (6-3-7), (3-7-6), (3-6-7)}. The calculation results for various sets are presented in Table V-6. As it can be seen, three different sets {(7-6-3), (7-3-6), (3-7-6)} have lower power losses than other sets.

Table V-6: Comparison of sources set in case analysis 3 (MSML)

Set number	Set	Node loss (W)	Edge loss (W)	Total loss (W)
1	7-6-3	850	700.5	1550.5
2	7-3-6	850	700.5	1550.5
3	6-7-3	620	947.1	1567.1
4	6-3-7	620	947.1	1567.1
5	3-7-6	850	700.5	1550.5
6	3-6-7	620	947.1	1567.1

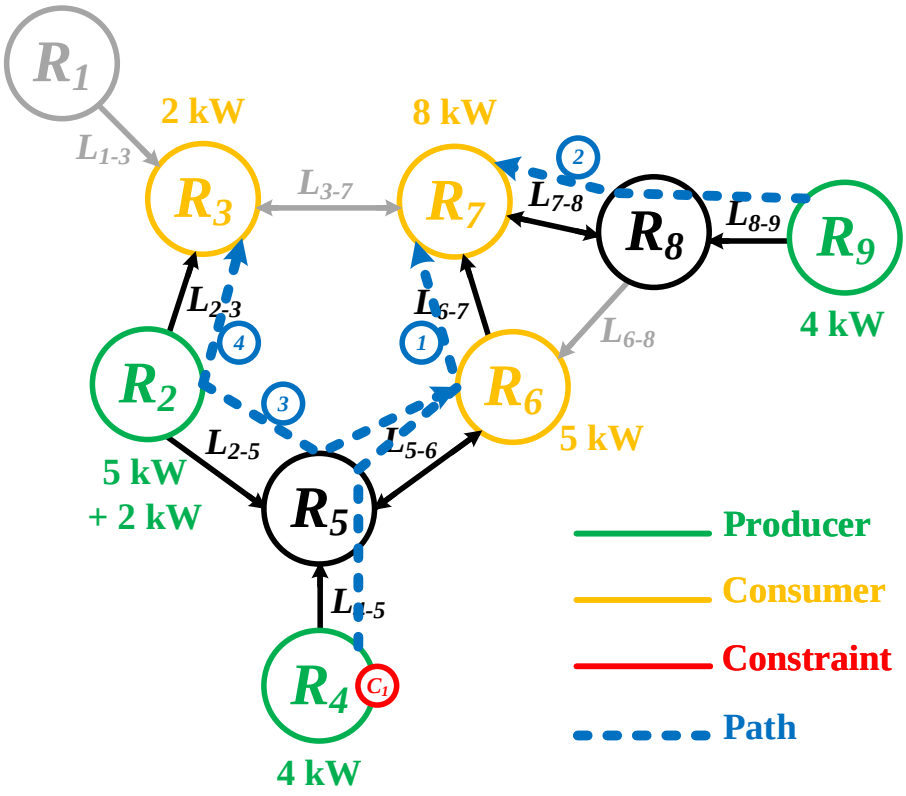

Figure V.8: Simulation result of case analysis 3.

The selected paths for the set 1 {(7-6-3)} are presented in Table V-7 and Figure V.8.

Table V-7: Simulation results for set 7-6-3 in case analysis 3 (MSML)

Priority	Load	Power demand (kW)	Source	Power supply (kW)	Best rout
1	MG_7	8	MG_4	4	4-5-6-7
			MG_9	4	9-8-7
2	MG_6	5	MG_2	5	2-5-6
3	MG_3	2	MG_2	2	2-3

V.4.1.d. Case analysis 4: Energy security and reliability

In this scenario, the importance of energy security and reliability are verified for the number of effective sources in the energy routers routing algorithm. As stated above, the purpose of the developed routing algorithm is to provide energy with the least power losses and employing involved sources. Now it is assumed that in case analysis 1, the surplus power of the MG_4 is limited to 5 kW.

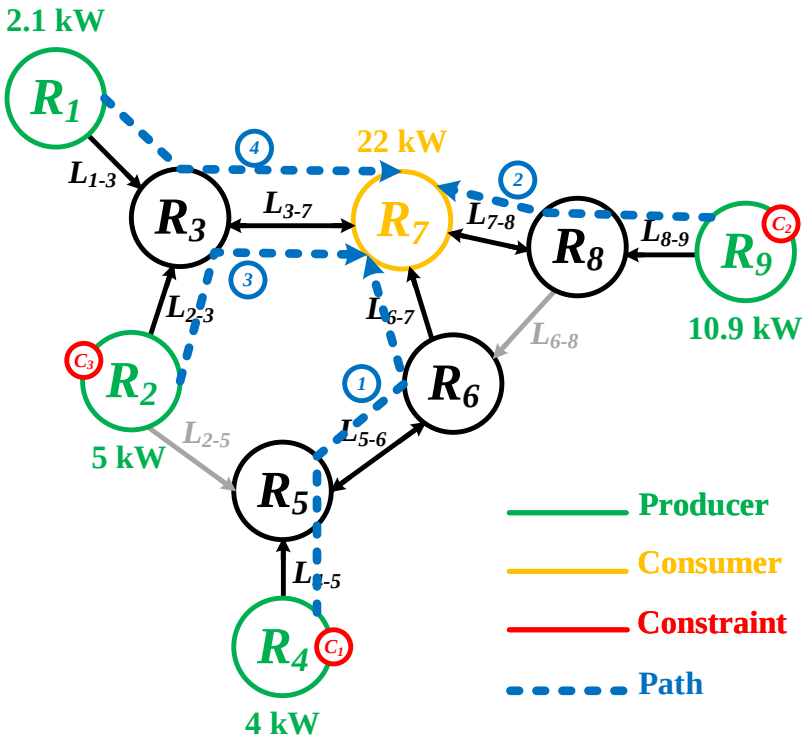

Figure V.9: Simulation result of case analysis 4.

As shown in Table V-8 and Figure V.9, the number of sources increases, and despite the limitations (restriction on the MG_4), the total cost of the system is reduced. These results clearly indicate that energy routing with lower losses is possible in Case Analysis 1, but the proposed algorithm prefers the presence of three sources to four sources. Although the reduction of system losses is not significant, the importance of energy security is shown in comparison with the system losses. In fact, in the usual case, the algorithm attempts to use a source that has not reached maximum power in order to decrease the complexity of energy routing selection and increase the reliability of the system.

Table V-8: Simulation results for case analysis 4 (MSML)

Priority	Source	Path (num.)	Power (kW)	Node loss (kW)	Edge loss (kW)	Total loss (kW)
1	MG_4	4, 5, 6, 7 (1)	4	0.240	0.145	0.385
2	MG_9	9, 8, 7 (2)	10.9	0.436	1.092	1.528
3	MG_2	2, 3, 7 (1)	5	0.350	0.287	0.637
4	MG_1	1, 3, 7 (1)	2.1	0.084	0.260	0.344
Total			22	1.110	1.784	2.894

Of course, in applying this strategy, a tradeoff can be made with the amount of loss that depends on the operator's decision. For example, if the losses related to set with more sources have n (%) reduction compared to other sets, the reliability constraint is ignored. In this structure, it is not reasonable to ignore the reliability and security constraints for a loss reduction of 70.4 W (2.4%).

V.4.2. Large microgrids system structure

In this section, the 30-MG model shown in Figure V.10 is considered for further analysis and to confirm the effectiveness of the proposed algorithm compared to [140]. The modified IEEE 30-node system is too complicated and meshed that is not usually available for a low-voltage MMG system. However, this topology is still investigated to show the performance of the routing algorithm for a larger and more complex MMG system. Also, the parameters are presented in Table V-9, Table V-10 and. In this structure, there are two surplus-energy MGs and three MGs with energy shortage. The results of the proposed routing algorithm are shown in Table V-12.

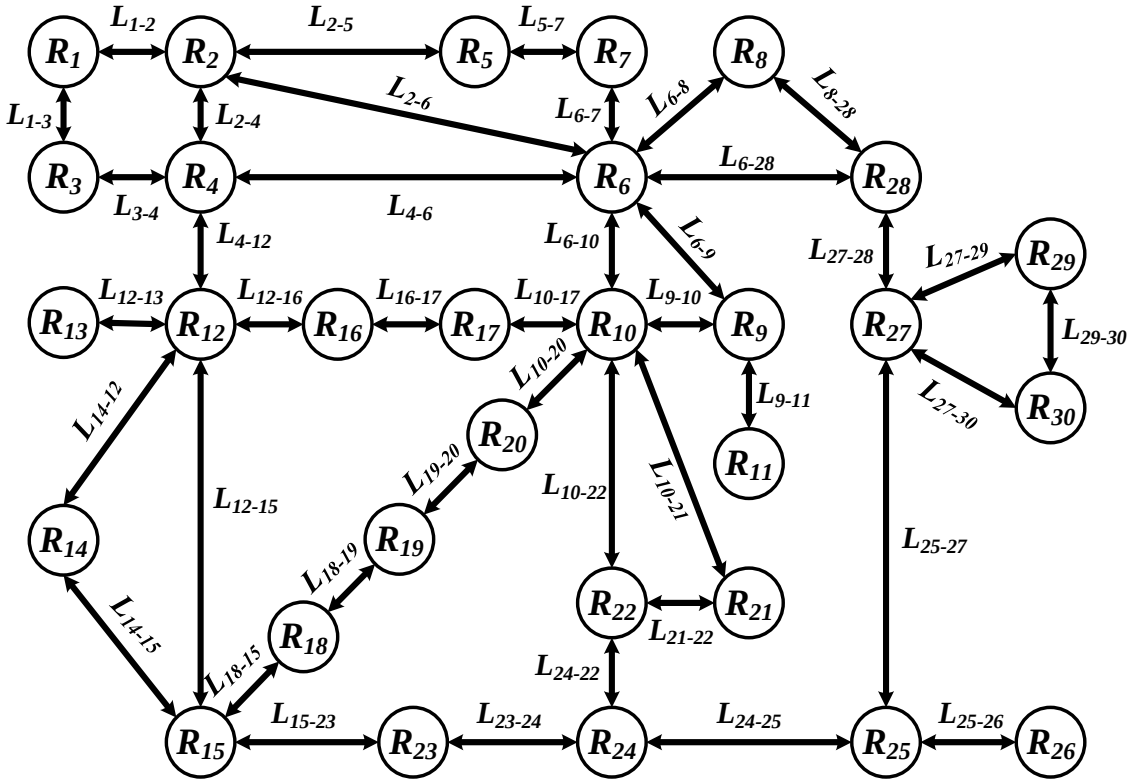

Figure V.10: Equivalent digraph of the modified 30-MGs system [140].

Table V-9: Multi – microgrid system parameters

Microgrid	Energy situation	Available power (MW)	Efficiency (%)
MG_2	Surplus	40	100
MG_8	Deficit	15	100
MG_{16}	Deficit	5	100
MG_{17}	Deficit	20	100
MG_{22}	Surplus	10	100

Table V-10: Energy routers parameters

Energy router	Available power (MW)	Efficiency (%)	Energy router	Available power (MW)	Efficiency (%)
R_1	130	98	R_{16}	32	98
R_2	130	99	R_{17}	32	97
R_3	130	98	R_{18}	16	98
R_4	130	97	R_{19}	32	99
R_5	130	99	R_{20}	32	98
R_6	130	98	R_{21}	32	99
R_7	130	98	R_{22}	32	97
R_8	32	99	R_{23}	16	99
R_9	65	98	R_{24}	16	98
R_{10}	65	97	R_{25}	16	99
R_{11}	65	99	R_{26}	16	97
R_{12}	65	98	R_{27}	65	99
R_{13}	65	98	R_{28}	65	98
R_{14}	32	99	R_{29}	16	99
R_{15}	32	99	R_{30}	16	98

Table V-11: Multi – microgrid DC transmission lines parameters

Line	Available power (MW)	Voltage (kV)	r (Ω)	Line	Available power (MW)	Voltage (kV)	r (Ω)
L_{1-2}	50	20	0.0192	L_{12-13}	65	33	0
L_{1-3}	60	20	0.0452	L_{12-14}	32	33	0.1231
L_{2-4}	25	20	0.0570	L_{12-15}	32	33	0.0662

L_{2-5}	32	20	0.0472	L_{12-16}	32	33	0.0945
L_{2-6}	25	20	0.0581	L_{14-15}	16	33	0.2210
L_{3-4}	40	20	0.0132	L_{15-18}	16	33	0.1073
L_{4-6}	25	20	0.0119	L_{15-23}	16	33	0.1000
L_{4-12}	65	20	0	L_{16-17}	16	33	0.0524
L_{5-7}	70	20	0.0460	L_{18-19}	16	33	0.0639
L_{6-7}	60	20	0.0267	L_{19-20}	32	33	0.0340
L_{6-8}	20	20	0.0120	L_{21-22}	16	33	0.0116
L_{6-9}	65	20	0	L_{22-24}	16	33	0.1150
L_{6-10}	32	20	0	L_{23-24}	16	33	0.1320
L_{6-28}	32	20	0.0169	L_{24-25}	16	33	0.1885
L_{8-28}	32	20	0.0636	L_{25-26}	16	33	0.2544
L_{9-10}	65	33	0	L_{25-27}	16	33	0.1093
L_{9-11}	65	11	0	L_{27-28}	65	20	0
L_{10-17}	32	33	0.0324	L_{27-29}	16	33	0.2198
L_{10-20}	32	33	0.0936	L_{27-30}	16	33	0.3202
L_{10-21}	32	33	0.0348	L_{29-30}	16	33	0.2399
L_{10-22}	32	33	0.0727				

Table V-12: Simulation results for 30-MGs system structure

Priority	Source	Path (num.)	Power (MW)	Node loss (MW)	Edge loss (MW)	Total loss (MW)
1	MG_2	2, 6, 8	15	0.6	0.0394	0.6394
2	MG_2	2, 6, 10, 17	10	0.9	0.0670	0.9670
3	MG_{22}	22, 10, 17	10	0.9	0.0097	0.9097
4	MG_2	2, 4, 12, 16	5	0.4	0.0057	0.4057
Total			40	2.8	0.1218	2.9218

In the first priority, MG_8 is fed by MG_2 through MG_6 at the lowest cost. After that, the power required by MG_{17} is also provided by MG_2, but the capacity limitation of power line L_{2-6} prevents providing this power completely. In fact, the capacity of line L_{2-6} is 25 MW, which the first priority has occupied 15 MW and the available capacity turns to be 10 MW. Therefore, in the third priority, another path ($\{R_{22}, R_{10}, R_{17}\}$) and MG_{22} provide the remained power of MG_{17} optimally. Finally, again, MG_2 satisfies the last MG with the proper path. The paths and power exchange obtained in the third and fourth priorities of this algorithm

are different from [140]. In other words, the proposed algorithm reduces power losses from 3.236 MW to 2.9218 MW (about 10%) by choosing better paths.

V.4.3. Performance evaluation

Table V-13: Performance comparison of different energy routers routing algorithms

Method / Feature	**E-LAN graph theory based method [90]**	**Secure based graph theory method** [136]	**Biased min-consensus based method** [139]	**Real-time transaction based method** [140]	**Proposed method**
Power loss minimization	Fair	Poor	Fair	Good	Excellent
MSML scenario	Not applicable	Not applicable	Not applicable	Not applicable	Applicable
MSSL scenario	Applicable	Applicable	Applicable	Not applicable	Applicable
Congestion management	Poor	Fair	Poor	Good	Good
Computation time	Medium	Medium	Low	High	Medium
Complexity	Medium	Low	High	High	Medium
Main limitation	Non-optimal congestion management	Loss minimization is not the main objective	High Complexity	Specify transactions between sources and loads	Considerable computation time for large systems

In order to emphasize the features and contributions of the proposed method, a rough comparison between the proposed routing algorithm and some recently published methods is shown in Table V-13. All strategies are based on graph theory and mainly are aimed at reducing the overall power losses in the MMG system via smart energy routing. The performance of the proposed method is compared in terms of power loss minimization, MSML and MSSL scenarios, congestion management, computation time and complexity, which is obtained from the literature and simulation results of this chapter.

As shown in the simulation results, the power loss minimization in other methods is not as good as the proposed algorithm. The weakest performance is related to the secure based method, where the security is preferred than the power losses. The MSML scenario has not been previously addressed in other methods. Even the transaction-based method has not considered the MSSL scenario. In contrast, in this chapter, all the loads are fed simultaneously, which is the case in the real application. In term of congestion management, the proposed and transaction-based algorithms can work better than [90] and [139] with respect to the presence of limited power lines. For instance, with the same system, the proposed method in the congestion management case study increases the losses by 25%

compare to the normal case study, while [90] and [139] cannot even find the available solution. The computation time of the proposed method is less than [140] and longer than [139]. In fact, the computational burden of the min-consensus based method is limited only to some nodes, while in the transaction-based method, the real-time transaction based on the bidding information exchange mechanism is added to the control system. Also, the transaction-based and min-consensus based methods have higher complexity due to the use of bidding information exchange mechanism and consensus algorithm, respectively. Therefore, under the same and fair conditions, the proposed routing algorithm obtains significant improvements for a large MMG systems with less than 50 MGs.

V.5. Conclusion

The multi-microgrid system is a good solution for the distributed and unpredictable nature of RESs. The energy routers interface is a key element in this structure, which provides bidirectional power and information flow. In this chapter, a novel energy routing algorithm was proposed based on graph theory to achieve P2P energy trading among MGs. The main objective of the proposed approach is to reduce power losses while maintaining energy security. In fact, the optimal path for power transmission is determined by the minimum power losses and minimum sources indexes. Therefore, the suggested scheme is able to determine the appropriate match between suppliers and consumers with the best load set, optimal sources and no-congestion minimum loss paths. Various analysis cases are investigated to confirm the performance and flexibility of the proposed algorithm. For the first time, the multi-sources and multi-loads scenario has been explored in the literature. Finally, simulation results are presented for different analysis cases which confirmed the superiority of the proposed method over the existing ones. In [90], [136], and [140], the power losses are about 16%, 29% and 10% higher than the proposed algorithm, respectively. Also, in term of congestion management, the proposed and transaction-based algorithms can work better than [90] and [139] with respect to the limited power lines.

CHAPTER VI :

Conclusions and perspectives

VI.1. General conclusions

This thesis has presented an energy router interfaces among microgrids in the multi-microgrid system structure. The DC-based architecture has been chosen for the energy router application in the clusters of microgrids. The works not only focus on modelling mathematical models but also consider the interaction and power, energy management in the system. Besides that, the battery sizing problem and the its operation in a remoted microgrid are also studied. The noteworthy results are achieved and concluded as follows.

- The proposed battery sizing process are developed with two modules. The load profiles, grid's data, the technical and economical constrains are given as the inputs. By applying an iterative method, the first part of the sizing method is able to estimate the optimal size of PV system. The proposed PV size is capable of supplying the load demands and optimizes the investment cost of the system. The second part of the sizing process is designed to minimize the battery storage size of the system with the optimal results from the first part as an input. The main component in the second module of the sizing program is the energy management system. A dynamic programming method is utilized in the energy management in the inner loop to optimize the system cost, with an iterative method in the outer loop to minimize the size of the storage system. The overall outputs of the developed sizing program are the optimal sizes of PV system, the optimal sizes of BESS and the optimal power schedule for the MG. Thanks to the application of the dynamic programming, the SOC of the BESS at the begin state and the final state is controlled, which is a significant advantage compared to other EMS methods. The simulation results are compared to the rule-based method in the literature to show the superiority of the developed strategy.
- To improve the efficiency and the lifespan of the BESS, a HESS concept is widely applied in the modern grid. The semi-active HESS topologies are

chosen for MG application because of its simple design, reliable and robust operation. The objectives of the control method are to reduce the stress of the FC system, following the pre-defined range SOC of BESS and minimize hydrogen consumption. Thus, a low-pass filter and an EMS are utilized in the control system to achieve these goals. A testing simulation model has been caried out and show that the stress of the FC system can be reduced by decomposing the high-frequency load and there is a tradeoff between following SOC of BESS and minimizing the hydrogen consumption with the developed EMS.

- The complementary energy exchange among MGs aims at decreasing the dependence on the main grid, reducing the size and cost of the energy storage units, and increasing energy efficiency. In this regard, the use of an energy router interface to connect the microgrids to the power system is necessary for controlling bidirectional power and data flow. In this thesis, mathematical models have been developed for the energy router and its control system. The main elements in the studied ER are voltage source controllers. The master/slave approach is proposed in this thesis for the interaction among MGs with the ER interface. The rule for choosing grid-forming unit relates to the amount of controllable energy in the MGs. These models and the control framework have been analyzed with numerous case studies. The simulation results have shown that the interconnection in the MMG with the DC link enhances the peer-to-peer energy trading between MGs so that the autonomous of the whole system has been improved.
- Unlike the AC interconnection, the AC MGs in the MMG system with the proposed ER interface can be electrical isolated. The fluctuation of the frequencies is not shared among MGs. Hence the “flexible” frequency approach can be applied. In this scenario, each MG in the cluster can work with a different range of frequency. The stability of the overall system is related to the stability of the DC voltage in the DC common link which is regulated by the grid-forming MG. The stability of this DC-link can be supported by using the concept of VSG or by improving the “inertia”. The thesis has also pointed

out that other members in the MMG system can contribute to the whole system stability by using a droop frequency characteristic with the grid-forming unit.

- With the ER application, one of the most crucial features in determining multi-microgrid system performance is the energy routing algorithm strategy based on graph theory. The objective of the routing algorithm is to minimize the overall power losses with respect to congestion and reliability in the MGs cluster. The optimal paths for power transmission among MGs are defined by the minimum power losses and minimum sources indexes. In this thesis, for the first time, the multi-sources and multi-loads case studies has been explored in the literatures. The new routing strategy has been proposed and examined for the multi-microgrid system with 9 MGs system and 30 MGs system. The encouraging simulation results are proved by comparing with various existing routing methods.

VI.2. Outlook on future research

The works and results presented in this thesis lead to new questions and studies, which opens a great number of future researches.

- First of all, the battery sizing problem considered in this thesis only focus on a single islanded microgrid system. In the future works, this sizing method can be applied to a microgrid working in a multi-microgrid system. Hence, the energy exchange process among microgrids can be taken into account in the energy management system in the sizing process. There will be new constrains and may be a new optimization function in this scheme, which can further reduce the size of the energy storage system.
- The strategy for operation of the hybrid energy storage system in this thesis aim to optimize the fuel cell consumption, stress and limit the SOC variation of the battery. In the future work, a multi-objective optimization approaches can be designed to optimize all the performance criteria.
- The DC-based energy router interface has been investigated with a single grid-forming unit. In a real implementation, there could be two or more grid-forming units, which will enhance the reliability of the multi-microgrid

system. Therefore, the strategy for load sharing and DC voltage control among these units need to be investigated.

- To improve the stability of the multi-microgrid system, the droop frequency method can be expanded with more than two participated microgrids. Another solution from the customers' side such as demand side management can also be considered.
- The application of graph-based routing algorithm is an ongoing research branch in the power system community. The proposed routing method in this thesis needs to be tested in the laboratory environment. Furthermore, the delay in the communication among energy routers is a very crucial problem and could be considered in the future research.

Publications

1. T. T. Mai, A. N. M. M. Haque, T. Vo, P. H. Nguyen and **M. C. Pham**, "Development of ICT Infrastructure for Physical LV Microgrids," *2018 IEEE International Conference on Environment and Electrical Engineering and 2018 IEEE Industrial and Commercial Power Systems Europe (EEEIC / I&CPS Europe)*, Palermo, 2018, pp. 1-6, doi: 10.1109/EEEIC.2018.8493788.
2. Q. T. Tran , **M. C. Pham**, L. Parent and K. Sousa, "Integration of PV Systems into Grid: From Impact Analysis to Solutions," *2018 IEEE International Conference on Environment and Electrical Engineering and 2018 IEEE Industrial and Commercial Power Systems Europe (EEEIC / I&CPS Europe)*, Palermo, 2018, pp. 1-6, doi: 10.1109/EEEIC.2018.8494400.
3. E. Amicarelli, Q. T. Tran , S. Bacha and **M. C. Pham,** "Capacity Limit Allocation for Active Congestion Management of Distribution Grids Using Flexible User's Profiles in Microgrids," *IECON 2018 - 44th Annual Conference of the IEEE Industrial Electronics Society*, Washington, DC, 2018, pp. 126-131, doi: 10.1109/IECON.2018.8591817.
4. **M. C. Pham**, Q. T. Tran , S. Bacha, A. Hably and L. N. An, "Optimal Sizing of Battery Energy Storage System for an Islaned Microgrid," *IECON 2018 - 44th Annual Conference of the IEEE Industrial Electronics Society*, Washington, DC, 2018, pp. 1899-1903, doi: 10.1109/IECON.2018.8591391.
5. **M. C. Pham**, R. Razi, A. Hably, S. Bacha, Q. T. Tran and H. Iman-Eini, "Power management in multi-microgrid system based on energy routers," *2020 IEEE International Conference on Industrial Technology (ICIT)*, Buenos Aires, Argentina, 2020, pp. 1178-1183, doi: 10.1109/ICIT45562.2020.9067200.
6. R. Razi, **M. C. Pham**, A. Hably, S. Bacha, Q. T. Tran and H. Iman-Eini, "Robust hybrid control of parallel inverters for accurate power-sharing in microgrid," *2020 IEEE International Conference on Industrial Technology (ICIT)*, Buenos Aires, Argentina, 2020, pp. 860-865, doi: 10.1109/ICIT45562.2020.9067116.
7. **M. C. Pham**, Q. T. Tran , A. Hably and S. Bacha, "Application of energy routers for frequency support in an AC/DC multi-microgrid system," *2021 IEEE International Conference on Environment and Electrical Engineering and 2021 IEEE Industrial and Commercial Power Systems Europe (EEEIC / I&CPS Europe)*, 2021, pp. 1-6, doi: 10.1109/EEEIC/ICPSEurope51590.2021.9584708.
8. R. Razi, **M. C. Pham**, A. Hably, S. Bacha, Q. T. Tran and H. Iman-Eini, "A Novel Graph-based Routing Algorithm in Residential Multi-Microgrid Systems," in IEEE Transactions on Industrial Informatics, doi: 10.1109/TII.2020.2997516.

Bibliography

[1] N. Hatziargyriou, *MICROGRIDS ARCHITECTURES AND CONTROL*, 1st ed. West Sussex, United Kingdom: John Wiley and Sons Ltd, 2014.

[2] A. M. Bouzid, J. M. Guerrero, A. Cheriti, M. Bouhamida, P. Sicard, and M. Benghanem, "A survey on control of electric power distributed generation systems for microgrid applications," *Renew. Sustain. Energy Rev.*, vol. 44, pp. 751–766, 2015, doi: 10.1016/j.rser.2015.01.016.

[3] O. Palizban and K. Kauhaniemi, "Energy storage systems in modern grids—Matrix of technologies and applications," *J. Energy Storage*, vol. 6, no. 2015, pp. 248–259, 2016, doi: 10.1016/j.est.2016.02.001.

[4] R. Lasseter, A. Akhil, C. Marnay, and J. Ste, "Consortium for Electric Reliability Technology Solutions White Paper on Integration of Distributed Energy Resources The MicroGrid Concept," no. April, 2002.

[5] N. Hatziargyriou *et al.*, "Microgrids - Large scale integration of microgeneration to low voltage grids," *41st Int. Conf. Large High Volt. Electr. Syst. 2006, CIGRE 2006*, 2006.

[6] DOE, "Summary report: 2012 DOE microgrid workshop," *U.S. Dep. Energy*, pp. 1–33, 2012, [Online]. Available: http://energy.gov/sites/prod/files/2012 Microgrid Workshop Report 09102012.pdf.

[7] A. Hirsch, Y. Parag, and J. Guerrero, "Microgrids: A review of technologies, key drivers, and outstanding issues," *Renew. Sustain. Energy Rev.*, vol. 90, no. March, pp. 402–411, 2018, doi: 10.1016/j.rser.2018.03.040.

[8] H. P, Barker; B, Johnson ; A, Maitra ; D, "Investigation of the Technical and Economic Feasibility of Micro-Grid- Based Power Systems," *Power Deliv. Util.*, no. December, p. 108, 2001, [Online]. Available: https://www.epri.com/research/products/1003973.

[9] R. K. Pachauri *et al.*, *Climate Change 2014: Synthesis Report. Contribution of Working Groups I, II and III to the Fifth Assessment Report of the Intergovernmental Panel on Climate Change*. Geneva, Switzerland: IPCC, 2014.

[10] S. Parhizi, H. Lotfi, A. Khodaei, and S. Bahramirad, "State of the art in research on microgrids: A review," *IEEE Access*, vol. 3, no. January, pp. 890–925, 2015, doi: 10.1109/ACCESS.2015.2443119.

[11] M. Munsell, “US Microgrid Capacity Will Exceed 1.8GW by 2018le.” https://www.greentechmedia.com/articles/read/us-microgrid-capacity-will-exceed-1-8-gw-by-2018#gs.kagzqb.

[12] P. Asmus and M. Lawrence, “Emerging Microgrid Business Models,” pp. 1–14, 2016.

[13] F. Bandeiras, E. Pinheiro, M. Gomes, P. Coelho, and J. Fernandes, “Review of the cooperation and operation of microgrid clusters,” *Renew. Sustain. Energy Rev.*, vol. 133, no. March, p. 110311, 2020, doi: 10.1016/j.rser.2020.110311.

[14] G. Shahgholian, “A brief review on microgrids: Operation, applications, modeling, and control,” *Int. Trans. Electr. Energy Syst.*, vol. 31, no. 6, pp. 1–28, 2021, doi: 10.1002/2050-7038.12885.

[15] M. H. Spiegel, E. M. S. P. Veith, and T. I. Strasser, “The spectrum of proactive, resilient multi-microgrid scheduling: A systematic literature review,” *Energies*, vol. 13, no. 17, 2020, doi: 10.3390/en13174543.

[16] E. Espe, V. Potdar, and E. Chang, “Prosumer Communities and Relationships in Smart Grids: A Literature Review, Evolution and Future Directions,” *Energies* , vol. 11, no. 10. 2018, doi: 10.3390/en11102528.

[17] “PARADISE.” http://www.gipsa-lab.fr/projet/PARADISE/publications.html.

[18] Y. Li *et al.*, “Optimal operation of multimicrogrids via cooperative energy and reserve scheduling,” *IEEE Trans. Ind. Informatics*, vol. 14, no. 8, pp. 3459–3468, 2018, doi: 10.1109/TII.2018.2792441.

[19] L. Cupelli, N. Barve, and A. Monti, “Optimal sizing of data center battery energy storage system for provision offrequency containment reserve,” in *IECON 2017 - 43rd Annual Conference of the IEEE Industrial Electronics Society*, 2017, pp. 7185–7190, doi: 10.1109/IECON.2017.8217257.

[20] M. R. Aghamohammadi and H. Abdolahinia, “A new approach for optimal sizing of battery energy storage system for primary frequency control of islanded Microgrid,” *Int. J. Electr. Power Energy Syst.*, vol. 54, pp. 325–333, 2014, doi: https://doi.org/10.1016/j.ijepes.2013.07.005.

[21] K. K. Mehmood, S. U. Khan, S.-J. Lee, Z. M. Haider, M. Rafique, and C. Kim, “Optimal sizing and allocation of battery energy storage systems with wind and solar power DGs in a distribution network for voltage regulation considering the lifespan of batteries,” *Iet Renew. Power Gener.*, vol. 11, pp. 1305–1315, 2017.

[22] K. Lai, Y. Wang, D. Shi, M. S. Illindala, Y. Jin, and Z. Wang, “Sizing battery storage

for islanded microgrid systems to enhance robustness against attacks on energy sources," *J. Mod. Power Syst. Clean Energy*, vol. 7, no. 5, pp. 1177–1188, 2019, doi: 10.1007/s40565-019-0501-1.

[23] K. Lai and M. S. Illindala, "Design and planning strategy for energy storage system in a shipboard dc hybrid power system," in *2017 IEEE/IAS 53rd Industrial and Commercial Power Systems Technical Conference (I&CPS)*, 2017, pp. 1–9, doi: 10.1109/ICPS.2017.7945094.

[24] C. K. Nayak and M. R. Nayak, "Optimal design of battery energy storage system for peak load shaving and time of use pricing," in *2017 Second International Conference on Electrical, Computer and Communication Technologies (ICECCT)*, 2017, pp. 1–7, doi: 10.1109/ICECCT.2017.8118030.

[25] H. Xiao, W. Pei, Y. Yang, and L. Kong, "Sizing of battery energy storage for micro-grid considering optimal operation management," in *2014 International Conference on Power System Technology*, 2014, pp. 3162–3169, doi: 10.1109/POWERCON.2014.6993661.

[26] H. Khorramdel, J. Aghaei, B. Khorramdel, and P. Siano, "Optimal Battery Sizing in Microgrids Using Probabilistic Unit Commitment," *IEEE Trans. Ind. Informatics*, vol. 12, no. 2, pp. 834–843, 2016, doi: 10.1109/TII.2015.2509424.

[27] S. Sharma, S. Bhattacharjee, and A. Bhattacharya, "Grey wolf optimisation for optimal sizing of battery energy storage device to minimise operation cost of microgrid," pp. 1–13, 2015, doi: 10.1049/iet-gtd.2015.0429.

[28] M. S. Id, N. A. Rahim, C. Tan, A. Muhammad, S. Rohani, and S. Raihan, "Optimal sizing and energy scheduling of isolated microgrid considering the battery lifetime degradation," pp. 1–28, 2019.

[29] J. P. Fossati, A. Galarza, A. Martín-Villate, and L. Fontán, "A method for optimal sizing energy storage systems for microgrids," *Renew. Energy*, vol. 77, pp. 539–549, 2015, doi: https://doi.org/10.1016/j.renene.2014.12.039.

[30] W. Li and G. Joos, "A power electronic interface for a battery supercapacitor hybrid energy storage system for wind applications," in *2008 IEEE Power Electronics Specialists Conference*, 2008, pp. 1762–1768, doi: 10.1109/PESC.2008.4592198.

[31] J. D. Maclay, J. Brouwer, and G. S. Samuelsen, "Dynamic modeling of hybrid energy storage systems coupled to photovoltaic generation in residential applications," *J. Power Sources*, vol. 163, no. 2, pp. 916–925, 2007, doi:

https://doi.org/10.1016/j.jpowsour.2006.09.086.

[32] S. Hajiaghasi, A. Salemnia, and M. Hamzeh, “Hybrid energy storage system for microgrids applications: A review,” *J. Energy Storage*, vol. 21, no. December 2018, pp. 543–570, 2019, doi: 10.1016/j.est.2018.12.017.

[33] W. Jing, C. H. Lai, S. H. W. Wong, and M. L. D. Wong, “Battery-supercapacitor hybrid energy storage system in standalone DC microgrids: Areview,” *IET Renew. Power Gener.*, vol. 11, no. 4, pp. 461–469, 2017, doi: 10.1049/iet-rpg.2016.0500.

[34] A. Etxeberria, I. Vechiu, H. Camblong, and J. M. Vinassa, “Hybrid energy storage systems for renewable energy sources integration in microgrids: A review,” *2010 9th Int. Power Energy Conf. IPEC 2010*, pp. 532–537, 2010, doi: 10.1109/IPECON.2010.5697053.

[35] Z. Li, Z. Zheng, L. Xu, and X. Lu, “A review of the applications of fuel cells in microgrids: opportunities and challenges,” *BMC Energy*, vol. 1, no. 1, p. 8, 2019, doi: 10.1186/s42500-019-0008-3.

[36] S. J. Moura, J. B. Siegel, D. J. Siegel, H. K. Fathy, and A. G. Stefanopoulou, “Education on vehicle electrification: Battery Systems, Fuel Cells, and Hydrogen,” in *2010 IEEE Vehicle Power and Propulsion Conference*, 2010, pp. 1–6, doi: 10.1109/VPPC.2010.5729150.

[37] S. Pay and Y. Baghzouz, “Effectiveness of battery-supercapacitor combination in electric vehicles,” in *2003 IEEE Bologna Power Tech Conference Proceedings,* 2003, vol. 3, p. 6 pp. Vol.3, doi: 10.1109/PTC.2003.1304472.

[38] A. Etxeberria, I. Vechiu, H. Camblong, and J.-M. Vinassa, “Comparison of three topologies and controls of a hybrid energy storage system for microgrids,” *Energy Convers. Manag.*, vol. 54, no. 1, pp. 113–121, 2012, doi: https://doi.org/10.1016/j.enconman.2011.10.012.

[39] S. M. Lukic, S. G. Wirasingha, F. Rodriguez, J. Cao, and A. Emadi, “Power Management of an Ultracapacitor/Battery Hybrid Energy Storage System in an HEV,” in *2006 IEEE Vehicle Power and Propulsion Conference*, 2006, pp. 1–6, doi: 10.1109/VPPC.2006.364357.

[40] E. Jamshidpour, S. Saadate, and P. Poure, “Energy management and control of a stand-alone photovoltaic/ultra capacitor/battery microgrid,” in *2015 IEEE Jordan Conference on Applied Electrical Engineering and Computing Technologies (AEECT)*, 2015, pp. 1–6, doi: 10.1109/AEECT.2015.7360584.

[41] J. L. Bernal-Agustín, R. Dufo-López, and D. M. Rivas-Ascaso, “Design of isolated hybrid systems minimizing costs and pollutant emissions,” *Renew. Energy*, vol. 31, no. 14, pp. 2227–2244, 2006, doi: https://doi.org/10.1016/j.renene.2005.11.002.

[42] T. Senjyu, D. Hayashi, A. Yona, N. Urasaki, and T. Funabashi, “Optimal configuration of power generating systems in isolated island with renewable energy,” *Renew. Energy*, vol. 32, no. 11, pp. 1917–1933, 2007, doi: https://doi.org/10.1016/j.renene.2006.09.003.

[43] “Photowatt PW2300-235 (235W) Solar Panel.” http://www.solardesigntool.com/components/module-panel-solar/Photowatt/853/PW2300-235/specification-data-sheet.html.

[44] Y. Riffonneau, “GESTION DES FLUX ÉNERGÉTIQUE DANS UN SYSTÈME PHOTOVOLTAÏQUE AVEC STOCKAGE CONNECTER AU RÉSEAU,” 2009.

[45] M. Broussely *et al.*, “Main aging mechanisms in Li ion batteries,” *J. Power Sources*, vol. 146, no. 1, pp. 90–96, 2005, doi: https://doi.org/10.1016/j.jpowsour.2005.03.172.

[46] M. Ecker *et al.*, “Development of a lifetime prediction model for lithium-ion batteries based on extended accelerated aging test data,” *J. Power Sources*, vol. 215, pp. 248–257, 2012, doi: https://doi.org/10.1016/j.jpowsour.2012.05.012.

[47] Y. Riffonneau, S. Bacha, F. Barruel, and S. Ploix, “Optimal Power Flow Management for Grid Connected PV Systems With Batteries,” *IEEE Trans. Sustain. Energy*, vol. 2, no. 3, pp. 309–320, 2011, doi: 10.1109/TSTE.2011.2114901.

[48] P. Malbranche, A. Delaille, F. Mattera, and E. Lemaire, “Assessment of Storage Ageing in Different Types of PV Systems: Technical and Economical Aspects,” 2008.

[49] M. Mendil, A. De Domenico, V. Heiries, R. Caire, and N. Hadjsaid, “Battery-Aware Optimization of Green Small Cells: Sizing and Energy Management,” *IEEE Trans. Green Commun. Netw.*, vol. 2, no. 3, pp. 635–651, 2018, doi: 10.1109/TGCN.2018.2829344.

[50] X. Li, D. Hui, and X. Lai, “Battery Energy Storage Station (BESS)-Based Smoothing Control of Photovoltaic (PV) and Wind Power Generation Fluctuations,” *IEEE Trans. Sustain. Energy*, vol. 4, no. 2, pp. 464–473, 2013, doi: 10.1109/TSTE.2013.2247428.

[51] S. Diaf, M. Belhamel, M. Haddadi, and A. Louche, “Technical and economic assessment of hybrid photovoltaic/wind system with battery storage in Corsica island,” *Energy Policy*, vol. 36, no. 2, pp. 743–754, 2008, doi: https://doi.org/10.1016/j.enpol.2007.10.028.

[52] T. Khatib, A. Mohamed, and K. Sopian, “A review of photovoltaic systems size optimization techniques,” *Renew. Sustain. Energy Rev.*, vol. 22, pp. 454–465, 2013, doi: https://doi.org/10.1016/j.rser.2013.02.023.

[53] A. Annuk *et al.*, “Increasing renewable fraction by Smoothing consumer power charts in grid-connected wind-solar hybrid systems,” *Oil Shale*, vol. 30, p. 257, Jan. 2013, doi: 10.3176/oil.2013.2S.06.

[54] M. C. Pham, T. Q. Tran, S. Bacha, A. Hably, and L. N. An, “Optimal Sizing of Battery Energy Storage System for an Islaned Microgrid,” in *IECON 2018 - 44th Annual Conference of the IEEE Industrial Electronics Society*, 2018, pp. 1899–1903, doi: 10.1109/IECON.2018.8591391.

[55] H. Suryoatmojo, “Artificial intelligence based optimal configuration of hybrid power generation system,” 2010.

[56] L. N. An, T. Quoc-Tuan, B. Seddik, and N. Be, “Optimal design of an isolated photovoltaic-diesel-battery hybrid system by using an iterative algorithm,” in *2014 IEEE PES General Meeting | Conference & Exposition*, 2014, pp. 1–5, doi: 10.1109/PESGM.2014.6939171.

[57] S. Njoya Motapon, L. A. Dessaint, and K. Al-Haddad, “A comparative study of energy management schemes for a fuel-cell hybrid emergency power system of more-electric aircraft,” *IEEE Trans. Ind. Electron.*, vol. 61, no. 3, pp. 1320–1334, 2014, doi: 10.1109/TIE.2013.2257152.

[58] S. N. M., O. Tremblay, and L. Dessaint, “A generic fuel cell model for the simulation of fuel cell vehicles,” in *2009 IEEE Vehicle Power and Propulsion Conference*, 2009, pp. 1722–1729, doi: 10.1109/VPPC.2009.5289692.

[59] K. B. Oldham, “A Gouy–Chapman–Stern model of the double layer at a (metal)/(ionic liquid) interface,” *J. Electroanal. Chem.*, vol. 613, no. 2, pp. 131–138, 2008, doi: https://doi.org/10.1016/j.jelechem.2007.10.017.

[60] O. Tremblay, L. Dessaint, and A. Dekkiche, “A Generic Battery Model for the Dynamic Simulation of Hybrid Electric Vehicles,” in *2007 IEEE Vehicle Power and Propulsion Conference*, 2007, pp. 284–289, doi: 10.1109/VPPC.2007.4544139.

[61] P. Garcia, L. M. Fernandez, C. A. Garcia, and F. Jurado, “Energy Management System of Fuel-Cell-Battery Hybrid Tramway,” *IEEE Trans. Ind. Electron.*, vol. 57, no. 12, pp. 4013–4023, 2010, doi: 10.1109/TIE.2009.2034173.

[62] P. Thounthong and S. Rael, “The benefits of hybridization,” *IEEE Ind. Electron.*

Mag., vol. 3, no. 3, pp. 25–37, 2009, doi: 10.1109/MIE.2009.933885.

[63] B. Vural *et al.*, "Fuel cell and ultra-capacitor hybridization: A prototype test bench based analysis of different energy management strategies for vehicular applications," *Int. J. Hydrogen Energy*, vol. 35, no. 20, pp. 11161–11171, 2010, doi: https://doi.org/10.1016/j.ijhydene.2010.07.063.

[64] A. Mannelli, F. Papi, G. Pechlivanoglou, G. Ferrara, and A. Bianchini, "Wind Turbine Power Using Li-Ion Batteries," 2021.

[65] X. Zhang, C. C. Mi, A. Masrur, and D. Daniszewski, "Wavelet-transform-based power management of hybrid vehicles with multiple on-board energy sources including fuel cell, battery and ultracapacitor," *J. Power Sources*, vol. 185, no. 2, pp. 1533–1543, 2008, doi: 10.1016/j.jpowsour.2008.08.046.

[66] P. García, J. P. Torreglosa, L. M. Fernández, and F. Jurado, "Viability study of a FC-battery-SC tramway controlled by equivalent consumption minimization strategy," *Int. J. Hydrogen Energy*, vol. 37, no. 11, pp. 9368–9382, 2012, doi: https://doi.org/10.1016/j.ijhydene.2012.02.184.

[67] Y. Wang, R. Pan, D. Yang, X. Tang, and Z. Chen, "Remaining Useful Life Prediction of Lithium-ion Battery Based on Discrete Wavelet Transform," *Energy Procedia*, vol. 105, pp. 2053–2058, 2017, doi: 10.1016/j.egypro.2017.03.582.

[68] D. Roberts, A. Chang, and Vox, "Meet the microgrid, the technology poised to transform electricity." 2018, [Online]. Available: https://www.vox.com/energy-and-environment/2017/12/15/16714146/greener-more-reliable-more-resilient-grid-microgrids.

[69] M. Chenine, E. Karam, and L. Nordström, "Modeling and simulation of wide area monitoring and control systems in IP-based networks," *2009 IEEE Power Energy Soc. Gen. Meet. PES '09*, pp. 1–8, 2009, doi: 10.1109/PES.2009.5275818.

[70] A. Mohamed, A. Ghareeb, T. Youssef, and O. A. Mohammed, "Wide area monitoring and control for voltage assessment in smart grids with distributed generation," *2013 IEEE PES Innov. Smart Grid Technol. Conf. ISGT 2013*, pp. 1–6, 2013, doi: 10.1109/ISGT.2013.6497849.

[71] A. D. Nguyen, V. H. Bui, A. Hussain, D. H. Nguyen, and H. M. Kim, "Impact of demand response programs on optimal operation of multi-microgrid system," *Energies*, vol. 11, no. 6, 2018, doi: 10.3390/en11061452.

[72] S. Vandael, B. Claessens, M. Hommelberg, T. Holvoet, and G. Deconinck, "A

scalable three-step approach for demand side management of plug-in hybrid vehicles," *IEEE Trans. Smart Grid*, vol. 4, no. 2, pp. 720–728, 2013, doi: 10.1109/TSG.2012.2213847.

[73] L. Che, M. Shahidehpour, A. Alabdulwahab, and Y. Al-Turki, "Hierarchical coordination of a community microgrid with AC and DC microgrids," *IEEE Trans. Smart Grid*, vol. 6, no. 6, pp. 3042–3051, 2015, doi: 10.1109/TSG.2015.2398853.

[74] H. Almasalma, J. Engels, and G. Deconinck, "Peer-to-Peer Control of Microgrids," in *Young Researchers Symposium*, Nov. 2017, [Online]. Available: http://arxiv.org/abs/1711.04070.

[75] A. Mehrizi-Sani, "Distributed Control Techniques in Microgrids," *Microgrid Adv. Control Methods Renew. Energy Syst. Integr.*, vol. 5, no. 6, pp. 43–62, 2016, doi: 10.1016/B978-0-08-101753-1.00002-4.

[76] D. Alaerts and J. De Turck, "Investigation and comparison of distributed algorithms for demand-side management," ESAT-ELECTA, KU Leuven, 2013.

[77] R. Schollmeier, "A definition of peer-to-peer networking for the classification of peer-to-peer architectures and applications," *Proc. - 1st Int. Conf. Peer-to-Peer Comput. P2P 2001*, no. September 2001, pp. 101–102, 2001, doi: 10.1109/P2P.2001.990434.

[78] S. D. J. McArthur *et al.*, "Multi-Agent Systems for Power Engineering Applications—Part I: Concepts, Approaches, and Technical Challenges," *IEEE Trans. Power Syst.*, vol. 22, no. 4, pp. 1743–1752, Nov. 2007, doi: 10.1109/TPWRS.2007.908471.

[79] D. Kempe, A. Dobra, and J. Gehrke, "Gossip-based computation of aggregate information," in *44th Annual IEEE Symposium on Foundations of Computer Science, 2003. Proceedings.*, 2003, pp. 482–491, doi: 10.1109/SFCS.2003.1238221.

[80] R. Olfati-Saber, J. A. Fax, and R. M. Murray, "Consensus and cooperation in networked multi-agent systems," *Proc. IEEE*, vol. 95, no. 1, pp. 215–233, 2007, doi: 10.1109/JPROC.2006.887293.

[81] Y. Wang, T.-L. Nguyen, Y. Xu, Q.-T. Tran, and R. Caire, "Peer-to-Peer Control for Networked Microgrids: Multi-Layer and Multi-Agent Architecture Design," *IEEE Trans. Smart Grid*, vol. 11, no. 6, pp. 4688–4699, 2020, doi: 10.1109/TSG.2020.3006883.

[82] J. Suh, D. H. Yoon, Y. S. Cho, and G. Jang, "Flexible Frequency Operation Strategy of Power System With High Renewable Penetration," *IEEE Trans. Sustain. Energy*,

vol. 8, no. 1, pp. 192–199, 2017, doi: 10.1109/TSTE.2016.2590939.

[83] W. Liu, W. Gu, Y. Xu, Y. Wang, and K. Zhang, "General distributed secondary control for multi-microgrids with both PQ-controlled and droop-controlled distributed generators," *IET Gener. Transm. Distrib.*, vol. 11, no. 3, pp. 707–718, 2016, doi: 10.1049/iet-gtd.2016.0613.

[84] C. Yuen, A. Oudalov, and A. Timbus, "The provision of frequency control reserves from multiple microgrids," *IEEE Trans. Ind. Electron.*, vol. 58, no. 1, pp. 173–183, 2011, doi: 10.1109/TIE.2010.2041139.

[85] A. Kargarian and M. Rahmani, "Multi-microgrid energy systems operation incorporating distribution-interline power flow controller," *Electr. Power Syst. Res.*, vol. 129, pp. 208–216, 2015, doi: 10.1016/j.epsr.2015.08.015.

[86] R. Majumder, "A hybrid microgrid with dc connection at back to back converters," *IEEE Trans. Smart Grid*, vol. 5, no. 1, pp. 251–259, 2014, doi: 10.1109/TSG.2013.2263847.

[87] ABB, "Ross Island research station - Power Generation References | ABB," 2009. http://new.abb.com/power-generation/references/ross-island-research-station.

[88] H. Pourbabak, T. Chen, and W. Su, *Centralized, decentralized, and distributed control for Energy Internet*. Elsevier Ltd, 2018.

[89] Z. Hu, L. Lu, G. Liu, J. Yi, and L. Zhaoc, "Research on Adaptability Evaluation Method of New Communication Technology Applied to Energy Internet Communication Network," *Proc. - 1st IEEE Int. Conf. Energy Internet, ICEI 2017*, pp. 250–255, 2017, doi: 10.1109/ICEI.2017.51.

[90] R. Wang, J. Wu, Z. Qian, Z. Lin, and X. He, "A Graph Theory Based Energy Routing Algorithm in Energy Local Area Network," *IEEE Trans. Ind. Informatics*, vol. 13, no. 6, pp. 3275–3285, 2017, doi: 10.1109/TII.2017.2713040.

[91] E. Foruzan, S. Asgarpoor, and J. M. Bradley, "Hybrid system modeling and supervisory control of a microgrid," *NAPS 2016 - 48th North Am. Power Symp. Proc.*, no. 1, pp. 1–6, 2016, doi: 10.1109/NAPS.2016.7747840.

[92] A. Q. Huang and J. Baliga, "FREEDM System: Role of power electronics and power semiconductors in developing an energy internet," *Proc. Int. Symp. Power Semicond. Devices ICs*, pp. 9–12, 2009, doi: 10.1109/ISPSD.2009.5157988.

[93] Y. Liu, Y. Fang, and J. Li, "Interconnecting microgrids via the energy router with smart energy management," *Energies*, vol. 10, no. 9, 2017, doi: 10.3390/en10091297.

[94] Y. Xu, J. Zhang, W. Wang, A. Juneja, and S. Bhattacharya, “Energy router: Architectures and functionalities toward energy internet,” *2011 IEEE Int. Conf. Smart Grid Commun. SmartGridComm 2011*, pp. 31–36, 2011, doi: 10.1109/SmartGridComm.2011.6102340.

[95] R. Majumder, A. Ghosh, G. Ledwich, and F. Zare, “Power management and power flow control with back-to-back converters in a utility connected microgrid,” *IEEE Trans. Power Syst.*, vol. 25, no. 2, pp. 821–834, 2010, doi: 10.1109/TPWRS.2009.2034666.

[96] R. Wu, B. Wang, Y. Zou, B. Fan, L. Li, and Z. Zhu, “Energy router interface model based on bidirectional flow control for intelligent park,” *Proc. IECON 2017 - 43rd Annu. Conf. IEEE Ind. Electron. Soc.*, vol. 2017-Janua, pp. 7771–7776, 2017, doi: 10.1109/IECON.2017.8217362.

[97] A. Shojaei and G. Joós, “A topology for three-stage Solid State Transformer,” in *2013 IEEE Power & Energy Society General Meeting*, 2013, pp. 1–5, doi: 10.1109/PESMG.2013.6672781.

[98] H. Guo, F. Wang, J. Luo, and L. Zhang, “Review of energy routers applied for the energy internet integrating renewable energy,” *2016 IEEE 8th Int. Power Electron. Motion Control Conf. IPEMC-ECCE Asia 2016*, no. 51577113, pp. 1997–2003, 2016, doi: 10.1109/IPEMC.2016.7512602.

[99] H. Wu, J. Zhang, and Y. Xing, “A Family of Multiport Buck–Boost Converters Based on DC-Link-Inductors (DLIs),” *IEEE Trans. Power Electron.*, vol. 30, no. 2, pp. 735–746, 2015, doi: 10.1109/TPEL.2014.2307883.

[100] T. Takuno, M. Koyama, and T. Hikihara, “In-Home Power Distribution Systems by Circuit Switching and Power Packet Dispatching,” in *2010 First IEEE International Conference on Smart Grid Communications*, 2010, pp. 427–430, doi: 10.1109/SMARTGRID.2010.5622079.

[101] H. Guo, F. Wang, G. James, L. Zhang, and J. Luo, “Graph theory based topology design and energy routing control of the energy internet,” *IET Gener. Transm. Distrib.*, vol. 12, no. 20, pp. 4507–4514, Nov. 2018, doi: 10.1049/iet-gtd.2018.6238.

[102] H. J. Yoo, T. T. Nguyen, and H. M. Kim, “Multi-frequency control in a stand-alone multi-microgrid system using a back-to-back converter,” *Energies*, vol. 10, no. 6, 2017, doi: 10.3390/en10060822.

[103] R. A. Serway, *Physics for scientists and engineers with modern physics*. Second

edition. Philadelphia : Saunders College Pub., 1986, c1983.

[104] F. M. Uriarte, C. Smith, S. VanBroekhoven, and R. E. Hebner, “Microgrid Ramp Rates and the Inertial Stability Margin,” *IEEE Trans. Power Syst.*, vol. 30, no. 6, pp. 3209–3216, 2015, doi: 10.1109/TPWRS.2014.2387700.

[105] A. Fernández-Guillamón, E. Gómez-Lázaro, E. Muljadi, and Á. Molina-García, “Power systems with high renewable energy sources: A review of inertia and frequency control strategies over time,” *Renew. Sustain. Energy Rev.*, vol. 115, p. 109369, 2019, doi: https://doi.org/10.1016/j.rser.2019.109369.

[106] A. Fernández-Guillamón, E. Gómez-Lázaro, E. Muljadi, and Á. Molina-Garcia, “A Review of Virtual Inertia Techniques for Renewable Energy-Based Generators,” *Renew. Energy - Technol. Appl.*, 2021, doi: 10.5772/intechopen.92651.

[107] A. Ulbig, T. S. Borsche, and G. Andersson, “Impact of low rotational inertia on power system stability and operation,” *IFAC Proc. Vol.*, vol. 19, pp. 7290–7297, 2014, doi: 10.3182/20140824-6-za-1003.02615.

[108] P. Denholm, T. Mai, R. W. Kenyon, B. Kroposki, and M. O. Malley, “Inertia and the Power Grid : A Guide Without the Spin,” no. May, 2020, [Online]. Available: https://www.nrel.gov/docs/fy20osti/73856.pdf.

[109] R. W. Kenyon, A. Hoke, J. Tan, and B. M. Hodge, “Grid-Following Inverters and Synchronous Condensers: A Grid-Forming Pair?,” *Clemson Univ. Power Syst. Conf. PSC 2020*, no. March, 2020, doi: 10.1109/PSC50246.2020.9131310.

[110] J. Matevosyan, “Evolution of ERCOT’s Frequency Control and Ancillary Services for Higher Levels of Inverter- Based Generation,” 2019, [Online]. Available: https://www.esig.energy/download/evolution-of-ercots-frequency-control-and-ancillary-services-for-higher-levels-of-inverter-based-generation-julia-matevosyan/#.

[111] M. Nedd, C. Booth, and K. Bell, “Potential solutions to the challenges of low inertia power systems with a case study concerning synchronous condensers,” *2017 52nd Int. Univ. Power Eng. Conf. UPEC 2017*, vol. 2017-Janua, pp. 1–6, 2017, doi: 10.1109/UPEC.2017.8232001.

[112] D. Bazargan, S. Filizadeh, and A. M. Gole, “Stability Analysis of Converter-Connected Battery Energy Storage Systems in the Grid,” *IEEE Trans. Sustain. Energy*, vol. 5, no. 4, pp. 1204–1212, 2014, doi: 10.1109/TSTE.2014.2337053.

[113] S. c, C. Yammani, and S. Maheswarapu, “Load Frequency Control of Multi-microgrid

System considering Renewable Energy Sources Using Grey Wolf Optimization," *Smart Sci.*, vol. 7, no. 3, pp. 198–217, 2019, doi: 10.1080/23080477.2019.1630057.

[114] M. Khederzadeh, H. Maleki, and V. Asgharian, "Frequency control improvement of two adjacent microgrids in autonomous mode using back to back Voltage-Sourced Converters," *Int. J. Electr. Power Energy Syst.*, vol. 74, pp. 126–133, 2016, doi: 10.1016/j.ijepes.2015.07.002.

[115] V. Bui, A. Hussain, and H.-M. Kim, "A Strategy for Flexible Frequency Operation of Stand-Alone Multimicrogrids," *IEEE Trans. Sustain. Energy*, vol. 9, no. 4, pp. 1636–1647, Oct. 2018, doi: 10.1109/TSTE.2018.2803342.

[116] "IEEE Recommended Practice for Emergency and Standby Power Systems for Industrial and Commercial Applications," *IEEE Std 446-1995 [The Orange Book]*. pp. 1–320, 1996, doi: 10.1109/IEEESTD.1996.85950.

[117] W. Wu *et al.*, "A Virtual Inertia Control Strategy for DC Microgrids Analogized with Virtual Synchronous Machines," *IEEE Trans. Ind. Electron.*, vol. 64, no. 7, pp. 6005–6016, 2017, doi: 10.1109/TIE.2016.2645898.

[118] J. Alipoor, "STUDIES ON STABILIZATION OF POWER SYSTEM WITH DISTRIBUTED GENERATIONS USING VIRTUAL SYNCHRONOUS GENERATOR," Osaka University, 2015.

[119] J. Liu, "Studies on Improving Dynamic Performance of Microgrids by Applying Virtual Synchronous Generator Control to Distributed Generators," *Dissertation*, no. January, p. 106, 2016.

[120] U. Tamrakar, D. Shrestha, M. Maharjan, B. P. Bhattarai, T. M. Hansen, and R. Tonkoski, "Virtual inertia: Current trends and future directions," *Appl. Sci.*, vol. 7, no. 7, pp. 1–29, 2017, doi: 10.3390/app7070654.

[121] U. Tamraker, "Improvement of Transient Stability of Photovoltaic- hydro Microgrids Using Virtual Synchronous Machines," 2015.

[122] R. Razi, M. Pham, A. Hably, S. Bacha, and S. Member, "A Novel Graph-based Routing Algorithm in Residential Multi-Microgrid Systems," *IEEE Trans. Ind. Informatics*, vol. 3203, no. c, 2020, doi: 10.1109/TII.2020.2997516.

[123] K. Wang *et al.*, "A Survey on Energy Internet: Architecture, Approach, and Emerging Technologies," *IEEE Syst. J.*, vol. 12, no. 3, pp. 2403–2416, 2018, doi: 10.1109/JSYST.2016.2639820.

[124] E. Harmon, U. Ozgur, M. H. Cintuglu, R. de Azevedo, K. Akkaya, and O. A.

Mohammed, “The Internet of Microgrids: A Cloud-Based Framework for Wide Area Networked Microgrids,” *IEEE Trans. Ind. Informatics*, vol. 14, no. 3, pp. 1262–1274, Mar. 2018, doi: 10.1109/TII.2017.2785317.

[125] J. Ahmad, M. Tahir, and S. K. Mazumder, “Improved Dynamic Performance and Hierarchical Energy Management of Microgrids With Energy Routing,” *IEEE Trans. Ind. Informatics*, vol. 15, no. 6, pp. 3218–3229, 2019, doi: 10.1109/TII.2018.2877739.

[126] H. Guo, F. Wang, L. Zhang, and J. Luo, “A Hierarchical Optimization Strategy of the Energy Router-Based Energy Internet,” *IEEE Trans. Power Syst.*, vol. 34, no. 6, pp. 4177–4185, Nov. 2019, doi: 10.1109/TPWRS.2019.2907323.

[127] M. Gao, K. Wang, and L. He, “Probabilistic Model Checking and Scheduling Implementation of an Energy Router System in Energy Internet for Green Cities,” *IEEE Trans. Ind. Informatics*, vol. 14, no. 4, pp. 1501–1510, Apr. 2018, doi: 10.1109/TII.2018.2791537.

[128] W. Shi, X. Xie, C. Chu, and R. Gadh, “Distributed Optimal Energy Management in Microgrids,” *IEEE Trans. Smart Grid*, vol. 6, no. 3, pp. 1137–1146, 2015, doi: 10.1109/TSG.2014.2373150.

[129] N. Nikmehr and S. N. Ravadanegh, “Optimal Power Dispatch of Multi-Microgrids at Future Smart Distribution Grids,” *IEEE Trans. Smart Grid*, vol. 6, no. 4, pp. 1648–1657, 2015, doi: 10.1109/TSG.2015.2396992.

[130] H. Gao, J. Liu, and L. Wang, “Decentralized Energy Management for Networked Microgrids in Future Distribution Systems,” *IEEE Trans. Power Syst.*, vol. 33, no. 4, pp. 3599–3610, 2018, doi: 10.1109/TPWRS.2017.2773070.

[131] Z. Wang, S. Member, B. Chen, J. Wang, S. Member, and J. Kim, “Decentralized Energy Management System for Networked Microgrids in Grid-Connected and Islanded Modes,” *IEEE Trans. Smart Grid*, vol. 7, no. 2, pp. 1097–1105, 2016, doi: 10.1109/TSG.2015.2427371.

[132] P. Yi, T. Zhu, B. Jiang, R. Jin, and B. Wang, “Deploying Energy Routers in an Energy Internet Based on Electric Vehicles,” *IEEE Trans. Veh. Technol.*, vol. 65, no. 6, pp. 4714–4725, Jun. 2016, doi: 10.1109/TVT.2016.2549269.

[133] P. Yi *et al.*, “Renewable energy transmission through multiple routes in a mobile electrical grid,” in *ISGT 2014*, 2014, pp. 1–5, doi: 10.1109/ISGT.2014.6816468.

[134] X. Tang, S. Bi, and Y. A. Zhang, “Distributed Routing and Charging Scheduling

Optimization for Internet of Electric Vehicles," *IEEE Internet Things J.*, vol. 6, no. 1, pp. 136–148, 2019, doi: 10.1109/JIOT.2018.2876004.

[135] A. O. Hariri, M. El Hariri, T. Youssef, and O. A. Mohammed, "A Bilateral Decision Support Platform for Public Charging of Connected Electric Vehicles," *IEEE Trans. Veh. Technol.*, vol. 68, no. 1, pp. 129–140, 2019, doi: 10.1109/TVT.2018.2879927.

[136] T. Zhu, S. Xiao, Y. Ping, D. Towsley, and W. Gong, "A secure energy routing mechanism for sharing renewable energy in smart microgrid," *2011 IEEE Int. Conf. Smart Grid Commun. SmartGridComm 2011*, pp. 143–148, 2011, doi: 10.1109/SmartGridComm.2011.6102307.

[137] J. S. Hong and M. Kim, "Game-Theory-Based Approach for Energy Routing in a Smart Grid Network," *J. Comput. Networks Commun.*, vol. 2016, pp. 1–8, 2016, doi: 10.1155/2016/4761720.

[138] J. Ma, L. Song, and Y. Li, "Optimal power dispatching for local area packetized power network," *IEEE Trans. Smart Grid*, vol. 9, no. 5, pp. 4765–4776, 2018, doi: 10.1109/TSG.2017.2669907.

[139] X. Shi, Y. Xu, and H. Sun, "A Biased Min-consensus Based Approach for Optimal Power Transaction in Multi-Energy-Router Systems," *IEEE Trans. Sustain. Energy*, vol. PP, no. c, p. 1, 2018, doi: 10.1109/TSTE.2018.2889643.

[140] H. Guo, F. Wang, L. Li, J. Zhang, and J. Luo, "A Minimum Loss Routing Algorithm Based on Real-Time Transaction in Energy Internet," *IEEE Trans. Ind. Informatics*, vol. 15, no. 12, pp. 1–1, 2019, doi: 10.1109/tii.2019.2904188.

[141] A. Ovalle, J. Fernandez, A. Hably, and S. Bacha, "An Electric Vehicle Load Management Application of the Mixed Strategist Dynamics and the Maximum Entropy Principle," *IEEE Trans. Ind. Electron.*, vol. 63, no. 5, pp. 3060–3071, May 2016, doi: 10.1109/TIE.2016.2516975.

[142] R. R. Shrivastwa, A. Hably, K. Melizi, and S. Bacha, "Understanding Microgrids and Their Future Trends," in *2019 IEEE International Conference on Industrial Technology (ICIT)*, 2019, pp. 1723–1728, doi: 10.1109/ICIT.2019.8754952.

[143] A. Ovalle, A. Hably, and S. Bacha, *Grid Optimal Integration of Electric Vehicles: Examples with Matlab Implementation*, vol. 137. Cham: Springer International Publishing, 2018.

[144] X. Li *et al.*, "Constrained Optimization of Multicast Routing for Wide Area Control of Smart Grid," *IEEE Trans. Smart Grid*, vol. 10, no. 4, pp. 3801–3808, 2019, doi:

10.1109/TSG.2018.2835487.

[145] Ş. Temel, V. Ç. Gungor, and T. Koçak, “Routing protocol design guidelines for smart grid environments,” *Comput. Networks*, vol. 60, pp. 160–170, Feb. 2014, doi: 10.1016/j.bjp.2013.11.009.

[146] H. Guo, F. Wang, G. James, L. Zhang, and J. Luo, “Graph theory based topology design and energy routing control of the energy internet,” *IET Gener. Transm. Distrib.*, vol. 12, no. 20, pp. 4507–4514, 2018, doi: 10.1049/iet-gtd.2018.6238.

[147] Q. Shafiee, T. Dragicevic, J. C. Vasquez, and J. M. Guerrero, “Hierarchical Control for Multiple DC-Microgrids Clusters,” *IEEE Trans. Energy Convers.*, vol. 29, no. 4, pp. 922–933, Dec. 2014, doi: 10.1109/TEC.2014.2362191.

[148] M. C. Falvo, D. Sbordone, I. S. Bayram, and M. Devetsikiotis, “EV charging stations and modes: International standards,” in *2014 International Symposium on Power Electronics, Electrical Drives, Automation and Motion*, Jun. 2014, pp. 1134–1139, doi: 10.1109/SPEEDAM.2014.6872107.